

Understanding and improving thermodynamic stability of austenite in low carbon carbide free bainitic steels via ausforming process

Von der Fakultät für Georessourcen und Materialtechnik
der Rheinisch-Westfälischen Technischen Hochschule Aachen

zur Erlangung des akademischen Grades eines
Doktors der Ingenieurwissenschaften
genehmigte Dissertation

vorgelegt von
Theerawat Kumnorkaew, Master of Engineering
aus Chiangmai, Thailand

Berichter: Univ.-Prof. Dr.-Ing. Wolfgang Bleck
Prof. Dr.-Ing. Junhe Lian

Tag der mündlichen Prüfung: 22.02.2023

Diese Dissertation ist auf den Internetseiten der Universitätsbibliothek online verfügbar

Declaration on publications

This dissertation includes the following articles that have been published in international peer-reviewed journals.

Chapter II - T. Kumnorkaew, J. Lian, V. Uthaisangsuk, and W. Bleck, Effect of ausforming on microstructure and hardness characteristics of bainitic steel, *Journal of Materials Research and Technology* 9 (2020), 13365–13374.

<https://doi.org/10.1016/j.jmrt.2020.09.016>.

Chapter III - T. Kumnorkaew, J. Lian, V. Uthaisangsuk, and W. Bleck, Kinetic Model of Isothermal Bainitic Transformation of Low Carbon Steels under Ausforming Conditions. *Alloys* 1 (2022), 93-115.

<https://doi.org/10.3390/alloys1010007>

Chapter IV - T. Kumnorkaew, J. Lian, V. Uthaisangsuk, J. Zhang, and W. Bleck, Low carbon bainitic steel processed by ausforming: Heterogeneous microstructure and mechanical properties. *Materials Characterization* 194 (2022), 112466.

<https://doi.org/10.1016/j.matchar.2022.112466>

For the articles published in international journals in Chapter II – Chapter IV, the data curation, kinetics model development, and parameters calibration have been performed by the candidate. The preparation of the original draft, including texts, figures and tables, has been provided by the candidate, who has also made the corresponding modifications and improvements in the papers following the suggestions provided by the reviewers.

To my family

Acknowledgments

I would like to express my most profound appreciation to my primary supervisor, Prof. Dr.-Ing. Wolfgang Bleck, for providing me the opportunity of working on this interesting research topic at the Steel Institute of RWTH Aachen University. I am also deeply thankful to Prof. Dr.-Ing. Junhe Lian from Alto University for his patient guidance and insightful discussions. I would like to sincerely thank Prof. Dr.-Ing. Sebastian Münstermann for giving me the opportunity to participate in all research events within the materials integrity group. In addition, I am sincerely grateful to my master's degree supervisor and my co-advisor for my doctoral study, Prof. Dr.-Ing. Vitoon Uthaisangsuk from King's Mongkut University of Technology Thonburi for his patience, enthusiasm, and immense knowledge.

I also would like to express my utmost gratitude to Dr.-Ing. Jiali Zhang from Institute for Materials Applications in Mechanical Engineering of RWTH Aachen University for her assistance and contribution to my last publication.

I gratefully acknowledge the funding received towards years of my doctoral study from Rajamangala University of Technology Krungthep and offices from the Office of Educational Affairs Royal Thai Embassy for their administrative support.

Moreover, I would like to thank Mrs. Christina Beumers, Mrs. Martina Sparrer, Dr.-Ing. Markus Könnemann, and Dr.-Ing. Michael Dölz for taking care of many administrative issues. I sincerely appreciate all the technical support from Mr. Malte Schmachtenberg from Institute for Materials Applications, Mr. Michael Schillheim, Mr. Wilhelm Meier, Mr. Sebastian Seibel, Mr. Jürgen Dartenne, Mr. Dietmar Sodar, Mr. Robert Gier, Mr. Wieslaw Tupiec, Ms. Monika Friedrichs and Mrs. Cornelia Freytag for their assistances regarding sample manufacturing, specimen preparation, and experiments. I am also very grateful to all my colleagues, especially Dr.-Ing. Seyedamirhossein Motaman, Dr.-Ing. Napat Vajaragupta, Mr. Peerapon Wechsuwanmanee, Dr.-Ing. Yuling Chang, Dr.-Ing. Marc Ackermann, and Mr. Ahmed Turnali for excellent scientific discussions.

I would also like to say a heartfelt thank you to my family for always believing in me and encouraging me to follow my dreams. The unconditional support and love from my parents have

been the greatest wealth in my life that helps me to overcome all the challenges and potholes along the way.

Finally, I wish to thank with love to my wife who has stood by me throughout all my travails. Without you believing in me, I never could have made it. It is time to celebrate; you earned this degree right along with me.

Theerawat Kumnorkaew

Aachen, February 2023

Abstract

Carbide-free bainitic (CFB) steel has become a new forefront of advanced high-strength steels owing to their outstanding balance in mechanical properties. Due to a thermodynamic instability of austenite in low carbon CFB steels, formations of only primary phase bainitic ferrite and secondary carbon enriched retained austenite phase are impracticable. The untransformed austenite at high temperatures could partially transform into fresh martensite during cooling operation, depending on the local carbon concentration in the austenite. A general consequence is that an excessive formation of fresh martensite may deteriorate ductility, despite the enhanced strength of the steel. Thus, controlling the thermodynamic stability of austenite has been a challenging issue in developing low-carbon carbide-free bainitic (CFB) steels, besides increasing mean carbon content and chemical compositions.

Ausforming as a thermomechanical heat treatment process is applied to compromise the formation of fresh martensite and to balance the phase constituent of the steels. This process combines plastic deformation of the untransformed austenite with the conventional process of isothermal heat treatment. Parameters of ausforming, such as deformation temperature, strain, and strain rate, are of significant importance in defining appropriate conditions for desirable microstructures and mechanical properties. The correlation between the ausforming conditions throughout the kinetics behavior of isothermal bainitic transformation, factors inherent in the martensite transformation, hardness, and tensile properties have been established.

A unified physics-based model has been developed based on nucleation rate theory to provide a better understanding of how ausforming influences the variations of activation energy, corresponding driving energy, and the evolution of carbon enrichment in austenite. In addition, the impact of the chemical compositions has been conducted to reveal a limitation of ausforming with respect to the deformation strain on improving the thermodynamic stability of austenite against the formation of fresh martensite. Throughout the dissertation, a systematic investigation in heterogeneous microstructure and mechanical properties subjected to ausforming conditions allows for establishing advanced high-strength steels with reasonable hardness and improved strength and ductility.

Kurzzusammenfassung

Karbidfreier bainitischer (CFB) Stahl hat sich aufgrund seiner hervorragenden Ausgewogenheit der mechanischen Eigenschaften zu einer neuen Vorreiterrolle bei den neuen hochfesten Stählen (Advanced High Strength Steels AHSS) entwickelt. Aufgrund einer thermodynamischen Instabilität von Austenit in kohlenstoffarmen CFB-Stählen ist die Bildung von nur primärphasigem bainitischem Ferrit mit der Sekundärphase kohlenstoffangereicherter Restaustenit nicht praktikabel. Der bei hohen Temperaturen nicht umgewandelte Austenit könnte sich während des Abkühlvorgangs teilweise in frischen Martensit umwandeln, abhängig von der lokalen Kohlenstoffkonzentration im Austenit. Eine allgemeine Konsequenz ist, dass eine übermäßige Bildung von frischem Martensit trotz der erhöhten Festigkeit des Stahls die Duktilität verschlechtern kann. Daher war die Kontrolle der thermodynamischen Stabilität von Austenit neben der Erhöhung des mittleren Kohlenstoffgehalts und der Legierungsmodifikation ein herausforderndes Problem bei der Entwicklung von karbidfreien bainitischen (CFB) Stählen mit niedrigem Kohlenstoffgehalt.

Ausforming als thermomechanischer Wärmebehandlungsprozess wird angewendet, um die Bildung von frischem Martensit zu beeinträchtigen und den Phasenbestandteil der Stähle auszugleichen. Dieser Prozess kombiniert die plastische Verformung des nicht umgewandelten Austenits mit dem konventionellen Prozess der isothermen Wärmebehandlung. Parameter des Ausforming, wie Verformungstemperatur, Dehnung und Dehnungsrate, sind von erheblicher Bedeutung beim Definieren geeigneter Bedingungen für wünschenswerte Mikrostrukturen und mechanische Eigenschaften. Die Korrelation der Ausforming-Bedingungen mit dem kinetischen Verhalten bei der isothermen bainitischen Umwandlung und mit den Faktoren, die der Martensit-Umwandlung, der Härte und den Zugeigenschaften innewohnen, wurde ermittelt.

Basierend auf der Keimbildungsratentheorie wurde ein einheitliches physikalisches Modell entwickelt, um ein besseres Verständnis dafür zu liefern, wie das Ausforming die Variationen der Aktivierungsenergie, der entsprechenden Antriebsenergie und der Entwicklung der Kohlenstoffanreicherung in Austenit beeinflusst. Darüber hinaus wurde der Einfluss der chemischen Zusammensetzungen analysiert, um eine Begrenzung des Ausforming in Bezug auf die Verformungsspannung bei der Verbesserung der thermodynamischen Stabilität von Austenit

gegen die Bildung von frischem Martensit aufzuzeigen. Durchgehend wird in der gesamten Dissertation eine systematische Untersuchung der heterogenen Mikrostruktur und der mechanischen Eigenschaften vorgenommen, um mittels Ausforming die Entwicklung neuer hochfester Stähle mit verbesserter Festigkeit und Duktilität zu ermöglichen.

Table of contents

Declaration on publications	i
Acknowledgments	v
Abstract.....	vii
Kurzzusammenfassung.....	viii
Table of contents	x
List of abbreviations	xi
List of symbols.....	xiii
Chapter I - Introduction.....	18
1.1 Fundamentals	22
1.2 Objectives and scope of the study.....	51
1.3 Original scientific contribution	54
1.4 References.....	59
Chapter II Effect of ausforming on microstructure and hardness characteristics of bainitic steel	69
Chapter III Kinetic model development of isothermal bainitic transformation of low carbon steels under ausforming conditions	92
Chapter IV Low carbon bainitic steel processed by ausforming: heterogeneous microstructure and mechanical properties	131
Chapter V Conclusions and future studies.....	165
Curriculum vitae.....	168

List of abbreviations

AFP	Age-hardenable Ferritic-Pearlitic
AIT	Ausforming followed by Isothermal Tempering
AN	Autocatalytic Nucleation
APT	Atom Probe Tomography
BCC	Body-Centered Cubic
BF	Bainitic Ferrite
CAL	CALculation
CCT	Continuous Cooling Transformation
CFB	Carbide Free Bainite
DLB	Degenerated Lower Bainite
DUB	Degenerated Upper Bainite
DQ	Direct Quenching
EBS	Electron BackScatter Diffraction
FCC	Face-Centered Cubic
FM	Fresh Martensite
GB	Grain Boundary
G-T	Greninger-Troiano
GND	Geometrically Necessary Dislocation
IPF	Inverse Pole Figure
IPS	Invariant Plane Strain
IQ	Image Quality
KAM	Kernel Average Misorientation
KM	Koistinen Marburger
K-S	Kurdjumov-Sachs
LOM	Light Optical Microscope
M/A	Martensite/Austenite
NS	Nucleation Site
N-W	Nishiyama-Wassermann

OR	Orientation Relationship
PAG	Prior Austenite Grain
PAGB	Prior Austenite Grain Boundary
PEEQ	Equivalent Plastic Strain
PIT	Pure Isothermal Tempering
Q&T	Quench and Tempering
RA	Retained Austenite
RT	Room Temperature
SE	Secondary Electron
SEM	Scanning Electron Microscope
SPSC	Semi-Product Simulation Center
TTT	Time-Temperature-Transformation
TRIP	TRansformation-Induced Plasticity
UA	Untransformed Austenite
UTS	Ultimate Tensile Strengths
WHR	Work-Hardening Rate
XRD	X-Ray Diffraction
YS	Yield Strength

List of symbols

A_{c1}	temperature at which austenite begins to form during heating
A_{c3}	temperature at which transformation of ferrite to austenite is completed during heating.
A_5	total elongation
b	Burgers vector
b_{AN}	parameter considering an effect of γ/α interfaces
b_{GB}	parameter considering an effect of γ/γ interfaces
B_s	bainite start temperature
C_1	proportional constant relating to temperature at the beginning of bainitic transformation and carbon content
C_2	proportional constant relating to temperature at the beginning of displacive transformation and carbon content
d	spacing between cubic planes
d_i	instantaneous diameter of specimen
d_P	dimension of cementite particle
d_s	constant parameter relating to austenite grain size
d_γ	average grain size of austenite
d_0	initial diameter of specimen
D	average crystal size
E^α	elastic modulus of bainite and martensite structures
E^γ	elastic modulus of austenite
f_{FM}	fresh martensite fraction after cooling to room temperature
f_{RA}	retained austenite fraction after cooling to room temperature
f_{UA}	untransformed austenite fraction at bainitic transformation stage
f_α	bainitic ferrite fraction formed during bainitic transformation
f_θ	cementite fraction formed during bainitic transformation
G_{dislo}	dislocation interaction energy due to bainitic stress field
G_N	universal nucleation function

G_{SB}	stored energy of bainite
G_{α}	shear modulus of bcc iron
G_{γ}	shear modulus of fcc iron
ΔG_{AN}	total free energy change for autocatalytic nucleation
ΔG_{ch}	chemical free energy change
ΔG_{chA}	chemical free energy change depending on degree of carbon enrichment in the austenite
ΔG_{chAi}	initial free energy change at the beginning of the transformation or grain boundary nucleation.
ΔG_{GB}	total free energy change for grain boundary nucleation
ΔG_i	total molar free energy of the associated event of nucleation
ΔG_m	maximum driving force available for para-equilibrium nucleation
$\Delta G^{\gamma \rightarrow \alpha}$	free energy difference between austenite and bainite
$\Delta G_{\gamma/\alpha}$	semi-coherent interfacial energy at γ/α interfaces
$\Delta G_{\gamma/\gamma}$	semi-coherent interfacial energy at γ/γ interfaces
h	Plank constant
k	material constant for XRD analysis
k_B	Boltzmann constant
K_1	fitting parameter
L_3	mean linear intercept corresponding to the dimension of a slip plane
M_f	martensite finish temperature
M_s	martensite start temperature
$M_{s,cal}$	martensite start temperature obtained from calculation
$M_{s,exp}$	martensite start temperature obtained from experiment
n	number of FCC cubic planes along nucleus thickness
n_{ch}	material constant depending chemical composition of steel
N_i	number density of pre-existing defects
N_0	nucleation function
Q_{AN}^*	activation energy required for autocatalytic nucleation
Q_{GB}^*	activation energy required for grain boundary nucleation

Q_i^*	activation energy required for individual process for nucleation
Q_0^*	initial energy required for phase transformation
ΔQ^*	total activation energy difference required for activating bainitic transformation at each iteration
R	gas constant
T	testing temperature
T_{def}	deformation temperature
T_h	displacive transformation temperature
$T_{h\bar{X}}$	temperature at the beginning of displacive transformation
T_{iso}	isothermal tempering temperature
T_{RM}	room temperature
T_0	temperature limit for a diffusionless transformation
T'_0	temperature limit for a diffusionless transformation, including a stored energy of 400 J/mol
$T'_{0,\text{ausforming}}$	temperature limit for a diffusionless transformation, including a stored energy of 400 J/mol and estimated energy due to ausforming
$T_{0\bar{X}}$	temperature at the beginning of isothermal bainitic transformation
V_α	average volume of bainitic ferrite sub-unit
V_{mol}	molar volume of austenite
V_0	initial volume of specimen
ΔV	volumetric change of specimen
\bar{w}	average carbon content of steel
w_α	carbon content in bainitic ferrite
$w_{\alpha'}$	carbon content in fresh martensite
w_γ	carbon content within untransformed austenite
$w_{\gamma,\text{RA}}$	carbon content in retained austenite
x_{Al}	aluminium content
x_{C}	carbon content
x_{Co}	cobalt content
x_{Cr}	chromium content
x_{Cu}	copper content

x_N	nitrogen content
x_{Nb}	niobium content
x_{Ni}	nickel content
x_{Mn}	manganese content
x_{Mo}	molybdenum content
x_{Si}	silicon content
x_{Ti}	titanium content
x_V	vanadium content
x_W	tungsten content
Z	material constant
α	material constant
α'	alpha phase fresh martensite
α_B	alpha phase ferrite or bainitic ferrite
α_c	material constant
α_{FM}	material parameter in the KM model
α_γ	lattice parameter of austenite
γ	gamma phase austenite
γ/α	interface boundary of austenite and ferrite
γ/γ	grain boundary in austenite
δ	effective thickness of prior austenite grain boundary
ε_L	longitudinal strain
ε_P	plastic strain
ε_R	radial strain
ε_1	microstrain within crystal domain
ε_{22}^{tr}	internal elastic strain state resulting from local strain instability between bainitic ferrite and untransformed austenite
ζ	dislocation half width
ν	Poisson ratio
ξ	material constant
ρ	average dislocation density

ρ_C	dislocation density due to the crystallite size contribution
ρ_S	dislocation density due to the microstrain contribution
σ_{hydro}	strength due to the effect of neighboring phases
σ_{y0}	initial yield strength value
$\sigma_{\gamma/\gamma}$	grain boundary energy per unit area
$\Delta\sigma_{\text{Fe}}$	strength due to pure iron
$\Delta\sigma_{\text{GS}}$	strength due to grain size reduction
$\Delta\sigma_{\text{P}}$	strength due to precipitation
$\Delta\sigma_{\rho}$	strength due to the contribution of dislocations
$\Delta\sigma_{\text{SS}}$	strength due to solid solution strengthening
τ_s	critical shear strain for bainitic transformation
Γ	material constant

Chapter I - Introduction

Due to its high strength and resilience of production cost, steel remains the best candidate material used in various industry sectors, particularly automotive manufacturing. The progress in research and technology allows the optimal balance of strength, performance, and weight reduction with the most negligible environmental impact [1–4]. Most lightweight components not only improve fuel efficiency but also reduce the rate of carbon emissions produced by the combustion engine. The forged steel components must be strong and tough in response to their loading conditions, whereas good machinability should not be avoided since subsequent machining is usually required after forging. Consequently, conventional quenched and tempered (Q&T) steel grades were made for automotive bolts and screws by which better cyclic tolerance is achieved with the feature of a hard and brittle martensitic structure. However, the three stages of heat treatment operation after the forging are cost intensive. Precipitation-hardened pearlitic ferritic (in German called AFP) steels have been then developed to shorten such processing routes by directly hardening while exhibiting inferior mechanical properties compared to Q&T steels [5]. To these drawbacks, lightweight and micro-alloyed bainitic steels have been developed as an alternative to Q&T and AFP steels, as shown in **Fig. 1a**. For example, a bainitic grade DIN-20MnCrMo7 is commercially available for applications to the common rail and injector body [6]. By additions of Mn, Cr, and Mo, the desired bainitic microstructure can be achieved via a single step of heat treatment operation, as illustrated in **Fig. 1b**. An essential aspect of the bainitic steels is their machinability, to which carbide formation and solid solution are significantly related. However, compared with Q&T steels, bainitic steel is more difficult to machine due to its higher hardness.

Alloying with Si or Al by an appropriate content can change carbon activity by rejecting carbon into the parent austenite when bainitic ferritic plates are formed. The enrichment of carbon into austenite thus results in austenite retention during cooling operation. The benefit of retained austenite is the transformation-induced plasticity (TRIP) effect, by which damage tolerance can be improved when the working component reaches its critical value. However, the TRIP effect should not be susceptible to bulk components design like sheet metal in which formability is extremely required. Therefore, a component with an appropriate fraction of the retained austenite may lead to a balance in strength-ductility when it is subjected to mechanical loading. There is a critical

concern regarding fresh martensite that could form while cooling operation for the steel producer. In particular, low-carbon steels where carbon enrichment within austenite is somewhat small, resulting in the thermodynamic instability of austenite. Although some fraction of the unstable austenite is transformed into fresh martensite, most of the retained austenite presented after the heat treatment operation is in the form of granular or blocky type. The problem is that if the size of blocky retained austenite is much coarsened, the austenite becomes less stable and prone to transform into high-carbon martensite under the influence of a small strain. Thus, this untempered and hard martensite embrittles the steel compromising its mechanical properties, even though the presence of fresh martensite gives rise to a strengthening point of view. In this dissertation, controlling balance in phase constituents by minimizing the total fraction of fresh martensite is necessary.

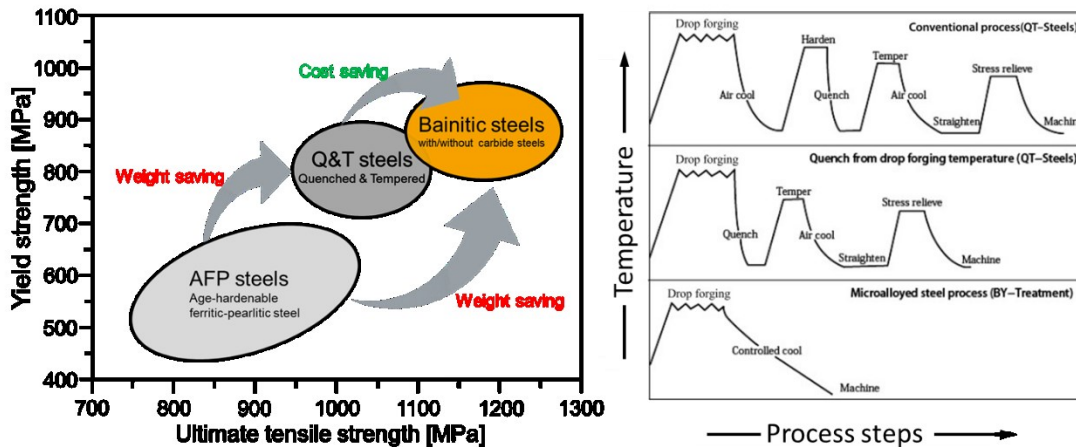


Fig. 1 (a) Mechanical properties of AFP, Q&T, and bainitic grade steels [7] and (b) heat-treatment process required for Q&T and bainitic grade steels [8].

Based on the displacive transformation theory of bainite, the carbon enrichment accompanying diffusionless growth of bainitic ferrite is limited by T_0 locus. The locus allows the design of a wide range of high-strength bainitic steels. By increasing the amount of bainitic ferrite, the rate of carbon-enriched austenite is simultaneously augmented. In general, this strategy becomes feasible when the mean carbon of the steel is increased so that a reduction in the start temperature of martensite allows the possibility of treating the steel at a lower temperature. Apart from that, various heat treatment techniques have been employed, including alloy modification, i.e., manganese. Most of them are associated with prior austenite grain reduction in which the available

nucleation sites for martensite are mostly prevented, despite the increased availability of bainitic transformation.

Ausforming, which combines plastic deformation of the untransformed austenite with an isothermal heat treatment process, is one of the thermomechanical treatments employed for such a purpose. However, only few research studies have paid attention to low-carbon steels. Even though the ausforming parameters, such as deformation temperature, strain, and strain rate, have been conducted, the effect of mechanical stabilization, which occurs during the transformation progress, has not been systematically and distinctly described. Therefore, the first objective of this dissertation is to establish a quantitative correlation between the ausforming parameters, bainitic transformation behavior, microstructural features, and strength behavior for 0.18C-1Si-2.5Mn-0.2Cr-0.2Ni-0.02B-0.03Ti steel. Also, understanding the effect of ausforming on phase transformations, including the kinetics behavior of isothermal bainitic transformation and subsequent formation of fresh martensite, is of importance.

Nonetheless, the role of ausforming parameters on the kinetics of isothermal bainitic transformation at the desired temperature and the mechanical stabilization to the thermodynamic stability improvement of austenite remains questioned. Because inconsistent outcomes regarding the kinetics of isothermal bainitic transformation with respect to alloying variations, including carbon, have been reported. In this regard, several models based on the classical nucleation rate theory have been proposed to describe the kinetics behavior of bainitic transformations under the influences of alloying elements and undercooling temperatures in terms of activation energy change. Nevertheless, none of them does consider the effect of ausforming on the variation of activation energy, driving pressure, and evolution of the carbon enrichment in austenite during isothermal bainitic transformation. Thus, a unified physics-based model has been later derived by considering the effect of ausforming. The model is proposed to give rise to an in-depth understanding of the nucleation rate influenced by changes in the activation energy and enriched carbon in the austenite. In aspects of mechanical stabilization of austenite, dislocation density involving ausforming and alloying elements (referring to 0.26C-1Si-1.5Mn-1Cr-1Ni-0.003B-0.03Ti steel) is also roughly estimated in this dissertation.

According to the statements above, the defects induced by ausforming lead to changes in grain size, morphology, carbon enrichment, and phase constituents, leading to variations in the

mechanical properties of the steel. However, the insight discussion on the effect of ausforming involving thermodynamic stability throughout tensile properties, including post-necking and fracture behaviors of the low carbon steels, has never been thoroughly characterized. Therefore, the insight discussion on the microstructural heterogeneity that responds to the tensile properties of low-carbon steel is proposed in this dissertation. In particular, the TRIP effect dependent on the retained austenite fraction and grain refinement associated with strengthening and resistance to fracture is also evaluated. To conclude, this dissertation provides approaches for designing and preparing bainitic steels with low carbon content via the ausforming process and facilitating the application of such steels.

1.1 Fundamentals

The following sections summarize the current research status of low-carbon bainitic TRIP steels, which is relevant to the inquiries conducted within the scope of this dissertation. In particular, scientific literature on the kinetics of bainitic transformation, the thermodynamic stability of high-temperature austenite, ausforming heat treatment, and the mechanical stability of retained austenite have been reviewed.

1.1.1. Overview of bainite

Bainite is a non-equilibrium transformation product of austenite as it forms at a high cooling rate, which is high enough to avoid pearlitic transformation but not as high as to transform into martensite. Apart from cooling, bainite can form under isothermal heat treatment at a temperature range between bainite start (B_S) and martensite transformation (M_S) temperatures [9]. Austenite decomposition into bainite is time-dependent; thus, the kinetics or progress of the bainitic transformation is represented by a lower C curve on the time-temperature-transformation (TTT) diagram, as shown in **Fig. 2**. Since the formation of bainite occurs between reconstructive pearlite (as in the upper C curve) and displacive martensite, the exact definition of bainitic transformation mechanism is relatively ambiguous. In particular, the growth nature that can be controlled by reconstructive or by displacive mechanism. Consequently, the transformation mechanism applicable to bainite has remained controversial among metallurgists up to the present.

Bainitic microstructures are commonly described as non-lamellar aggregates of bainitic ferrite (BF) laths or platelets as the primary phase, separated by a carbon-enriched phase like cementite, fresh martensite (FM) or retained austenite (RA) [10]. The enriched carbon phase as a secondary phase is inevitable during bainitic transformation, which remains untransformed upon the growth of BF. The term BF stands for the formation of ferrite components in bainite [11]. The aggregates of BF platelets are called sheaves, and the platelets within each sheaf are sub-units. **Fig. 3** shows a schematic representation of a characteristic of bainitic sheaf at the prior boundary of austenite. The sub-units within each sheaf are not isolated from each other by the second phase. They are connected in three dimensions since they share a common crystallographic orientation and habit plane. Bainite can generally be classified into two types according to the transformation temperature, i.e., upper bainite and lower bainite. The difference in morphology is the formation of cementite interlath between or within BF lath. Upper bainite forms at higher temperatures where

the diffusion rate is fast to allow carbon diffusion to the lath boundaries. Lower bainite forms at relatively lower temperatures where the carbon is entrapped within the growing plate of BF as the diffusion rate is low. Hence, carbon is precipitated within BF.

However, those upper and lower bainite can not be fully described for all features that form during the transformation because of variations of plate or lath, depending on carbon concentration, alloying elements, and heat treatment. Other aspects of the bainitic classification were suggested by Krauss and Thompson [12], Lotter and Hougardy [13], or by Ohmori et al. [14], and Bramfitt and Speer [15]. Zajac et al. [16] proposed a summary of bainitic classification. As shown in **Fig. 4**, bainite is distinguished into five categories based on the arrangement of primary phase bainitic ferrite and secondary carbon enriched phase. Apart from the common well-known upper and lower bainite structures, degenerated features of upper/lower bainite (DUB/DLB) and granular bainite was obtained. The degenerated upper bainite has so-called martensite/retained austenite (M/A) constituent on the lath boundaries, while the degenerated lower bainite has M/A dispersed inside the ferrite laths. Granular bainite is defined as irregular ferrite with carbon-enriched second phases distributed between these irregular grains.

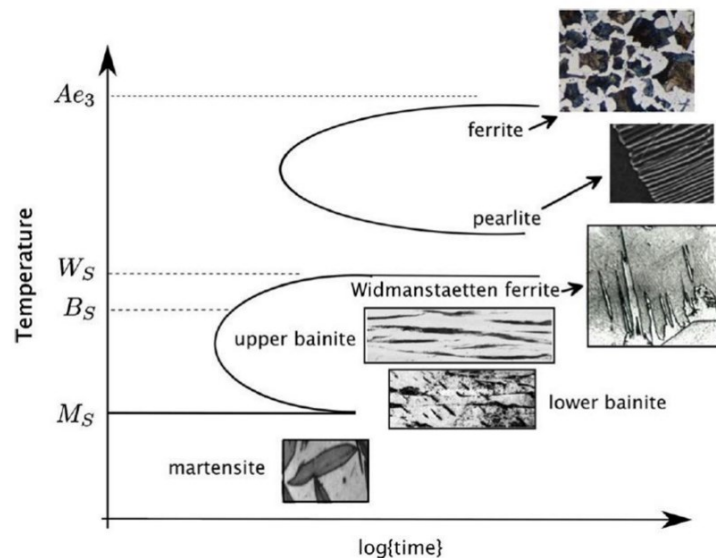


Fig. 2 A time-temperature-transformation (TTT) diagram for steel showing microstructural features that can be achieved by heat treatment [17].

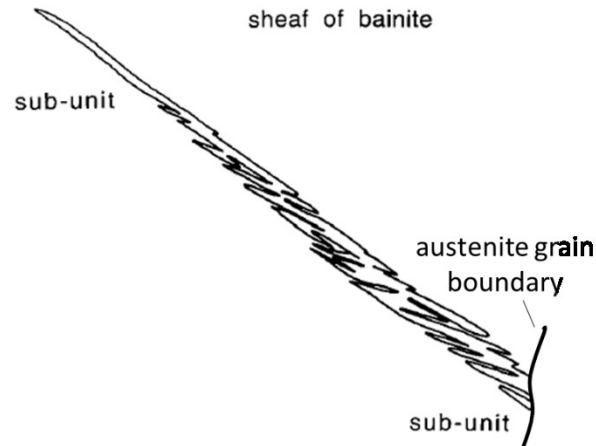


Fig. 3 Schematic representation of the sheaf structure of bainite [10].

Generally, the carbon-rich second phase is not cementite. It is any transformation product developed from carbon-enriched austenite, which can be characterized into five categories: (i) degenerated pearlite or debris of cementite, (ii) retained austenite, (iii) mixture of ‘incomplete’ transformation products, (iv) M/A, and (v) martensite. The advantage of this scheme is that it covers various bainitic microstructures and can be easily used and understood in common parlance.

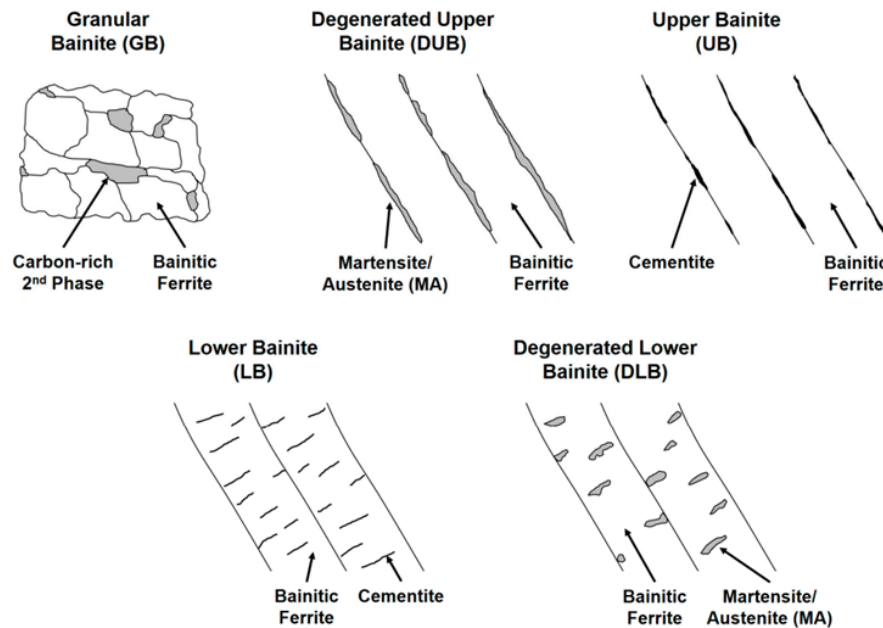


Fig. 4 Graphical illustration of microstructural features of bainite summarized by Zajac et al. [16].

1.1.2. Growth mechanism of bainite

Since the bainitic transformation occurs between displacive martensite and reconstructive pearlite, in some instances, it exhibits both characteristic features of martensite and pearlite. As such, the mechanism of bainitic transformation has been the subject of earnest debate thus far, whether it grows by diffusive or displacive mode [18,19], as the comprehensive understanding has not been clarified yet. The diffusive fashion elucidates that bainitic formation is controlled by carbon diffusion. Bainitic ferrite formed by the ledge mechanism, where it has been postulated that the interface area, has a disordered structure. By using hot stage microscopic to examine the growth mechanism of bainitic ferrite, Ko and Cottrell in 1952 [20] found that bainitic transformation was continuous process and it grown relatively slow compared with the growth rate of martensite plates. Later, this mechanism was also experimentally confirmed by other publications [21,22]. They claimed that the diffusion of carbon atoms plays an essential role in controlling the edgewise growth of a plate at γ/α interface boundary. Growing plates ceased when they reached the austenite grain boundary. Although surface relief was also observed, the bainitic ferrite plates did not cross the austenite grain or even at twin boundaries.

In view of the displacive approach, this theory was first proposed by Hultgren in 1926 [23], where the formation of bainitic ferrite seemed to be governed by a shear mechanism similar to that of martensite. This mechanism involves the motion of carbon atoms across a glissile interface and a generation of an invariant plane shear strain or IPS caused by shape change during the bainitic ferrite formation. The shape change accompanied by the formation of individual sub-unit requires plastic accumulation in austenite. This leads to an accumulation of transformation strain energy and a loss of coherency of the interface boundary that requires for nucleation of a new sub-unit of bainitic ferrite. During the transformation, carbon immediately rejected from bainitic ferrite is enriched into the adjacent parent austenite due to the shear mechanism, even though at the nucleation stage the diffusion of carbon under paraequilibrium condition is taking place [24]. However, most researchers accepted that the bainitic transformation is processed by diffusionless rather than diffusion if the transformation occurs nearly above the start temperature of martensite [9,18,25]. A short summary of the structures formed by the diffusive and displacive mechanisms is illustrated in **Fig. 5**.

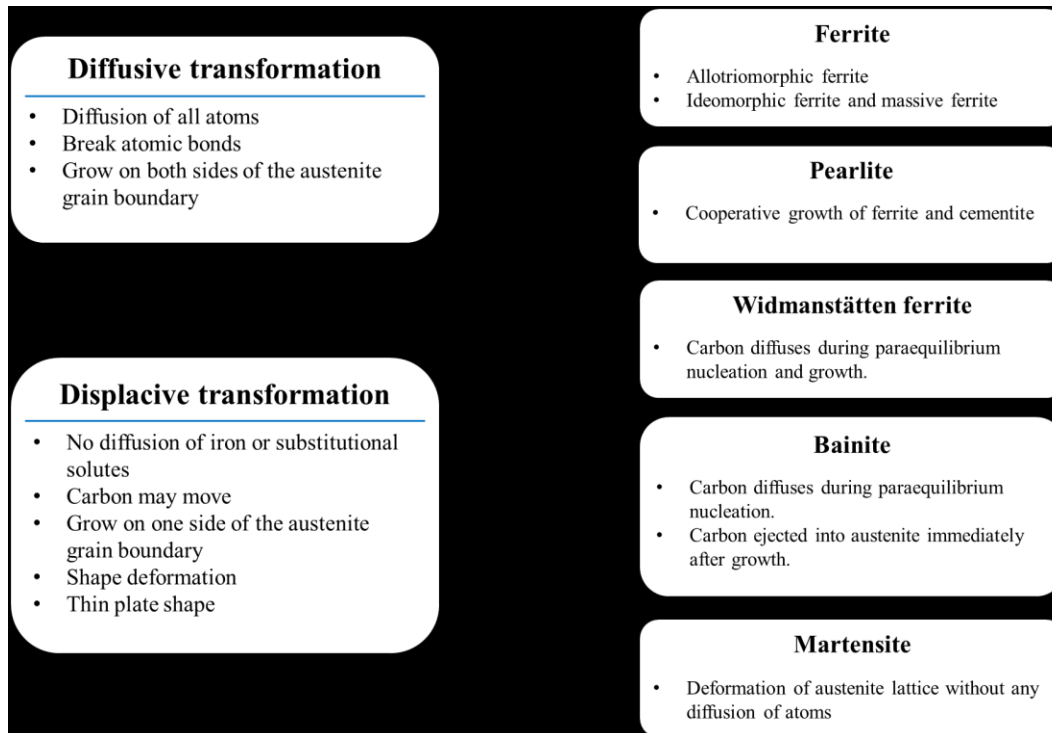


Fig. 5 Characteristics of diffusive and displacive transformations in steels, modified from [10].

From the displacive theory point of view, the kinetics of austenite decomposition is represented on the TTT diagrams. The formation of bainite proceeds by the nucleation and growth mechanisms. The kinetics of transformation of austenite is represented on the time-temperature-transformation diagrams. The nucleation occurs by spontaneous dissociation of specific dislocation defects presented in the parent phase, while the growth progresses autocatalytically at the adjacent defects on freshly formed bainitic ferritic sub-units without any diffusion. The individual mechanisms are controlled by the rate of bainitic ferritic nucleation with respect to the driving force and mobility of alloys caused by partitioning. In steels containing the alloying elements such as Cr, Mo, and B, the reaction can be separated C-curve nature of the TTT diagram at which the characteristic flat top of bainite at a temperature of T_h appears (illustrated in **Fig. 2**). This indicates the highest temperature where ferrite can form by a displacive mechanism. However, the nucleation reaction of Widmanstätten ferrite and bainite possesses the same mechanism, opposing the growth mechanism. The same nucleus can develop into either phase based on the available thermodynamic conditions.

1.1.3. Incomplete reaction phenomenon

In displacive manner, bainite starts with paraequilibrium nucleation and grows without carbon diffusion. The bainitic growth arises soon after carbon supersaturated from bainitic ferrite is rejected into the residual austenite. The residual austenite enriched with carbon defines a characteristic of diffusionless growth that the transformation of bainite would never reach its equilibrium. On the Fe-C phase diagram (**Fig. 6**), the T_0 curve is the locus of all points where the austenite and ferrite of the same composition have identical free energy. This curve lies between ferrite and austenite phase boundaries. Ae_1 refers to the $(\gamma + \alpha)/\alpha$ phase boundary and Ae_3 refers to the paraequilibrium phase boundary of $(\gamma + \alpha)/\gamma$. A plate of bainitic ferrite grows by diffusionless of carbon as any excess of carbon from the supersaturated bainitic ferrite plate is rejected into the residual austenite. The next plate is thus forced to grow from carbon-enriched austenite. This process can continue until the mean carbon concentration of steel reaches the carbon concentration of the residual austenite at T_0 locus. Therefore, the decomposition of austenite into bainite caused by the carbon enrichment can only take place below the T_0 curve. The T'_0 curve has the similar meaning, but it takes into account the strain energy term of ferrite due to shape change in the growth process [26,27]. Regarding shape deformation, the elastic strain component caused by the IPS is accommodated in the residual austenite. The strain energy associated with the deformation is estimated to be about 400 J/mol, which is higher than that for Widmanstätten ferrite (~200 J/mol) but lower than martensite (~600 J/mol).

The transformation of bainite follows that the maximum amount of bainite can be achieved at any temperature by the fact that the carbon concentration of retained austenite must be lower than the T'_0 curve. Hereby, the transformation incompletes as it is expected to fall between austenite and ferrite. The incomplete reaction phenomenon was initially introduced by Zener [28] and modified by Aaronson et al. [25]. The transformation of austenite under such a phenomenon explains why the degree of transformation to bainite is zero at the B_S temperature and increases with undercooling below the B_S temperature of steels. A benefit of the T'_0 curve is allowing the design of advanced high strength bainitic steels which comprises mainly bainitic ferrite with a certain amount of retained austenite [29]. The schematic illustration of the T_0 and the modified T'_0 curves are shown in **Fig. 7**. According to this concept, Takahashi and Bhadeshia [30] proposed that there are three possibilities for steel design to achieve the maximum amount of bainitic ferrite: by

adjusting the T'_0 curve to greater carbon concentration by controlling the average carbon concentration and by minimizing the transformation temperature. These strategies are based on the following relationship:

$$V_{\alpha\text{BF}}^{\text{max}} = \frac{x_{T'_0} - \bar{x}}{x_{T'_0} - x_{\alpha\text{BF}}} \quad (1)$$

where $x_{T'_0}$ is the molar carbon concentration of the residual austenite given by the T'_0 locus, \bar{x} is the mean carbon concentration in steel, and $x_{\alpha\text{BF}}$ is the molar carbon concentration of bainitic ferrite. However, this condition is feasible if the following two thermodynamic conditions are met below the T'_0 temperature.

$$\Delta G_{\text{m}} < G_{\text{N}} \text{ and } \Delta G^{\gamma \rightarrow \alpha} < -G_{\text{SB}} \quad (2)$$

where the first condition describes nucleation of bainite. ΔG_{m} is the maximum molar Gibbs free energy change for the bainitic nucleation, G_{N} is the universal nucleation function depending on a dislocation mechanism associated with martensite nucleation [31,32]. The term G_{N} depends on the transformation temperature and chemical composition. The second condition describes the limit to the growth of bainitic ferrite formation. $\Delta G^{\gamma \rightarrow \alpha}$ is the free energy change accompanying the decomposition of austenite without any change in chemical composition. G_{SB} is the stored energy of bainite that considers the strain energy due to invariant plane strain shape changes accompanying the growth of bainitic ferrite [27].

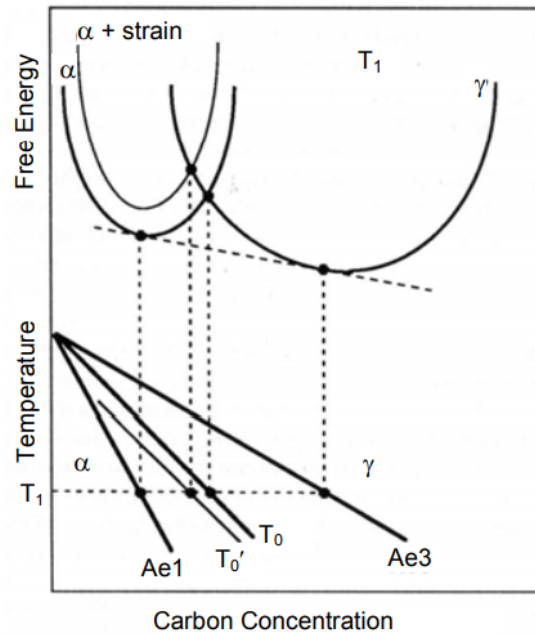


Fig. 6 Schematic illustration of the origin of the T_0 construction on the Fe-C phase diagram. The T_0' curve represents T_0 which takes into consideration of the strain energy term of ferrite [25].

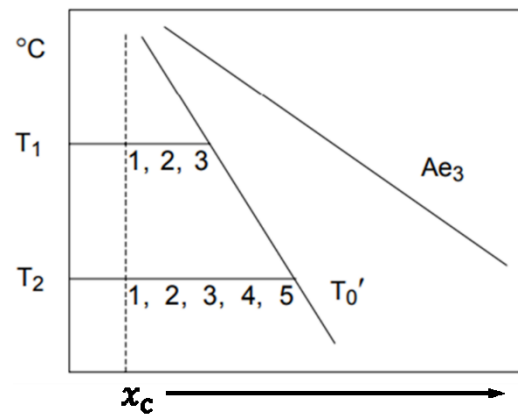


Fig. 7 Illustration of the incomplete reaction phenomenon. A plate of bainitic ferrite grows without diffusion, then partitions its excess carbon into the retained austenite. The next plate is stimulated to grow from carbon-enriched austenite, starting from the bulk carbon concentration x_c and through points 1,2,3,...,5 [29].

1.1.4. Developments of low carbon carbide free bainitic steel and heat treatments

In the early stage of bainitic steels developments, Edmond and co-workers [11,33–35] show that carbide-free bainitic steels are an ideal microstructure. Instead of the microstructure combined between bainitic ferrite laths and interlaths of carbide, it comprises bainitic ferrite laths embedded

in thin films of untransformed retained austenite. The steel reveals a relatively impressive high resistance to cleavage fracture and void formation owing to the absence of the precipitates of carbide. Moreover, developing such a microstructure can simultaneously improve the strength and further enhance the ductility by TRIP effect. Based on original experiments conducted by Bhadeshia and Edmond [11], they highlight the role of the T'_0 curve in greatly influencing the mechanical properties of carbide-free bainitic steels. Nevertheless, the experimental alloys designed for their work are not optimum for mechanical property improvement. Afterward, Caballero et al. [36,37], design alloys based on the concept of T'_0 curve to obtain a bainitic microstructure with a satisfied hardenability after forging and subsequent air cooling. The hardenability is achieved by alloyed 3.5Ni-1.4Cr-0.1V (wt.%), while the addition of 1.5 wt.%Si suppresses the precipitation of cementite during bainitic transformation. The minimum strength of about 1100 MPa is reached when 0.3 wt.%C is added to the two designed steels. The steels are forged to a thickness of 25 mm at an austenitizing temperature of 950°C before air cooled to room temperature. Desired microstructure consisting of bainitic ferrite and film-like retained austenite achieves toughness values of nearly 130 MPa/m^{1/2} and strength in the range of 1500-1700 MPa. Recently, Wirth [38] adjusted alloys by lowering carbon to 0.18 wt.%C with Mn of about 2.5 wt.% for hardenability and B of 0.0018 wt.% to retard bainitic reaction. Minimized Si concentration to ~1 wt.% is found to sufficiently suppress carbide formation during the bainitic reaction, conducted in three different processing routes, as shown in **Fig. 8**. The first processing route (**Fig. 8a-I**) is that the steel is forged at a high temperature above A_{c3} temperature, then cooled to room temperature. For the second route (**Fig. 8a-II**), the forged steel is cooled at a controlled rate immediately after austenitizing heat treatment. In the other route, the forged steel is austenitized at a temperature above A_{c3} temperature similar to the first and second routes then cooled to a temperature in the bainitic regime above M_s prior to isothermally transform into bainite according to **Fig. 8a-III**. The microstructures obtained from these processing routes (**Fig. 8b**) show that the steel processed by isothermal tempering at 400°C for 1 hr. provides a better suppression of fresh martensite formation and balance in strength and ductility ranged of 1000-1200 MPa and 8-12%, respectively. However, the large amount of small fresh martensite remains an issue for further development since it limits the range of ductility with the initiation of damage at the early stage of the deformation.

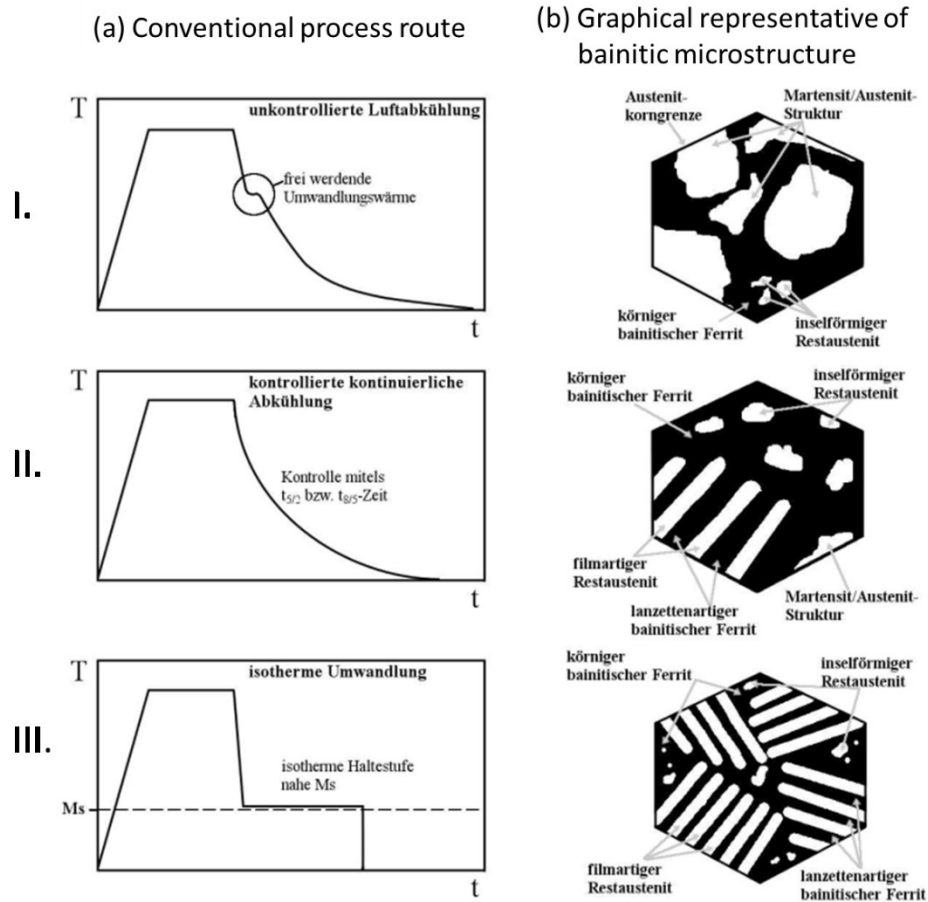


Fig. 8 (a) conventional process routes for bainitic forged steel (b) graphical representative of bainitic microstructure comprising bainitic ferrite, retained austenite, and fresh martensite in the form of martensite in retained austenite (M/A) [38].

Also, Buchmayr [39] suggests that from the optimal mechanical properties point of view, isothermal heat treatment offers a better reduction of fresh martensite with appropriate balance in bainitic ferrite and retained austenite fractions. **Fig. 9** shows that the strength and ductility of carbide-free bainitic steels, which lie above comparable other commercial grades, can be improved by adjusting alloys and optimal process parameters of isothermal heat treatment.

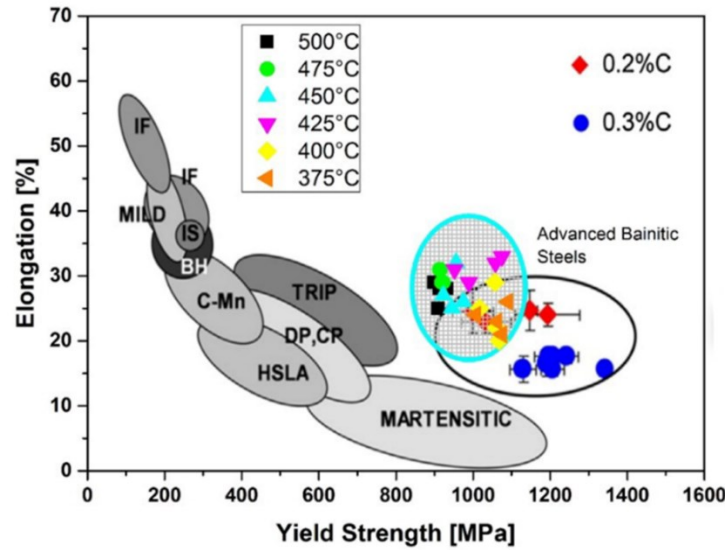


Fig. 9 Yield strength and total elongation of advanced bainitic steels compared with other commercial automotive steels [39].

1.1.5. Thermodynamic stability of austenite

Austenite or gamma phase configured with face-centered cubic (FCC) structure is considered a common phase in the Fe-C phase diagram, being stable at high temperatures above the recrystallized temperature. While cooling, austenite can be decomposed into other phases due to structural instability. The resistance of austenite against transformation during temperature changes is referred to as its thermodynamic stability, characterized by any change in phase transition temperatures [40]. Apart from that, the most essential evaluation of the thermodynamic stability of austenite is the variation of martensite start temperature.

Carbon is known as the most effective element that can either expand or restrict the austenite (γ) phase region in the equilibrium phase diagram. Moreover, alloying elements such as nitrogen (N), manganese (Mn), and nickel (Ni) are classified into those that expand the γ -field by decreasing the A_4 temperature and deviating the A_3 temperature, which is the ferrite phase field. **Fig. 10** shows the enthalpy difference of alloying elements in austenite and ferrite calculated from the following equations.

$$\Delta G^{\gamma \rightarrow \alpha'} = (1 - x)\Delta G_{Fe}^{\gamma \rightarrow \alpha'} + x\Delta H^{\gamma \rightarrow \alpha'} \quad (3)$$

$$\Delta H = H_\gamma - H_\alpha \quad (4)$$

Negative values of the latent heat of transformation for the allotropic $\gamma \rightarrow \alpha$ transformation result in an increase of the A_4 temperature and a decrease in the A_3 temperature [41]. These values are responsible for an expansion of the γ -phase field. In contrast, positive values of the heat transformation for the allotropic $\gamma \rightarrow \alpha$ transformation of the latent heat for the $\gamma \rightarrow \alpha$ transformation cause a decrease in the A_4 temperature and an increase in the A_3 temperature, thus corresponding to a reduction of the γ -phase field. The negative values are indicators of the relative strength of an element as austenite-former elements, while the positive values are indicators of ferrite-former elements.

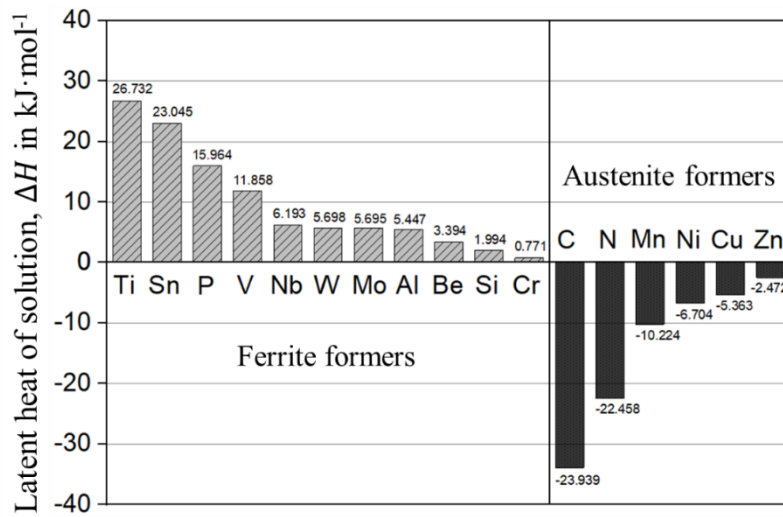


Fig. 10 Relative strength of various alloying elements acting as ferrite-or austenite formers [41].

The start temperatures of bainite and martensite are good indicators for the thermodynamic stability evaluation. Several quantitative investigations have been conducted to determine the relationship between the alloying element additions and the variation of those critical temperatures. Based on such a relationship, many empirical equations have been proposed to predict the B_s and M_s temperatures. However, these temperatures depend not only on the chemical composition of steel but also on the prior austenite grain sizes (PAGs). It has been found that the B_s temperature decreases with increasing carbon content, some alloying elements, and decreasing the PAGs. An empirical equation proposed by Kang et al. [42] taken into consideration of alloying addition and PAGs is presented as follows.

$$B_s(^{\circ}\text{C}) = 634.8 - 193.1C + 102.4C^2 - 31.2Mn - 4.6Si - 18.6Ni - 32.4Cr - 15.6Mo + 10.36 \cdot \ln(d_\gamma) \quad (5)$$

where d_γ is the PAGs in μm . Similarly, a decrease in the M_s temperatures were represented by an empirical equation proposed by Arlazarov et al. [43].

$$M_s(^{\circ}\text{C}) = 565 - 27Mn - 7Si + 10Al - 16Cr - 600 \cdot [1 - e^{-0.96C}] - 90(d_\gamma)^{-1/3} \quad (6)$$

He [44] compiled intrinsic and extrinsic factors that delay phase transformation temperatures expressed in terms of thermodynamic resistance. All factors that resisted phase transformation are directly associated with the strength of austenite grains, which depends upon heat treatment and chemical composition. As known, the strengthening of austenite increases with decreasing PAGs according to the concept of the Hall-Petch relationship [45]. PAGs in the range from 6 to 185 μm , obtained by varying austenitizing temperatures or applying cyclic heat treatments after austenitization, were studied by Casero et al. [46]. The result of grain refinement not only shifts the M_s temperature to lower values but also accelerates the transformation at the initial stage due to the increased density of nucleation sites.

With respect to displacive transformation, the growths of martensite, bainite, and Widmanstätten ferrite are accompanied by a change in the shape of the transformed region. A change is described by the IPS with a large shear component [47]. When the transformation occurs at a temperature where the shape change cannot be accommodated elastically, the plastic deformation driven by the shape change causes the accumulation of dislocations in austenite and their product phases. The creation of dislocation debris in the austenite then resists further progress of the transformation by a phenomenon known as mechanical stabilization of austenite [48–50]. Later, Chatterjee et al. [51] derived an equation to elucidate this phenomenon that occurs when the stress driving the interface and the opposing stresses are equivalent. The equation can be used to estimate the critical strain that is satisfied for mechanical stabilization.

$$b\Delta G_{\text{ch}} = \frac{1}{8\pi(1-\nu)} G_\gamma b^{3/2} \left(\frac{\varepsilon}{L}\right)^{1/2} + \tau_s b \quad (7)$$

where b is the Burgers vector, ΔG_{ch} is the chemical driving energy change of the transformation. It is a function of temperature and the chemical composition of steel. ν is the Poisson ratio, G_γ is the shear modulus of austenite, ε/L is the aspect ratio of the austenite grain, and τ_s is the critical

shear strain for the transformation. Pickering [52] determined the dislocation density accumulated in these phases. It mainly depends on the transformation temperature. Garcia-Mateo et al. [53] then conducted an X-Ray line profile analysis to estimate dislocation density based on a change in lattice strain. The dislocation density conducted by this analysis increases due to increasing isothermal tempering temperatures for bainite, as shown in **Fig. 11**. The specimen after isothermally heat-treated at 200, 300, and 450°C had dislocation densities of 8.8×10^{15} , 2.1×10^{15} , and $1.4 \times 10^{14} \text{ m}^{-2}$, respectively.

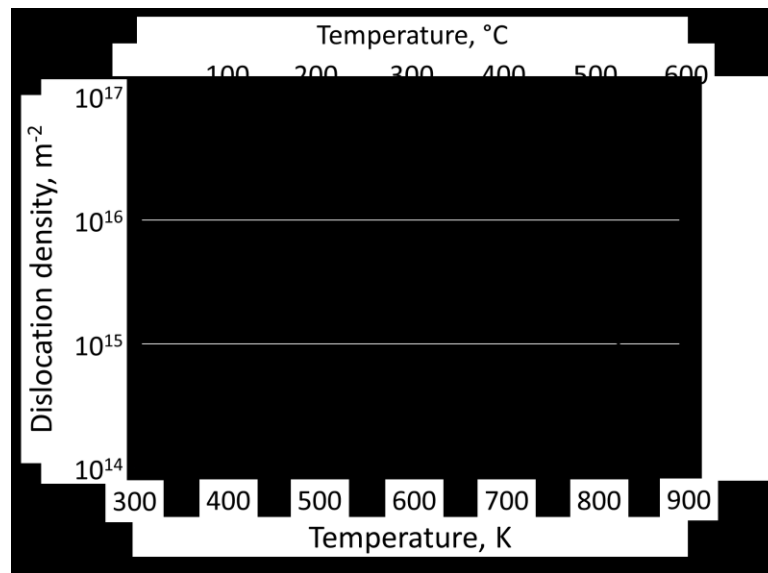


Fig. 11 Dislocation density as a function of transformation temperature obtained from XRD line profile analysis [53].

In terms of microstructural features, retained austenite as a product of the carbon enrichment during the austenite decomposition usually forms in two types of morphology, including film-like/thin-film and blocky/granular types, respectively, as depicted in **Fig. 12**. The thermodynamic stability of the austenite reflects the formation of these features during heat treatment since their carbon contents are somewhat different from each other. Increasing mean carbon content in steel improves the thermodynamic stability of the austenite against martensitic transformation, leading to a more fraction of film-like retained austenite after the heat treatment operation. Sugimoto et al. [54] also found that apart from carbon concentration, film-like retained austenite is influenced by more hydrostatic pressure from adjacent phases, unlike in the blocky type. Based on an experiment of Caballero et al. [55], changes in mean carbon concentration in low alloy steels provide an

explicitness that low carbon steels have a much more blocky type of retained austenite than medium and high carbon steels. It is owing to low carbon enrichment in austenite grain.

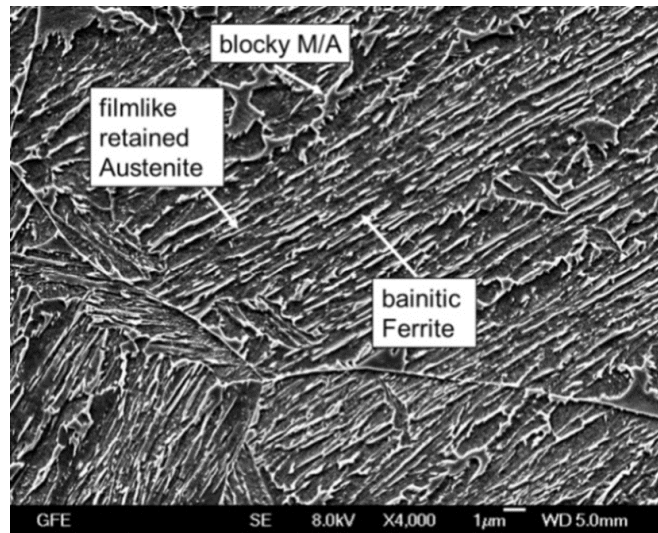


Fig. 12 (a) SEM micrograph of a specimen isothermally treated at 375°C for 15 min after austenitized at 950°C, showing microstructure of bainitic ferrite, with minority of blocky martensite/austenite (M/A) and film-like retained austenite [56]

The presence of either film-like or blocky-type is mostly dependent on the rate of carbon enrichment in the austenite and local carbon content, which is entrapped within retained austenite and its surrounding phases [57]. According to atom probe tomography (APT) measurement shown in **Fig. 13a**, Caballero et al. [58] found that both film-like and blocky-type entrapped between bainitic ferrite/retained austenite interface have different carbon concentrations. Carbon concentration profiles obtained from APT reveal that the nano-scale film-like retained austenite has a greater carbon content than the sub-microscale blocky type due to higher defect density, which induces more carbon enriched in untransformed austenite during isothermal tempering at 400°C (**Fig. 13b**).

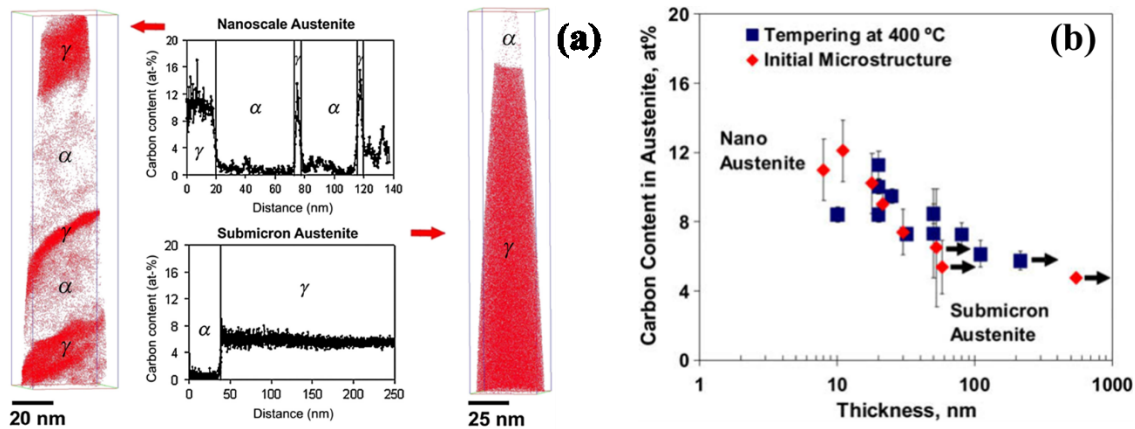


Fig. 13 (a) Carbon atom maps obtained from atom probe tomography (APT) measurement and corresponding concentration profiles across austenite-bainite interfaces for nano-scale film and sub-microscale blocky retained austenite, (b) carbon content in austenite measured by APT as a function of the thickness of the analyzed austenite regions in the initial microstructure and after tempering at 400 °C [58].

1.1.6. Ausforming heat treatment

Ausforming is a thermo-mechanical heat treatment process that combines a prior plastic deformation of austenite with a typical heat treatment process, either control cooling or isothermal tempering. A general consequence is to improve strength without deteriorating ductility. The deformation reduces the effective grain size of austenite, leading to more refined final microstructures [59]. The microstructural refinement gives two prospects for the mechanical property development of bainitic steels [60]. The strength is controlled by the refined bainitic ferrite thickness and the accumulated dislocation density, whereas ductility is mainly occupied by retained austenite fraction. The fraction of retained austenite is simply evaluated by the transformability of retained austenite during plastic deformation or TRIP effect. Chen et al. [61] investigated phase transformation behavior and microstructural change in medium carbon steel comprised of 0.43C-1.90Si-2.83Mn-0.57Al-0.06Cu (wt.%) affected by ausforming. After plastically deformed with a strain of 0.2 at a strain rate of 1 s^{-1} , the kinetics of austenite decomposition into bainite is accelerated during isothermally treated at 573 K for 60 min but ceased much earlier when compared with the specimen treated without ausforming (see in **Fig. 14a and b**). The cessation is overwhelmed by dislocation-induced mechanical stabilization of austenite. The effect of mechanical stabilization leads to a drastic increase in retained austenite

volume from 7% to 23%, with a much reduction of fresh martensite formation from 38% to 13.5%. Owing to a benefit in shortening the onset of bainitic transformation, ausforming has been utilized mostly in high carbon ($>0.5\text{C}\%$ wt.) and medium carbon (0.3 to $0.5\text{C}\%$ wt.) steels. Because the decomposition of austenite into bainite is generally time consuming in those materials [62–64]. Two major outcomes were found during ausforming. Firstly, more defects introduced into austenite provide available nucleation sites for subsequent phase transformation. The substantial nucleation sites enhance the free energy change for the bainitic transformation, thus accelerating the nucleation process. Secondly, the maximum fraction of bainitic ferrite is reduced due to the high dislocation density accumulated within the austenite matrix during the bainitic transformation progress, referred to as the mechanical stabilization of austenite. Recently, many research efforts have conducted experimental validations by considering the influence of processing parameters, such as strain, strain rate, and temperature, on changes in the kinetics behavior of bainitic transformation. For instance, Fan et al. [65] performed ausforming experiments at the deformation temperatures of 700°C , 600°C , and 300°C with strains upon 50%. Bainitic ferrite fraction increases with decreasing the deformation temperature, whereas ausforming conducted at 300°C with various strains shows significant outcomes. An increase in ausforming strain accelerates the kinetics of transformation and then promotes the total fraction of bainitic ferrite. In contrast, it increases the fraction of blocky retained austenite while reducing the amount of film-like retained austenite. A similar approach was carried out by Hu et al. [66,67], but the fraction of bainitic ferrite reduces, and that of retained austenite increases when the plastic strain increases. Chen et al. [68] evaluated the influence of ausforming strain rate on the kinetics transformation behavior of bainite, and it shows a slight difference in the kinetic evolution when increasing the strain rates (from $0.01\text{--}5\text{ s}^{-1}$) at a constant temperature at 400°C . But there is a critical strain rate, which is 1 s^{-1} providing the maximum retained austenite fraction of 35% by volume with a carbon concentration of 0.75%. The carbon concentration in retained austenite of ausformed material lies in between para-equilibrium T_0 and equilibrium A_{c3} loci and even higher than isothermally treated material [66]. However, there is no clear conclusion on the kinetics transformation and microstructural evolution for this range of carbon steels. In terms of mechanical properties, an excellent comprehensive mechanical property of the steel with an ultimate tensile strength value of 1850 MPa and total elongation of 23% is achieved in the ausformed 0.7%wt.C steel [69]. The improved tensile strength is attributed to the volume fraction of 68.3% of nanostructure bainitic ferrite with a

thickness of ~ 60 nm, while the extended elongation is contributed by 34.2% of retained austenite with a considerable reduction of its blocky size to ~ 0.28 μm . Apart from that, the increase in the proportion of film-like retained austenite and decrease in the block size is associated with an almost parallel alignment of bainitic ferrite grains and a decrease in number of variants in a single austenite grain [70]. In low carbon steels, Zhao et al. [71] explore the possibility of producing superfine bainitic ferrite structure with improved mechanical properties in a 0.15C-1.41Si-1.88Mn (% wt) steel. A great balance in mechanical properties with an ultimate tensile strength of 1650 MPa and engineering strain of 0.28 is achieved when plastic deformation of austenite was conducted at temperatures below M_S temperature. However, the ductility of the steel ausformed at a temperature above M_S temperature needs to be improved due to a presence of a large amount of brittle fresh martensite. Although the approach of improving the mechanical property of low-carbon steel is proposed, other contributing factors to the microstructure development, including thermodynamics of transformation, and dislocation density, are not considered.

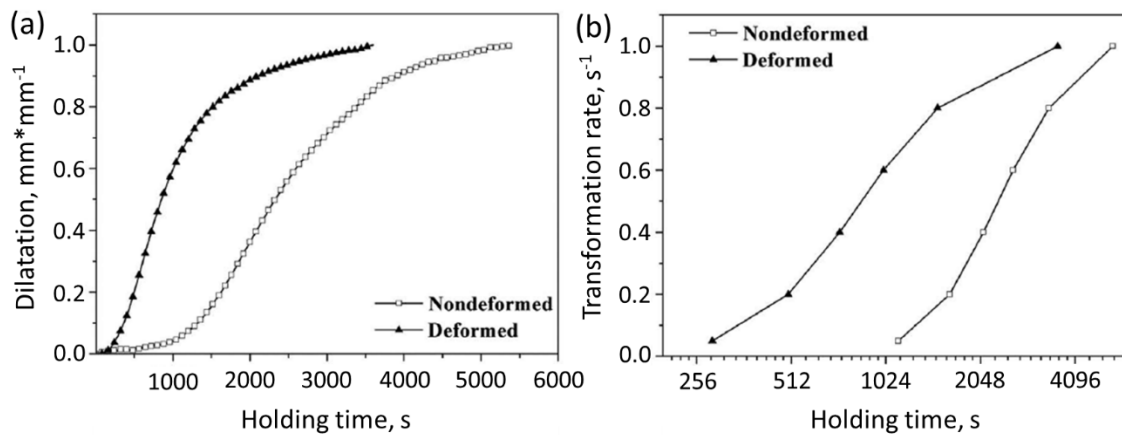


Fig. 14 (a) Dilatation change versus time during isothermal bainitic transformation at 300°C, and (b) transformation rates in non-ausformed and ausformed specimens, showing a much faster kinetics of bainite transformation after a plastic deformation of austenite at a strain of 0.2 [61].

1.1.7. Analysis of crystallographic arrangement

Based on the crystallographic relationship between face-centered cubic (fcc) and body-centered cubic (bcc) systems, the parallelism of their crystallographic planes and directions can be theoretically described through the most common four major orientation relationships (OR) models: Bain OR [72], Kurdjumov-Sachs (K-S) OR [73], Nishiyama-Wassermann (N-W) OR

[74,75], and Greninger-Troiano (G-T) OR [76]. These OR are listed in **Table 1**. The Bain OR was first proposed in 1924 to explain the martensite transformation in carbon steel in terms of a simple set of orthogonal strains that would transform the austenite lattice directly to the martensite lattice. It is now well known that Bain distortion alone is insufficient to describe the martensitic transformation in carbon steels [77], and the Bain OR is not observed for martensite in these alloys. However, it is found that the Bain OR has been observed in Fe₃Pt martensite and Fe₃Al-C martensite [78] but has never been reported for ferrite and austenite microstructure. The K-S and N-W ORs are the most frequently reported relationships for fcc-bcc systems, including martensite in steels, and they are the only ones reported for austenite-ferrite microstructures. These two relationships differ from each other by a small relative rotation of 5.26 deg. The G-T OR is reported for martensite in steel containing 0.8%C-22%Ni. It always lies between the K-S and N-W ORs, which are separated by approximately 2.5 deg. from the N-W OR.

Table 1 four commonly used orientation relationship models for face-centered cubic (fcc) to body-centered cubic (bcc) transformation.

OR	Plane	Direction
Bain	$\{010\}_\gamma \parallel \{010\}_\alpha$	$\langle 001 \rangle_\gamma \parallel \langle 101 \rangle_\alpha$
Kurdjumov-Sachs	$\{111\}_\gamma \parallel \{110\}_\alpha$	$\langle 110 \rangle_\gamma \parallel \langle 111 \rangle_\alpha$
Nishiyama-Wassermann	$\{111\}_\gamma \parallel \{010\}_\alpha$	$\langle 011 \rangle_\gamma \parallel \langle 001 \rangle_\alpha$ or $\langle 112 \rangle_\gamma \parallel \langle 110 \rangle_\alpha$
Greninger-Troiano	$\{111\}_\gamma \sim 1^\circ \parallel \{110\}_\alpha$	$\langle 12,17,5 \rangle_\gamma \parallel \langle 17,17,7 \rangle_\alpha$

For bainitic steels, Tari et al. [79] analyzed pole figure obtained Electron BackScatter Diffraction (EBSD) technique and found that the OR between bainitic ferrite and retained austenite is strongly dependent on isothermal temperature. At high temperature of about 350-450°C, the OR between parent and daughter phases is closed to N-W OR with twelve variants, while it is closed to K-S OR with twenty four variants when the transformation is employed at low temperatures below 200°C. The closest orientations to N-W and K-S ORs are confirmed by Suikkanen et al. [80] and Hu et al. [81]. However, not wholly N-W and K-S ORs are observed in bainitic steels. As shown in **Fig. 15**, a few variants are identified as K-S OR, while other variants are closely related to the N-W relationship. They claimed that the multiple ORs might be attributed to the accommodation of transformation strain associated with the bainitic transformation.

From the EBSD result, the inverse pole figure (IPF) image showed that the prior austenite grain is divided into several packets that consist of one or more blocks. Each block contains few bainitic ferrite laths and retained austenite with a similar orientation, as shown in **Fig. 16**. When the transformation of bainitic ferrite is conducted at a high temperature above 350°C, Beladi et al. [82] showed that the microstructure becomes coarsen and the formation of crystallographic variants becomes smaller. The strong variant selection is obtained due to a presence of high dislocation density in bainitic ferrite. This evidence is attributed to the plastic strain formed during the bainitic transformation.

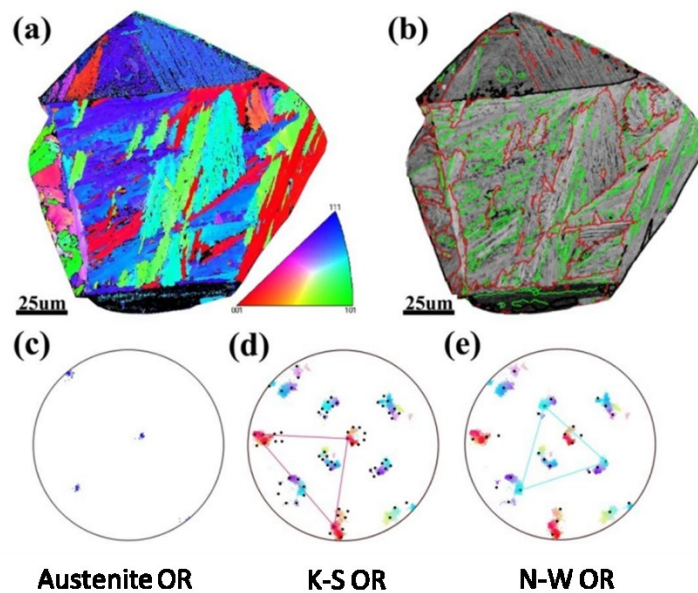


Fig. 15 (a) Inverse pole figure (IPF) map of BF in the region of ~0.38 wt.% C, which was transformed at 410 °C. (b) band contrast image overlaid with grain boundaries indexed as block (green) and packet (red). (c) $\{100\}_\gamma$ pole figure, with blue dots showing experimental orientation of austenite. (d) and (e) $\{100\}_\alpha$ pole figure, with the black dots showing poles predicted by (d) K-S and (e) N-W orientation relationship [81].

Recently, Wang et al. [83] analyzed area fraction distributions of misorientation angles of two multiphase steels with different Ni contents, namely 0.080C-2.43Ni (Low Ni) and 0.074C-4.29Ni (High Ni) steels. These steels have three structural components (bainite, martensite, and retained austenite), and only martensite and bainite share similar crystallographic orientations. According to the distributions of misorientation angles shown in **Fig. 17a**, the misorientation angle of

martensite/bainite boundaries and retained austenite is about 45° , while that of martensite and bainite grain boundary are about $50\text{--}60^\circ$ degrees. They interpret that the misorientation angles between bainite and prior austenite in the N-W relationship are approximately $53\text{--}54^\circ\langle 110\rangle$ and that between martensite and prior austenite in the K-S relationship is $60^\circ\langle 111\rangle$. However, there remained difficulty in discriminating between martensite and bainite structures by these angles. Therefore, they continue using image quality (IQ) values to resolve this complication. By fitting the Gaussian distribution function with the IQ values, the threshold value between martensite and bainite is obtained by the intersection point between the martensite and the bainite, represented by green, and red curves, respectively (**Fig. 17b**).

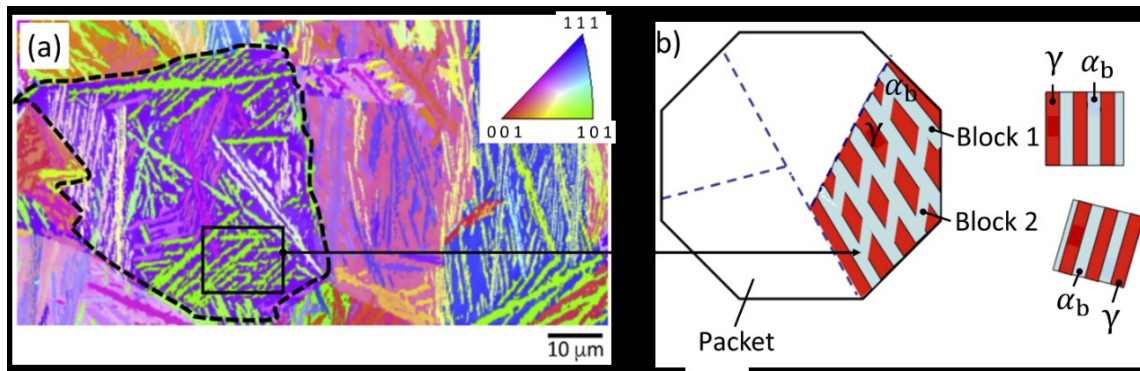


Fig. 16 (a) IPF-EBD image of fully bainitic microstructure formed at 350°C isothermal temperature, and (b) Schematic representation of bainitic ferrite and retained austenite arrangement in a given parent austenite grain [82].

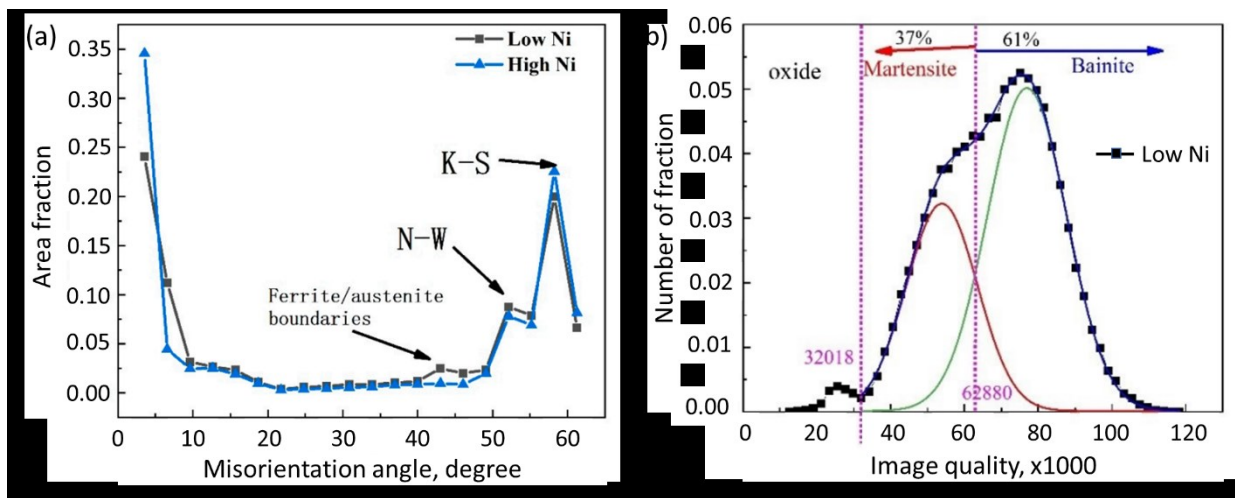


Fig. 17 (a) Area fraction distributions of misorientation angles of $0.080\text{C}\text{--}2.43\text{Ni}$ (Low Ni) and $0.074\text{C}\text{--}4.29\text{Ni}$ (High Ni) steels, and (b) a Gaussian distribution curve of image quality (IQ)

values for Low Ni steel, analyzed to quantify the volume fraction of bainite and martensite by thresholding method [83].

1.1.8. Impact of microstructure on mechanical properties

➤ Strengthening of a mixed structure of fresh martensite and bainitic ferrite

According to works dedicated by Bhadeshia [10], the strengthening of the mixed structures can be factorized into five components: the intrinsic strength of iron ($\Delta\sigma_{Fe}$), solid solution strengthening ($\Delta\sigma_{SS}$), precipitation ($\Delta\sigma_P$), dislocations ($\Delta\sigma_\rho$), and grain size ($\Delta\sigma_{GS}$). By adding up the values of these factors, the strengthening of bainitic ferrite can be estimated as follows.

$$\Delta\sigma_b = \Delta\sigma_{Fe} + \Delta\sigma_{SS} + \Delta\sigma_P + \Delta\sigma_\rho + \Delta\sigma_{GS} \quad (8)$$

As shown in **Fig. 18a**, pure bcc iron in the fully annealed condition and substitutional solutes that do not partition during the growth of either martensite or bainitic ferrite formation are the major contribution of the strengthening of the steel. Kashyap et al. [84] proposed that the stress involving pure bcc iron can be calculated by Peierls–Nabarro equation.

$$\Delta\sigma_{Fe} = \frac{2G_\alpha}{(1-\nu)} \exp\left(\frac{-4\pi\zeta}{b}\right) \quad (9)$$

where G_α is the shear modulus of bcc iron, ν is the Poisson ratio, ζ is the half-width of the dislocation, and b is the Burgers vector. This stress represents the lattice friction stress required for the movement of edge dislocations from one position to another. Meanwhile, among various equations expressing the effect of the solid solution on the strengthening of alloyed steels, Kang et al. [85] proposed an equation covering the contribution of carbon (x_C), manganese (x_{Mn}), silicon (x_{Si}), and titanium (x_{Ti}).

$$\Delta\sigma_{SS} = 4570x_C + 37x_{Mn} + 83x_{Si} + 80x_{Ti} \quad (10)$$

Apart from that, **Fig. 18b** also shows estimated contributions by other factors. Precipitation strengthening is another beneficial mechanism, and the strengthening due to a uniform dispersal of spherical cementite particles is given by

$$\Delta\sigma_P \approx 0.52f_\theta d_P^{-1} \quad (11)$$

where f_θ is the volume fraction of the cementite, and d_P is the particle spacing. However, in bainitic steels, most of carbon is enriched into the residual austenite and remains in solution rather than precipitating as carbides.

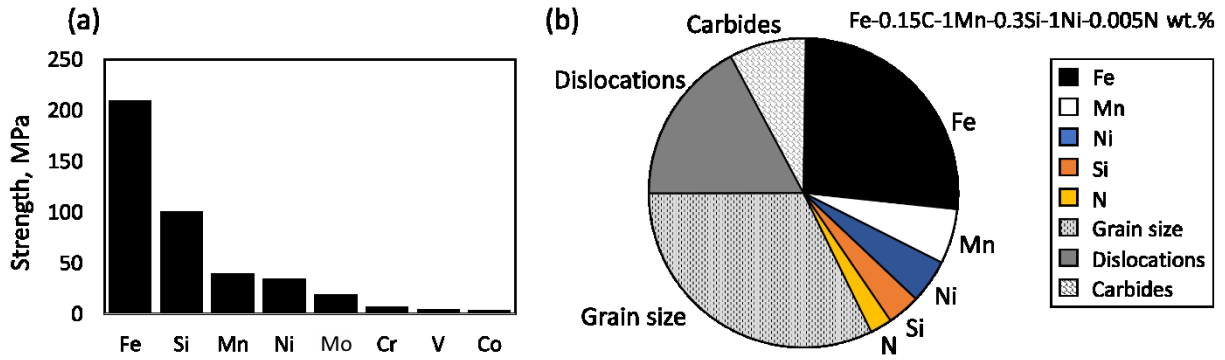


Fig. 18 (a) Typical solid solution strengthening contributions per wt.% of solute atoms in bainitic ferrite, (b) Estimated contributions to the strength of bainitic steel. The graphical illustration is modified from [10].

Since the diffusionless growth of both fresh martensite and bainitic ferrite causes the shape change of the transformed region, the plastic deformation that is driven by large shear components as the IPS generates the accommodation of dislocations in both phases. In this regard, Takahashi and Bhadeshia [86] found that the tendency for plastic accommodation is largely dependent on the transformation temperature. They suggested that although the equation was valid for most low alloy steels, the transformation temperature that would fit this equation should be lower than 370 K. Later, Young and Bhadeshia [87] conducted this investigation at higher temperatures and found that the dislocation density of composite structures increases with decreasing the transformation temperature. This correspondence with the increase in undercooling temperature.

An experimental validation proposed by Bailey and Hirsch [88] indicates that the strengthening of low alloy steels also depends on the chemical composition and volume fraction of phases. These factors must also affect the increased dislocation density in alloys. Thus, the strengthening caused by the contribution of dislocation density can be estimated using the following equation.

$$\Delta\sigma_p = M\alpha b G_\alpha \rho^{1/2} \quad (12)$$

where M is the Taylor factor, α is a constant depending on crystal structure, and ρ is the dislocation density, which forms by those factors. In terms of grain size, it is associated with the lath shape of fresh martensite and bainitic ferrite and could be described by the morphology of platelets. In low alloy steels, if the dimensional shapes of both structures are relatively small, the strengthening due to the fine lath size can be estimated by the mean values of the largest diameter of slip planes [89,90] and given by

$$\Delta\sigma_{GS} \approx 115L_3^{-1} \quad (13)$$

Where L_3 is the mean linear intercept corresponding to the thickness of the subjected plate.

➤ Strengthening of retained austenite

The resistance of retained austenite to transformation into fresh martensite upon deformation is referred to as its mechanical stability. It is a significant factor used to evaluate the mechanical response in multiphase steels. Pereloma et al. [91] summarized that the mechanical stability of retained austenite depends on various factors such as alloying elements, carbon concentration, retained austenite grain size, the nature of neighboring phases, orientation, and stress state. In this study, some factors relevant to the mechanical stability of retained austenite are reviewed as follows.

I. Effect of retained austenite grain size

According to a number of experimental studies, the mechanical stability of retained austenite is inversely related to its grain size. The retained austenite with small grain sizes is more stable than that with the coarser grains, which is unstable and prone to transform into fresh martensite at low strain. This feature provides only a limited contribution to the total ductility of steel. In contrast, although a majority of fine grain retained austenite is strongly beneficial to TRIP effect, very fine retained austenite grains may not transform into fresh martensite even at fracture and make themselves useless for TRIP effect. Timokhina et al. [92] analyzed the sensitivity of retained austenite grain diameter to the formation of fresh martensite at different stages of tensile deformation based on EBSD measurements. **Fig. 19** shows that retained austenite grains prior to tensile testing have an average grain size of up to 2 μm whereas the vast majority of the retained

austenite at fracture has sizes of less than $0.7\text{ }\mu\text{m}$. They concluded that the retained austenite grain size restricts the number of available nucleation sites for fresh martensite formation [93]. If the effect of chemical elements is not disregarded, the number of available nucleation sites is proportional to their surface area [94]. The very fine grains are prone to hinder the plastic accumulation accompanying the fresh martensite formation and control the interfacial energy of fresh martensite.

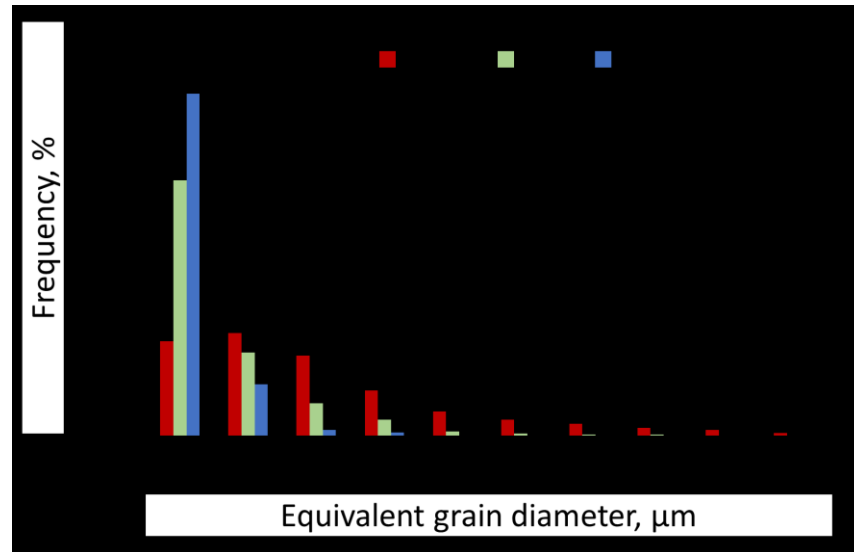


Fig. 19 Effective grain diameter of retained austenite measured at different tensile deformation stages [92].

II. Effect of neighboring phases

The effect of neighboring phases on the mechanical stability of retained austenite is examined in carbide-free bainitic steels and dual-phase TRIP steels by Sugimoto et al. [54]. The retained austenite grains located between polygon ferrite grains are less stable and are being transformed at a small strain, then leaving some retained austenite with coarse grains untransformed. Likewise, the retained austenite located between very fine layers of bainitic ferrite laths is more stable, resulting in a remaining some fraction of retained austenite after fracture. They concluded that the size of retained austenite is likely similar to that of bainitic ferrite. With this expression, Radcliffe and Schatz [95] described that if the surrounding phase is hard, it exerts hydrostatic pressure on the retained austenite. The factors affecting the hydrostatic pressure are correlated by the following equation.

$$\sigma_{\text{hydro}} = \frac{2}{3} \left(\sigma_{y0} + 2 \frac{\Delta\sigma}{\Delta\varepsilon} \varepsilon_p \right) + \frac{2}{3} \sigma_{y0} \ln \left(\frac{E^\alpha \varepsilon_p}{(1-\nu)\sigma_{y0}} \right) \quad (14)$$

where σ_{y0} and $\frac{\Delta\sigma}{\Delta\varepsilon}$ are the yield stress and the work hardening rate of the surrounding retained austenite matrix, respectively. E^α is the elastic modulus of bainite and martensite structures, and ε_p is the plastic strain. Sugimoto et al. [54] also reported that the much higher stability of retained austenite film located between the bainitic ferrite laths has a much higher σ_{hydro} value than the lower stability of blocky retained austenite located between granular bainitic ferrite matrix. However, if the retained austenite is in contact with fresh martensite or a strong bainitic ferrite matrix, the direct propagation of stress to the retained austenite will raise the total driving force of the austenite to transform into fresh martensite.

III. Effect of retained austenite orientation and stress state

As reported by Wang et al. [96], the orientation-dependent mechanical stability of retained austenite is defined by the Schmid factor, which relates the maximum resolved shear stress with respect to the loading direction. In **Fig. 20(a) and (c)**, the different shades of green embedded within the bainitic ferrite matrix show Schmid factor distributions in the 0.25C-4Mn-1.88Al-0.6Si specimens before and after tensile deformation, respectively. It is clear by the Schmid factor histogram, shown in **Fig. 20(b) and (d)**, that before the deformation, most of the retained austenite has Schmid factor greater than 0.4, in contrast to the others after fracture most of the Schmid factors of the remaining grains shift to smaller values around 0.3. This means the retained austenite grains with high mechanical stability have small values of the Schmid factor. It can also be noted that most granular or blocky grains of retained austenite presented in the fractured specimen exhibit high mechanical stability, whereas the elongated grains have low mechanical stability.

Also, to account for the effect of retained austenite and ferrite grain orientations on the tensile loading, a micromechanical model proposed by Tjahjanto et al. [97] shows the evolution of transformation of grains of retained austenite in different orientations to the martensitic transformation. As illustrated in **Fig. 21a**, they given that the cubic structure of a TRIP steel consisting of 27 grains of retained austenite evenly distributed in a ferrite matrix composed of 81 grains is subjected to uniaxial tensile load at a rate of 10^{-3} s^{-1} . The results (in **Fig. 21b**) show that orientations of the retained austenite and ferrite grains play a vital role in the transformability of

retained austenite during tensile loading. Regardless of the orientation of ferrite grains, the specimens containing $[1\ 0\ 0]_A$ -loaded austenitic grains transform relatively slowly compared to those with $[1\ 1\ 1]_A$ -loaded austenitic grains. This means any grains of retained austenite oriented in $[1\ 0\ 0]_A$ possesses high mechanical stability than those oriented in the other planes.

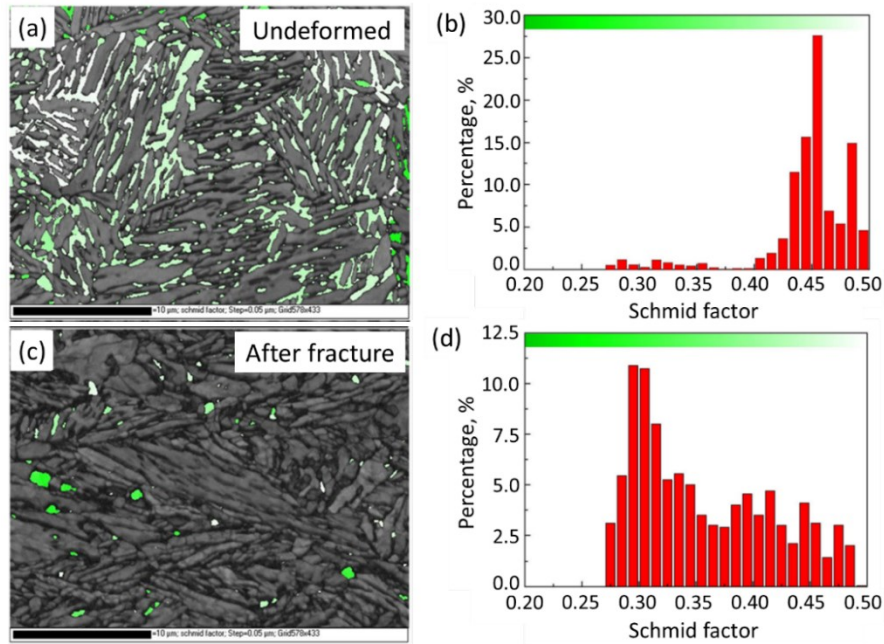


Fig. 20 (a), (c) Schmid factor distribution map and (b), (d) corresponding statistical data of Schmid factor distribution of retained austenite grain analyzed by EBSD: (a), (b) undeformed specimen and (c), (d) fractured specimen of 0.25C-4Mn-1.88Al-0.6Si steel [96].

Regarding the macroscopic stress state, the influence of the different loading paths on the mechanical stability of retained austenite is analyzed by Shan et al. [98]. **Fig. 22** shows the volume fraction of retained austenite dependent on effective strain under different loading paths, such as simple shear, uniaxial tension, plane strain, and equibiaxial stretching. These results imply that retained austenite under equibiaxial stretching is drastically sensitive to transformation into fresh martensite while straining contrast to that under simple shear, which is partially transformed during the deformation. This is because the equibiaxial stretching possesses higher stress triaxiality and promotes martensitic transformation.

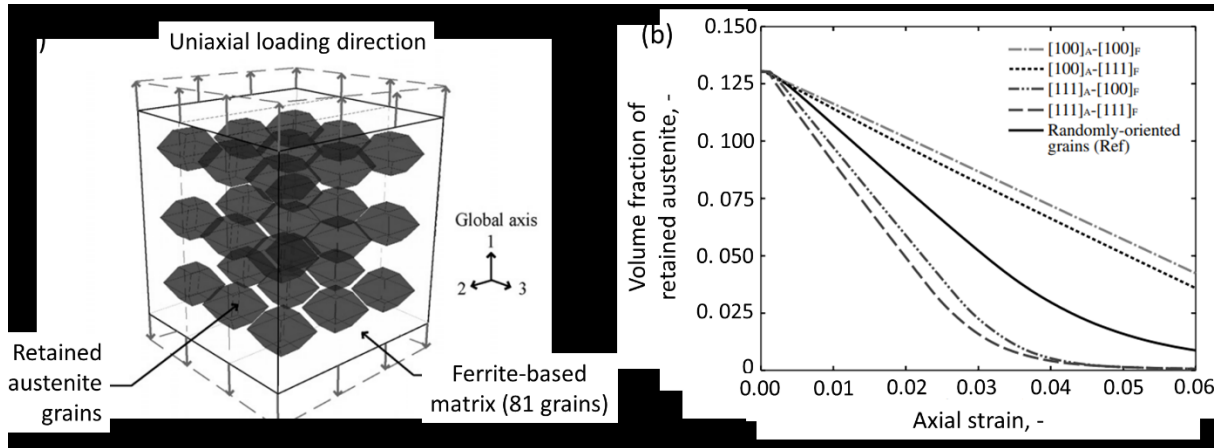


Fig. 21 (a) a micromechanical model representing the microstructure of TRIP steel, and (b) evolution of transformation of retained austenite grains as a function of axial strain. The microstructure consists of 37 grains of retained austenite embedded in a matrix of 81 grains of ferrite [97].

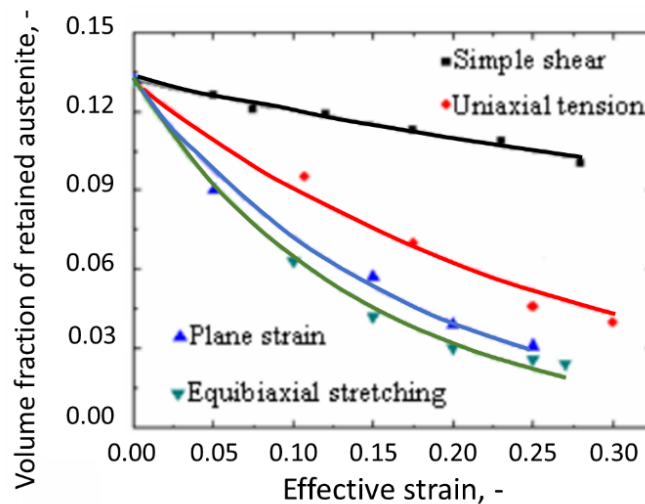


Fig. 22 Volume fractions of retained austenite dependent on effective strain under different loading paths [98].

➤ Retained austenite on ductility

As known that retained austenite is the main parameter affecting ductility of TRIP steels. As described previously, retained austenite is found to be located between laths or granular bainitic ferrite. In a study by Miihkinen and Edmonds [39], retained austenite films were found to improve deformation, while the impact of blocky retained austenite was negligible. The research conducted

by Chiang et al. [99] shows that retained austenite in equiaxed microstructure transforms faster in the early stage of straining. It is then completely transformed into fresh martensite at a high strain of about 0.25 (**Fig. 23a**). By contrast, retained austenite in the lamellar microstructure transforms relatively slowly and remains untransformed by 20% after cessation of the transformation. Regarding the optical micrographs shown in **Fig. 23b**, the equiaxed microstructure of retained austenite corresponds to the “blocky” types, while the lamellar microstructure is referred to as a mixture of “elongated” and “film-like” types of retained austenite. It should be noted that the retained austenite in lamellar microstructure has higher mechanical stability and would also be beneficial for desirable steel undergoing the TRIP effect.

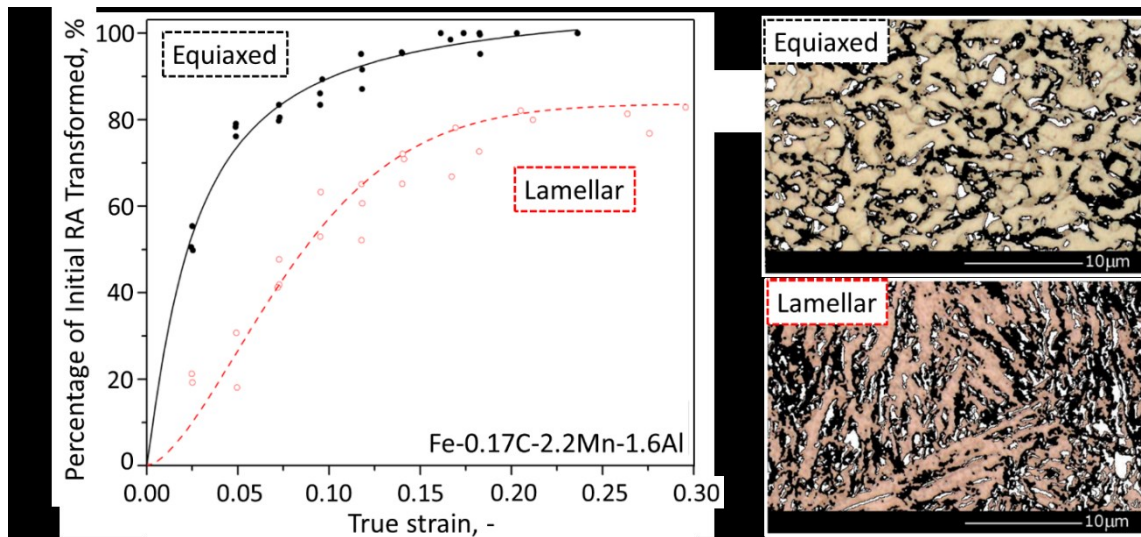


Fig. 23 (a) Percentage of retained austenite in different microstructures transformed into fresh martensite as a function of strain, and (b) optical micrograph of retained austenite in the equiaxed and lamellar microstructures [99].

1.2 Objectives and scope of the study

As an excessive formation of fresh martensite remains a critical issue in developing low carbon (<0.2 %wt.) carbide-free bainitic steels, it may deteriorate a balance in their mechanical properties. Thus, various heat treatment techniques, including ausforming, have been utilized to deal with martensitic transformation during cooling operations. Despite numerous research efforts utilizing ausforming to improve the mechanical properties of the steels, an understanding of how plastically deformed austenite interacts with the kinetics of phase transformation and microstructural development remains unclear. In particular, the effect of ausforming parameters on the kinetics of isothermal bainitic transformation, microstructure heterogeneity, and mechanical properties has never been comprehensively investigated. Thus, this dissertation is expected to explore the possibility of establishing high-strength low-carbon bainitic steels with a better understanding of phase transformation and microstructure development affected by the process parameters of ausforming. Furthermore, the scientific questions are addressed as follows.

- How do the process parameters of ausforming affect the kinetics behavior of isothermal bainitic transformation, the resistance to the formation of fresh martensite, the development of microstructural features, and finally the mechanical properties of low-carbon steel?
- How to understand the nucleation rate influenced by changes in the activation energy and carbon enrichment in the austenite due to ausforming and chemical compositions? How much is the dislocation density affected by the ausforming strain and chemical compositions?
- Is there any possibility of establishing heterogeneous microstructures with improving strength and ductility for low-carbon bainitic steels?

Experiments and a physical model are carried out to address these scientific questions. The hypotheses have been provided as follows.

- The kinetics behavior of isothermal bainitic transformation, the resistance to the formation of fresh martensite, microstructures, and the mechanical properties affected by the process parameters of ausforming should be systematically correlated.

- A unified physics-based model can provide an in-depth understanding of the nucleation rate influenced by changes in the activation energy, driving pressure, and carbon enrichment in the austenite. The dislocation density enhanced by ausforming and chemical compositions can be estimated by XRD analysis.
- A systematic investigation of the transformation behavior and analysis of microstructural heterogeneity that responds to the tensile properties might allow a possibility of improving strength and ductility by an appropriate balance in phase constituents.

In order to achieve these objectives, the kinetics of bainitic transformation affected by ausforming has been monitored via a thermomechanical heat treatment simulator. The nucleation rate influenced by changes in the activation energy, driving pressure, and enriched carbon in the austenite has been examined through constitutive equations derived from the classical nucleation rate theory. Mechanical properties such as hardness and uniaxial tensile tests have been conducted based on the standard individual testing method. Finally, this dissertation elaborates on all corresponding methodologies and results in three chapters.

Chapter II examines low-carbon steel comprised of 0.18C-0.97Si-2.5Mn-0.002B-0.033Ti by weight percent. The effects of ausforming temperature, strain, and strain rate on martensitic start temperature and kinetics of isothermal bainitic transformation are investigated using a thermomechanical heat treatment simulator. Microstructure, the volume fraction of each phase, and hardness behavior have also been evaluated. A comprehensive evaluation establishes a correlation between the ausforming parameters, the kinetics of isothermal bainitic transformation, microstructure, and hardness property.

Chapter III proposes a unified physics-based model for isothermal bainitic transformation by considering the effect of ausforming strain and chemical compositions. This model is derived from the theoretical basis of displacive transformation concerning a modified T_0 concept and the empirical Koistinen-Marburger (KM) equation. The nucleation rate influenced by changes in the activation energy, driving pressure, and carbon enrichment in the austenite is correlated with the kinetics of isothermal bainitic transformation. Regarding mechanical stabilization of austenite,

dislocation density involving ausforming and the impact of chemical compositions are roughly estimated.

Chapter IV takes representative steel from the previous chapters to analyze the evolution of heterogeneous microstructure affected by ausforming and without ausforming using SEM and EBSD measurements. Uniaxial tensile tests are used to validate such microstructural changes that respond to mechanical properties. In particular, yield strength, ultimate strength, post-necking behavior, and elongation are described in this regard. WHR behavior of the heat-treated steels is described with respect to the transformation of retained austenite, and the post-necking behavior is explained through the ability of microstructure refinement against fracture.

The results summarized in each chapter address the scientific questions mentioned above respectively. When the results from all three chapters are connected, a better understanding of the effect of ausforming on the kinetics behavior of isothermal bainitic transformation, resistance to fresh martensite formation, microstructural features, phase constituents, hardness, and tensile properties is established.

1.3 Original scientific contribution

After isothermal bainitic transformation, dealing with fresh martensite formation upon cooling was the majority of this work. Based on this scenario, the plastic deformation of austenite, called ausforming, was adapted to bring about a certain amount of planar dislocations into austenite so that the thermodynamic stability of this phase was enhanced significantly. Parameters of ausforming, such as deformation temperature, strain, and strain rate, are of significant importance to address for a better understanding of how they affect the kinetics of isothermal bainitic transformation based on the microstructure refinement. Based on nucleation rate theory, a physics-based model is developed to elucidate the physical parameters, such as driving energy, activation energy, nucleation rate, and carbon enrichment, subjected to ausforming and alloy modifications. The influence of ausforming on heterogeneous microstructure and mechanical properties of the ausformed steel is of importance to explore the possibility of establishing advanced high-strength steels to improve strength and ductility via the ausforming process.

➤ **Correlation between process parameters of ausforming, the kinetics of isothermal bainitic transformation, and hardness property**

The effect of ausforming parameters on the kinetics of isothermal bainitic transformation has been investigated in many research studies. However, most of them have been conducted in medium and high carbon steels with a majority of increasing strength without sacrificing ductility, including accelerating the onset of the transformation. Since the isothermal holding time for bainitic transformation is very time-consuming, which takes, for instance, dozens of hours to complete the reaction at a temperature range of 200-300°C. Ausforming parameters such as deformation temperature, strain, and strain rate are of importance for controlling the transformation behavior throughout the mechanical properties of the steels. Although these parameters have also been correlated with the kinetics behavior, microstructure, and mechanical properties, the contribution of ausforming parameters has not been comprehensively concluded due to separate investigations, including dissimilar alloying conditions. In low carbon steels (<0.2%wt.), there has been a critical issue involving the thermodynamic stability of austenite due to lower resistance against phase transformation at a lower temperature, especially during cooling. In this stage, the austenite could be transformed into fresh martensite, which may not be desirable for bainitic steels if an excessive amount of fresh martensite is formed. However, there are no

systematic investigations concerning the ausforming parameters. The effect of mechanical stabilization, which occurs during the transformation progress, has not been adequately described. Therefore, this research fills the scientific gap by establishing a quantitative correlation between the ausforming parameters, bainitic transformation behavior, microstructure features, and strength behavior for low-carbon bainitic steel.

According to the ausforming parameters, there are three process scenarios to carry out separately. For the first scenario, the plastic deformation of austenite is performed at temperatures of 650, 700, 750, and 800°C, with a deformation strain of 0.78 at a constant rate of 1 s⁻¹. The second scenario is that the austenite is plastically deformed at a temperature of 650°C and at 1 s⁻¹ of strain rate by changing the deformation strains from 0.15 to 0.78. The strain-dependent experiment is also compared with the one without deformation. Finally, the last scenario is strain rate dependence, which varies from 0.1 to 10 s⁻¹. The deformation temperature is the same as in the second scenario, while the deformation strain is 0.78. After deformation, the kinetics variables, including martensite start temperature, and dilatational change during isothermal transformation at 400°C, are monitored. All materials treated by individual scenarios are characterized using a light optical microscope and scanning electron microscope for microstructural analysis. The phase fraction is quantified by combining XRD measurement and image analysis using an adaptive threshold method. The latter is adapted for structural characterization, particularly those almost identical structures of bainitic ferrite and fresh martensite. The strength of the materials is then evaluated by the Macro-Vickers hardness test. It is observed that the martensite start temperature decreases after lowering the ausforming temperature. The decreased M_s temperatures are due to an increase in austenite strengthening, leading to triggering a mechanism called mechanical stabilization of austenite.

However, the enhanced strengthening of austenite, in turn, contributes to the onset of bainitic transformation. Lowering the temperature of ausforming also introduces substantial crystal defects, which act as available nucleation sites, enhancing the dilatational rate for bainitic transformation. Similar to those affected by ausforming strain and strain rate, the number of defect densities depends on the magnitude of plastic deformation of austenite and the decrease in strain rate. In the aspect of the microstructural feature, crystal defects induced by ausforming refines the prior austenite grain. Even though grain refinement accelerates the onset of bainitic transformation,

the displacive shear transformation of bainitic ferrite accompanied with dislocation debris eventually stabilizes the austenite in the later stage of the transformation. The enhancement of thermodynamic stability of austenite then resists a formation of fresh martensite during subsequent cooling operation, thus resulting in more volume fraction of retained austenite. The amount of fresh martensite formed during cooling predominantly affects the material strengthening evaluated from the micro-hardness value.

➤ **A unified physics-based model predicts the kinetics of isothermal bainitic formation of low-carbon steels by considering the effects of ausforming and alloy modification.**

Since the thermodynamic stability of austenite is a significant factor controlling the kinetics of isothermal bainitic transformation and the formation of fresh martensite during cooling operation, understanding physical parameters interplay with those phase transformations is of importance. In particular, when the plastic deformation of austenite and chemical composition are involved. Although numerous works have been proposed to describe the solid-state bainitic transformation kinetics, the chemical change and undercooling conditions have only been considered, and the effect of ausforming has been barely investigated. Therefore, a unified physics-based model proposed in this work is derived to thoroughly describe the macroscopic kinetics of isothermal bainitic transformation undergoing ausforming strains and chemical compositions. The kinetics model is derived based on the nucleation control mechanism in conjunction with the modified Koistinen-Marburger (KM) relationship to predict the amount of fresh martensite and retained austenite after the subsequent cooling. The nucleation-control approach is based on the displacive and diffusionless characteristics of forming bainitic ferrite sub-units. The basic idea is that the sub-units of bainitic ferrite (BF) are formed by activated nucleation at the interfaces of the austenite grain boundary and developed autocatalytically on the pre-existing platelets surrounding the ferrite/austenite interface. The growth of individual sub-unit is fast enough so that the transformation rate is determined by the successive nucleation events of bainitic ferrite. The nucleation events are time-temperature dependent and mainly governed by carbon enrichment in austenite and activation energy as an energy barrier required for nucleation. As observed experimentally, ausforming accelerates the nucleation reaction, then gradually becomes sluggish due to the mechanical stabilization of austenite. An explicit acceleration of grain boundary

nucleation is owing to the increased magnitude of ausforming strain and reduced mean carbon content of the steel.

On the other hand, being slow in the autocatalytic process is associated with carbon enrichment and dislocation density induced by bainitic ferrite formation during the transformation progress. An increase in the magnitude of ausforming strain decreases the amount of bainitic ferrite fraction, while a reduction of mean carbon concentration provides a more fraction of bainitic ferrite. A fitted parameter representing the initial energy barrier can be used to examine the activation energy change required for the nucleation processes, affected by ausforming and alloying variation. It is observed that a decrease in the energy barrier allows the acceleration of the transformation. While the transformation progresses, the driving energy for autocatalytic nucleation becomes smaller due to the increment of the dislocation density in the austenite. Also, minimizing mean carbon concentration in steel decreases the net activation energy difference with the increase of the nucleation rate. The result allocates a higher density of nucleation sites with more bainitic ferrite fractions. It is also obtained that a higher degree of ausforming is more applicable in steel with lower carbon content. With the substantial development of nucleation sites, the result effectively resists the formation of fresh martensite by improving the thermal stability of austenite, even though they provide a slightly lower fraction of bainitic ferrite.

➤ **Effects of ausforming on heterogeneous microstructure and mechanical property.**

Owing to the microstructure heterogeneity of low-carbon CFB steels, it is significantly responsible for their mechanical properties, including strength and ductility. In particular, when ausforming followed by the process of isothermal transformation of bainite at 400°C above M_s temperature is exploited to deal with microstructure constituents. The effects of ausforming on microstructures and mechanical properties have been investigated in a wide range of carbon steels. Generally, the investigation is aimed at shortening the incubation period for isothermal bainitic transformation and increasing the strength of the steel without sacrificing ductility according to the concept of nanostructured bainite steel. However, it has been given less attention in low carbon ($C < 0.2$ wt%) steels because of a lack of carbon content in austenite and a less possibility of achieving bainitic ferrite thickness of less than 100 nm. But even so, ausforming remains crucial for minimizing the formation of fresh martensite during cooling operation. If dislocations introduced by ausforming into prior austenite adequately suspend the formation of fresh martensite, more remaining austenite

would be achievable due to increased thermodynamic stability of the austenite. In terms of mechanical response, the retained austenite plays an essential role in enhancing strength and ductility via TRIP effect. Several efforts have been attempted to describe the thermodynamic stability of austenite dependence on the dislocation density in connection to the heat treatment process, microstructure evolution, and tensile properties. However, the insight discussion on the effect of ausforming involving thermodynamic stability throughout tensile properties, including post-necking and fracture behaviors of the low carbon steels, has never been thoroughly characterized.

This work systematically investigates the isothermal transformation kinetics, phase constituents, and mechanical properties related to the microstructural evolution of a low carbon bainitic steel that is processed either by the conventional process of isothermal heat treatment or by applying ausforming prior to the isothermal heat treatment is proposed. The results show that ausforming improves the thermodynamic stability of austenite. Increasing the number of substructures with high GND density reduces the nucleation sites available for martensitic transformation and leaves more austenite untransformed. Strength and ductility are enhanced by the heterogeneous microstructure developed during the ausforming process. A large fraction of retained austenite significantly impacts the enhancement of both uniform elongation and strength due to TRIP effect. Furthermore, grain boundary strengthening and a large fraction of highly stable retained austenite lead to effective retardation of void nucleation, consequently preventing the formation of macro/micro-cracks during post-necking.

1.4 References

- [1] J. Njuguna (Ed.), *Lightweight composite structures in transport: design, manufacturing, analysis and performance*, 1st ed., Woodhead Publishing, 2016.
- [2] A. Giampieri, J. Ling-Chin, Z. Ma, A. Smallbone, A.P. Roskilly, A review of the current automotive manufacturing practice from an energy perspective, *Appl. Energy* 261 (2020) 114074. <https://doi.org/10.1016/j.apenergy.2019.114074>.
- [3] T.P. Hovorun, K.V. Berladir, V.I. Pererva, S.G. Rudenko, Martynov A.I., Modern materials for automotive industry, *J. Eng. Sci.* 4 (2017) 8–18. [https://doi.org/10.21272/jes.2017.4\(2\).f8](https://doi.org/10.21272/jes.2017.4(2).f8).
- [4] A.T. Mayyas, A.R. Mayyas, M. Omar, Sustainable lightweight vehicle design, in: J. Njuguna (Ed.), *Lightweight composite structures in transport: design, manufacturing, analysis and performance*, firstst, Woodhead Publishing, 2016, pp. 267–302.
- [5] T. Sourmail, K. Maminska, A. Roth, E. D'eraimo, A. Galtier (Eds.), *30 years of bainitic forging steels*, Stuttgart, 2017.
- [6] T. Wurm, A. Busse, H.-W. Raedt, The Lightweight Forging Initiative -, *ATZ Worldw.* 121 (2019) 16–21. <https://doi.org/10.1007/s38311-018-0226-1>.
- [7] ArcelorMittal Europe Communications, Comparison of mechanical & quenchability properties of AFP, Q+T and bainitic grades, 2013. <https://barsandrods.arcelormittal.com/productsapplications/2755/forging>.
- [8] E.V. Edmonds, Innovation in the processing of tonnage materials: examples from the steel and aluminium industries, *J. Mater. Process. Technol (Journal of Materials Processing Technology)* 83 (1998) 1–13. [https://doi.org/10.1016/s0924-0136\(98\)00037-5](https://doi.org/10.1016/s0924-0136(98)00037-5).
- [9] H. Bhadeshia, The mechanism of bainite formation in steels, *Acta Metallur.* 28 (1980) 1265–1273. [https://doi.org/10.1016/0001-6160\(80\)90082-6](https://doi.org/10.1016/0001-6160(80)90082-6).
- [10] H. Bhadeshia (Ed.), *Bainite in Steels: Theory and Practice*, 3rd ed., Taylor & Francis Group, CRC Press, 2001.

-
- [11] H. Bhadeshia, D.V. Edmonds, Bainite in silicon steels: new composition–property approach Part 1, *Met. Sci. J.* 17 (1983) 411–419.
<https://doi.org/10.1179/030634583790420600>.
- [12] G. Krauss, S.W. Thompson, Ferritic microstructures in continuously cooled low-and ultralow-carbon steels, *ISIJ Int.* 35 (1995) 937–945.
<https://doi.org/10.2355/isijinternational.35.937>.
- [13] U. Lotter, H.P. Hougardy, The characterisation of bainitic microstructures, *Prakt. Metallogr.* 29 (1992) 151–156. <https://doi.org/10.1515/pm-1992-290305>.
- [14] Y. Ohmori, Y. Ohtani, T. Kunitake, The bainite in low carbon low alloy high strength steels, *Tetsu-to-Hagane.* 57 (1971) 1690–1705.
https://doi.org/10.2355/tetsutohagane1955.57.10_1690.
- [15] B.L. Bramfitt, J.G. Speer, A perspective on the morphology of bainite, *MTA.* 21 (1990) 817–829. <https://doi.org/10.1007/BF02656565>.
- [16] S. Zajac, V. Schwinn, K.-H. Tacke, Characterisation and quantification of complex bainitic microstructures in high and ultra-high strength linepipe steels, *MSF.* 500-501 (2005) 387–394. <https://doi.org/10.4028/www.scientific.net/MSF.500-501.387>.
- [17] S.G. Schawlann, High performance wear resistant bainitic steels for agricultural application. Master Thesis, Trondheim, June/2021.
- [18] L. Fielding, The bainite controversy, *Mater. Sci. Technol.* 29 (2013) 383–399.
<https://doi.org/10.1179/1743284712Y.00000000157>.
- [19] R.F. Hehemann, K.R. Kinsman, H.I. Aaronson, A debate on the bainite reaction, *Metall. Mater. Trans. A.* 3 (1972) 1077–1094. <https://doi.org/10.1007/BF02642439>.
- [20] T. Ko, S.A. Cottrell, The formation of bainite, *J. Iron Steel Inst* 172 (1952) 307–313.
- [21] G.R. Speich, M. Cohen, The growth rate of bainite, *Trans. Metall. Soc. AIME* 218 (1960) 1050–1059.
- [22] R.H. Goodenow, S.J. Matas, R.F. Hehemann, Growth kinetics and the mechanism of the bainite transformation, *Trans. Metall. AIME* 227 (1963) 651–658.

-
- [23] A. Hultgren, Bainitic transformation, *J. Iron Steel Inst* 114 (1926) 421–422.
- [24] H. Bhadeshia (Ed.), The nature, mechanism and properties of strong bainite, The Iron and Steel Institute of Japan, Tokyo, 2007.
- [25] H.I. Aaronson, W.T. Reynolds, G.J. Shiflet, G. Spanos, Bainite viewed three different ways, *MTA*. 21 (1990) 1343–1380. <https://doi.org/10.1007/BF02672557>.
- [26] M.J. Peet, H. Bhadeshia, Surface relief due to bainite transformation at 473 K (200 °C), *Metall. Mater. Trans. A*. 42 (2011). <https://doi.org/10.1007/s11661-011-0755-3>.
- [27] H. Bhadeshia, A rationalisation of shear transformations in steels, *Acta Metallur.* 29 (1981) 1117–1130.
- [28] C. Zener, Kinetics of the decomposition of austenite, *Trans. Am. Inst. Min. Metall. Eng.* 167 (1946) 550–595.
- [29] H. Bhadeshia (Ed.), Bainite: the incomplete-reaction phenomenon and the approach to equilibrium, The Metallurgical Society of the AIME, Warrendale, PA, USA., 1981.
- [30] M. Takahashi, H. Bhadeshia, The interpretation of dilatometric data for transformations in steels, *J. Mater. Sci. Lett.* 8 (1989) 477–478. <https://doi.org/10.1007/BF00720712>.
- [31] J.R. Patel, M. Cohen, Criterion for the action of applied stress in the martensitic transformation, *Acta Metallur.* 1 (1953) 531–538. [https://doi.org/10.1016/0001-6160\(53\)90083-2](https://doi.org/10.1016/0001-6160(53)90083-2).
- [32] G.B. Olson, M. Cohen, A general mechanism of martensitic nucleation: Part III. Kinetics of martensitic nucleation, *MTA*. 7 (1976) 1915–1923. <https://doi.org/10.1007/BF02659824>.
- [33] V.T.T. Miihkinen, D.V. Edmonds, Microstructural examination of two experimental high-strength bainitic low-alloy steels containing silicon, *Mater. Sci. Technol.* 3 (1987) 422–431. <https://doi.org/10.1179/mst.1987.3.6.422>.
- [34] V.T.T. Miihkinen, D.V. Edmonds, Tensile deformation of two experimental high-strength bainitic low-alloy steels containing silicon, *Mater. Sci. Technol.* 3 (1987) 432–440. <https://doi.org/10.1179/mst.1987.3.6.432>.

-
- [35] V.T.T. Miihkinen, D.V. Edmonds, Fracture toughness of two experimental high-strength bainitic low-alloy steels containing silicon, *Mater. Sci. Technol.* 3 (1987) 441–449. <https://doi.org/10.1179/mst.1987.3.6.441>.
- [36] F.G. Caballero, H. Bhadeshia, K. Mawella, D.G. Jones, P. Brown, Design of novel high strength bainitic steels: Part 2, *Mater. Sci. Technol.* 17 (2001) 517–522. <https://doi.org/10.1179/026708301101510357>.
- [37] F.G. Caballero, H. Bhadeshia, K. Mawella, D.G. Jones, P. Brown, Design of novel high strength bainitic steels: Part 1, *Mater. Sci. Technol.* 17 (2001) 512–516. <https://doi.org/10.1179/026708301101510348>.
- [38] V. Wirths, Prozessführung und zyklisches Werkstoffverhalten von karbidfreien bainitischen Stählen. Doctoral thesis, Aachen, Germany, 2016.
- [39] B. Buchmayr, Critical Assessment 22: bainitic forging steels, *Mater. Sci. Technol.* 32 (2016) 517–522. <https://doi.org/10.1080/02670836.2015.1114272>.
- [40] A. Arlazarov, M. Gouné, O. Bouaziz, A. Hazotte, Critical factors governing the thermal stability of austenite in an ultra-fined grained Medium-Mn steel, *Philos. Mag. Lett.* 97 (2017) 125–131. <https://doi.org/10.1080/09500839.2017.1290293>.
- [41] W. Bleck (Ed.), *Material Science of Steel: Textbook for Student at RWTH Aachen*, IEHK institute, 2016.
- [42] S. Kang, S. Yoon, S.J. Lee, Prediction of bainite start temperature in alloy steels with different grain sizes, *ISIJ Int.* 54 (2014) 997–999. <https://doi.org/10.2355/isijinternational.54.997>.
- [43] A. Arlazarov, E. Soares Barreto, N. Kabou, D. Huin, Evolution of Ms temperature as a function of composition and grain size, *Metall. Mater. Trans. A.* 51 (2020) 6159–6166. <https://doi.org/10.1007/s11661-020-06022-6>.
- [44] B. He, On the factors governing austenite stability: Intrinsic versus Extrinsic, *Mater.* 13 (2020). <https://doi.org/10.3390/ma13153440>.
- [45] N. Hansen, Hall–Petch relation and boundary strengthening, *Scripta Materialia* 51 (2004) 801–806. <https://doi.org/10.1016/j.scriptamat.2004.06.002>.

-
- [46] C.C. Casero, J. Sietsma, M.J. Santofimia, The role of the austenite grain size in the martensitic transformation in low carbon steels, *Mater. Des.* 178 (2019) 1–10. <https://doi.org/10.1016/j.matdes.2019.107625>.
- [47] H. Bhadeshia, BCC-BCC orientation relationships, surface relief and displacive phase transformation in steels, *Scr. Metall* 14 (1980) 821–824. [https://doi.org/10.1016/0036-9748\(80\)90296-3](https://doi.org/10.1016/0036-9748(80)90296-3).
- [48] J.R. Yang, C.Y. Huang, W.H. Hsieh, C.S. Chiou, Mechanical stabilization of austenite against bainitic reaction in Fe-Mn-Si-C bainitic steel, *JIM*. 37 (1996) 579–585. <https://doi.org/10.2320/matertrans1989.37.579>.
- [49] S.B. Singh, H. Bhadeshia, Quantitative evidence for mechanical stabilization of bainite, *Mater. Sci. Technol.* 12 (1996) 610–612. <https://doi.org/10.1179/mst.1996.12.7.610>.
- [50] P.H. Shipway, H. Bhadeshia, Mechanical stabilisation of bainite, *Mater. Sci. Technol.* 11 (1995) 1116–1128. <https://doi.org/10.1179/mst.1995.11.11.1116>.
- [51] S. Chatterjee, H.S. Wang, J.R. Yang, H. Bhadeshia, Mechanical stabilisation of austenite, *Mater. Sci. Technol.* 22 (2006) 641–644. <https://doi.org/10.1179/174328406X86128>.
- [52] F.B. Pickering, The structure and properties of bainite in steels, in: *Transformation and Hardenability in Steels*. Climax Molybdenum, Ann Arbor, Michigan, USA,, pp. 109–132.
- [53] C. Garcia-Mateo, F.G. Caballero, C. Capdevila, C.G. de Andres, Estimation of dislocation density in bainitic microstructures using high-resolution dilatometry, *Scripta Materialia* 61 (2009) 855–858. <https://doi.org/10.1016/j.scriptamat.2009.07.013>.
- [54] K. Sugimoto, M. Misu, M. Kobayashi, H. Shirasawa, Effects of second phase morphology on retained austenite morphology and tensile properties in a TRIP-aided dual-phase steel sheet, *ISIJ Int.* 33 (1993) 775–782. <https://doi.org/10.2355/isijinternational.33.775>.
- [55] F.G. Caballero, C. García-Mateo, C. Capdevila, C.G. Andrés, Advanced ultrahigh strength bainitic steels, *Mater. Manuf. Process.* 22 (2007) 502–506. <https://doi.org/10.1080/10426910701236023>.

-
- [56] V. Wirths, W. Bleck, R. Wagener, T. Melz (Eds.), *Bainitic forging steels*, 2014.
- [57] L.C. Chang, H. Bhadeshia, Austenite films in bainitic microstructures, *J. Mater. Sci. Technol.* 11 (1995) 874–882. <https://doi.org/10.1179/mst.1995.11.9.874>.
- [58] F.G. Caballero, M.K. Miller, A.J. Clarke, C. Garcia-Mateo, Examination of carbon partitioning into austenite during tempering of bainite, *Scr. Mater.* 63 (2010) 442–445. <https://doi.org/10.1016/j.scriptamat.2010.04.049>.
- [59] M. Zorgani, C. Garcia-Mateo, M. Jahazi, The role of ausforming in the stability of retained austenite in a medium-C carbide-free bainitic steel, *J. Mater. Res. Technol.* 9 (2020) 7762–7776. <https://doi.org/10.1016/j.jmrt.2020.05.062>.
- [60] M. Kabirmohammadi, B. Avishan, S. Yazdani, Transformation kinetics and microstructural features in low-temperature bainite after ausforming process, *Mater. Chem. Phys.* 184 (2016) 306–317. <https://doi.org/10.1016/j.matchemphys.2016.09.057>.
- [61] G. Chen, H. Hu, G. Xu, J. Tian, X. Wan, X. Wang, Optimizing microstructure and property by ausforming in a medium-carbon bainitic steel, *ISIJ Int.* 60 (2020) 2007–2014. <https://doi.org/10.2355/isijinternational.ISIJINT-2020-054>.
- [62] H. Bhadeshia, Nanostructured Bainite, in: H. Bhadeshia (Ed.), *Bainite in Steels: Theory and Practice*, Third Edition, CRC Press, London, 2019, pp. 455–494.
- [63] F.G. Caballero, M.K. Miller, S. Babu, C. Garcia-Mateo, Atomic scale observations of bainite transformation in a high carbon high silicon steel, *Acta Mater.* 55 (2007) 381–390. <https://doi.org/10.1016/j.actamat.2006.08.033>.
- [64] H. Amel-Farzad, H.R. Faridi, F. Rajabpour, A. Abolhasani, S. Kazemi, Y. Khaledzadeh, Developing very hard nanostructured bainitic steel, *Mater. Sci. Eng. A.* 559 (2013) 68–73. <https://doi.org/10.1016/j.msea.2012.08.020>.
- [65] H. Fan, A. Zhao, Q. Li, H. Guo, J. He, Effects of ausforming strain on bainite transformation in nanostructured bainite steel, *Int. J. Miner. Metall.* 24 (2017) 264–270. <https://doi.org/10.1007/s12613-017-1404-7>.

-
- [66] H. Hu, G. Xu, L. Wang, M. Zhou, Z. Xue, Effect of ausforming on the stability of retained austenite in a C-Mn-Si bainitic steel, *Met. Mater. Int.* 21 (2015) 929–935. <https://doi.org/10.1007/s12540-015-5156-5>.
- [67] H. Hu, G. Xu, L. Wang, M. Zhou, Effects of strain and deformation temperature on bainitic transformation in a Fe-C-Mn-Si alloy, *Steel Res.* 88 (2017) 1600170. <https://doi.org/10.1002/srin.201600170>.
- [68] G. Chen, G. Xu, H.S. Zurob, H. Hu, X. Wan, Effect of strain rate on the bainitic transformation in Fe-C-Mn-Si medium-carbon bainitic steels, *Metall. Mater. Trans. A.* 50 (2019) 573–580. <https://doi.org/10.1007/s11661-018-5051-z>.
- [69] H. Guo, X. Feng, A. Zhao, Q. Li, M. Chai, Effects of ausforming temperature on bainite transformation kinetics, microstructures and mechanical properties in ultra-fine bainitic steel, *J. Mater. Res. Technol.* 9 (2020) 1593–1605. <https://doi.org/10.1016/j.jmrt.2019.11.085>.
- [70] H. Guo, Y. Fan, Z. Li, Q. Li, X. Feng, Effect of ausforming parameters on strain-induced phase transformation and isothermally transformed bainite, *J. Mater. Res. Technol.* 11 (2021) 982–991. <https://doi.org/10.1016/j.jmrt.2021.01.087>.
- [71] L. Zhao, L. Qian, Q. Zhou, D. Li, T. Wang, Z. Jia, F. Zhang, J. Meng, The combining effects of ausforming and below-Ms or above-Ms austempering on the transformation kinetics, microstructure and mechanical properties of low-carbon bainitic steel, *Mater. Des.* 183 (2019) 108123. <https://doi.org/10.1016/j.matdes.2019.108123>.
- [72] E.C. Bain, N.Y. Dunkirk, The nature of martensite, *Trans. AIME* 70 (1924) 25–46.
- [73] G. Kurdjumow, G. Sachs, Über den Mechanismus der Stahlhärtung, *Mater. Chem. Phys.* 64 (1930) 325–343. <https://doi.org/10.1007/BF01397346>.
- [74] Z. Nishiyama, X-ray investigation of the mechanism of the transformation from face centered cubic lattice to body centered cubic, *Sci. Rep. Tohoku Univ.* 23 (1934) 637–664.
- [75] G. Wassermann, Einfluß der α - γ -Umwandlung eines irreversiblen Nickelstahls auf Kristallorientierung und Zugfestigkeit, *Steel Res.* 6 (1933) 347–351. <https://doi.org/10.1002/srin.193300427>.

-
- [76] A.B. Greninger, A.R. Troiano, The mechanism of martensite formation, *Trans. AIME*. 185 (1949) 590–598.
- [77] C.S. Barrett, T.B. Massalski (Eds.), *Structure of Metals*, 3rd ed., Pergamon Press Oxford, Toronto, Sydney, Paris Frankfurt, 1980.
- [78] K. Shimizu, Z. Nishiyama, Electron microscopic studies of martensitic transformations in iron alloys and steels, *MT*. 3 (1972) 1055–1068. <https://doi.org/10.1007/BF02642437>.
- [79] V. Tari, A.D. Rollett, H. Beladi, Back calculation of parent austenite orientation using a clustering approach, *J. Appl. Crystallogr.* 46 (2013) 210–215. <https://doi.org/10.1107/S002188981204914X>.
- [80] P.P. Suikkanen, C. Cayron, A.J. DeArdo, L.P. Karjalainen, Crystallographic analysis of isothermally transformed bainite in 0.2C–2.0Mn–1.5Si–0.6Cr steel using EBSD, *J. Mater. Sci. Technol.* 29 (2013) 359–366. <https://doi.org/10.1016/j.jmst.2013.01.015>.
- [81] H. Hu, B. Imed-Eddine, G. Xu, J. Tian, M. Zhou, Y. Bréchet, H.S. Zurob, Effect of temperature, carbon content and crystallography on the lengthening kinetics of bainitic ferrite laths, *Mater. Charact.* 187 (2022) 111860. <https://doi.org/10.1016/j.matchar.2022.111860>.
- [82] H. Beladi, V. Tari, I.B. Timokhina, P. Cizek, G.S. Rohrer, A.D. Rollett, P.D. Hodgson, On the crystallographic characteristics of nanobainitic steel, *Acta Mater.* 127 (2017) 426–437. <https://doi.org/10.1016/j.actamat.2017.01.058>.
- [83] J. Wang, X. Di, C. Li, D. Wang, The Influence of Ni on Bainite/Martensite Transformation and Mechanical Properties of Deposited Metals Obtained from Metal-Cored Wire, *Metals* 11 (2021) 1971. <https://doi.org/10.3390/met11121971>.
- [84] K.T. Kashyap, A. Bhat, P.G. Koppad, K.B. Puneeth, On Peierls Nabarro stress in Iron, *Comput. Mater. Sci.* 56 (2012) 172–173. <https://doi.org/10.1016/j.commatsci.2011.12.033>.
- [85] Y. Kang, Q. Han, X. Zhao, M. Cai, Influence of nanoparticle reinforcements on the strengthening mechanisms of an ultrafine-grained dual phase steel containing titanium, *Mater. Des.* 44 (2013) 331–339. <https://doi.org/10.1016/j.matdes.2012.07.068>.

-
- [86] M. Takahashi, H. Bhadeshia, A model for the microstructure of some advanced bainitic steels, *JIM*. 32 (1991) 689–696. <https://doi.org/10.2320/matertrans1989.32.689>.
- [87] C.H. Young, H. Bhadeshia, Strength of mixtures of bainite and martensite, *Mater. Sci. Technol.* 10 (1994) 209–214. <https://doi.org/10.1179/mst.1994.10.3.209>.
- [88] J.E. Bailey, P.B. Hirsch, The dislocation distribution, flow stress, and stored energy in cold-worked polycrystalline silver, *Philos. Mag. Lett.* 5 (1960) 485–497. <https://doi.org/10.1080/14786436008238300>.
- [89] J.P. Naylor, Grain boundaries, *Metall. Mater. Trans. A*. 10A (1979) 861–873.
- [90] J. Daigne, M. Guttman, J.P. Naylor, The influence of lath boundaries and carbide distribution on the yield strength of 0.4% C tempered martensitic steels, *Mater. Sci. Eng. A*. 56 (1982) 1–10. [https://doi.org/10.1016/0025-5416\(82\)90176-8](https://doi.org/10.1016/0025-5416(82)90176-8).
- [91] E.V. Pereloma, A.A. Gazder, I.B. Timokhina (Eds.), *Retained austenite: transformation-induced plasticity*, CRC Press, Boca Raton, Florida, 2016.
- [92] I.B. Timokhina, P.D. Hodgson, E.V. Pereloma, Effect of microstructure on the stability of retained austenite in transformation-induced-plasticity steels, *Metall. Mater. Trans. A*. 35 (2004) 2331–2341. <https://doi.org/10.1007/s11661-006-0213-9>.
- [93] C. Magee, R. Davies, The structure, deformation and strength of ferrous martensites, *Acta Metallur.* 19 (1971) 345–354. [https://doi.org/10.1016/0001-6160\(71\)90102-7](https://doi.org/10.1016/0001-6160(71)90102-7).
- [94] T. David, Kinetics of solidification of supercooled liquid mercury droplets, *J. Chem. Phys.* 20 (1952) 411–424. <https://doi.org/10.1063/1.1700435>.
- [95] S. Radcliffe, M. Schatz, The effect of high pressure on the martensitic reaction in iron-carbon alloys, *Acta Metallur.* 10 (1962) 201–207. [https://doi.org/10.1016/0001-6160\(62\)90117-7](https://doi.org/10.1016/0001-6160(62)90117-7).
- [96] H. Wang, G. Yuan, M. Lan, J. Kang, Y. Zhang, G. Cao, R.D.K. Misra, G. Wang, Microstructure and mechanical properties of a novel hot-rolled 4% Mn steel processed by intercritical annealing, *J. Mater. Sci.* 53 (2018) 12570–12582. <https://doi.org/10.1007/s10853-018-2512-0>.

- [97] D.D. Tjahjanto, A. Suiker, S. Turteltaub, P. Del Rivera Diaz Castillo, S. van der Zwaag, Micromechanical predictions of TRIP steel behavior as a function of microstructural parameters, *Comput. Mater. Sci.* 41 (2007) 107–116.
<https://doi.org/10.1016/j.commatsci.2007.03.005>.
- [98] T.K. Shan, W.G. Zhang, Z.Q. Lin, S.H. Li, The effect of macroscopic stress state on transformation rate in TRIP-assisted steels, *KEM.* 340-341 (2007) 1067–1072.
<https://doi.org/10.4028/www.scientific.net/KEM.340-341.1067>.
- [99] J. Chiang, B. Lawrence, J.D. Boyd, A.K. Pilkey, Effect of microstructure on retained austenite stability and work hardening of TRIP steels, *Mater. Sci. Eng. A.* 528 (2011) 4516–4521. <https://doi.org/10.1016/j.msea.2011.02.032>.

Chapter II Effect of ausforming on microstructure and hardness characteristics of bainitic steel

Theerawat Kumnorkaew, Junhe Lian, Vitoon Uthaisangsuk, Wolfgang Bleck

Journal of Materials Research and Technology 2020; 9(6):13365-13374

<https://doi.org/10.1016/j.jmrt.2020.09.016>

Chapter II investigates the influence of ausforming parameters, including deformation temperature, strain, and strain rate on prior austenite grain size, martensitic and isothermal bainitic transformations, and hardness property of 0.18C-0.97Si-2.5Mn-0.002B-0.033Ti steel. A quantitative correlation between the parameters, microstructure features, and strength behavior of the steel is established. Ausforming enhances the stability of austenite, decreases the martensitic start temperature, and accelerates the kinetics of bainitic transformation. The mechanical driving force and more nucleation sites increase the total extent of isothermal bainitic transformation. Microstructural refinement is highly effective when ausforming is conducted under low temperature, low strain rate, and high strain. The martensite fraction mainly defines hardness property.

Effect of ausforming on microstructure and hardness characteristics of bainitic steel

Theerawat Kumnorkaew^{a,*}, Junhe Lian^{b,**}, Vitoon Uthaisangsuk^c, and Wolfgang Bleck^a

^a Steel Institute of RWTH Aachen University, 52072 Aachen, Germany

^b Advanced Manufacturing and Materials, Department of Mechanical Engineering, Aalto University, Puumiehenkuja 3, 02150 Espoo, Finland

^c Department of Mechanical Engineering, King Mongkut's University of Technology Thonburi, 10140 Bangkok, Thailand

theerawat.kumnorkaew@iehk.rwth-aachen.de; junhe.lian@aalto.fi; vitoon.uth@kmutt.ac.th; bleck@iehk.rwth-aachen.de

Highlights:

- A quantitative correlation is established between the ausforming parameters, microstructure features and strength behavior for the low-carbon carbide free bainitic steel.
- Ausforming enhances the stability of austenite, decreases the martensitic start temperature, and accelerates the kinetics of bainitic transformation.
- Mechanical driving force and more nucleation sites contribute to increase in total extent of isothermal bainitic transformation.
- Microstructural refinement is highly effective when ausforming conducted under low temperature, low strain rate, and high strain.
- Hardness is mainly defined by the martensite fraction

Abstract:

Effects of process parameters of the ausforming such as temperature, strain and strain rate on the martensitic start temperature, kinetics of isothermal bainitic transformation and microstructure refinement of a low carbon carbide-free bainitic steel were investigated. It was found that applying plastic deformation to untransformed austenite during intermediate temperatures decreased the martensite start temperature of steel and enabled isothermal bainitic transformation at low temperatures. Hereby, ausforming significantly generated heterogeneous nucleation sites, which accelerated the overall kinetics of bainitic transformation and thus increased bainitic phase fraction in steel. In addition, the ausforming enhanced the stability of austenite that led to reduced amount of martensite after cooling down to room temperature. Finally, the ausforming parameters and observed microstructure features were correlated and discussed along with the hardness of steel.

Keywords: Ausforming; Low-carbon CFB steel; M/A constituent; Grain refinement; Deformation temperature; Strain rate

1. Introduction

The requirement of high-performance steels with lower production cost and better machinability has led to development of carbide free bainitic (CFB) steel. This CFB steel mainly consisted of fine lath matrix of bainitic ferrite (BF) embedded with retained austenite (RA). This RA was certainly a residual product from the process of carbon partitioning between supersaturated bainitic ferrite and surrounding austenite during a bainitic transformation. Such partitioning resulted in a formation of film-like or blocky RA that exhibited different stabilities [1]. The strengthening mechanism of CFB steel was mostly controlled by the contribution of BF, whereas its toughness and ductility are governed by the volume fraction and shape of RA [2,3]. According to Caballero and Mateo [4], RA could affect the strengthening mechanism of steel by the transformation-induced plasticity (TRIP) effect. It was obviously shown that controlling the stability of RA played an important role in balancing mechanical properties (ductility, strength, and toughness) regarding the TRIP effect, which strongly depended on its chemical composition and morphological feature.

As reported in [5,6] a film-like RA was a slender phase and located between BF sheaves. The film-like RA was more stable and difficult to be transformed to untempered martensite during either final quenching or deformation at a lower temperature in comparison to the blocky type RA due

to its higher degree of carbon enrichment. The blocky RA was usually found in the form of an inequiaxed blocky shape and dispersed among the granular matrix of BF, in which its stability directly depended on the block size. Liu et al. [5] showed that large blocky RA was unstable and could partially transformed into high-carbon brittle martensite during cooling down to room temperature, while smaller RA blocks were more stable. However, blocky RA exhibited lower stability than the film-like RA. Such unstable feature was often called ‘M/A’ phase, because it basically contained both martensite and untransformed RA. This untransformed RA could be completely transformed into a fully martensitic structure during an early stage of deformation [6–8]. Although the existence of brittle martensite was beneficial to hardness and strength in general, it was a major factor for deteriorating ductility and impact toughness of steels, since it could lead to a severe localization of neighboring phases due to the large difference in terms of strength [9].

Numerous works have been conducted in the past decades, in which the M/A constituents were replaced with fine and stable structures by different methods [5,10,11]. It was suggested that increasing the volume fraction of bainite and the possibility of austenite decomposition could be solutions of this critical issue [12]. Principally, the bainitic transformation started by para-equilibrium nucleation and grew through shear mechanism induced by diffusionless transformation [13]. Nevertheless, the transformation will be completely terminated when carbon was partitioned into austenite immediately after the bainitic growth approached the T'_0 locus of equilibrium phase diagram, in which the strain energy of BF was taken into account [7,14,15]. It is also known that carbon is the main element which governed the phase transformation in steel. Increasing of carbon concentration enhanced the thermal stability of austenite and subsequently decreased the transformation temperature. Bhadeshia [16] reported that microstructure refinement of low-alloy bainitic steels was achieved well at very low transformation temperatures for steel containing 0.3-1.0%C. On the other hand, the phase transformation in those high/medium-carbon steels was time-consuming, possibly taking several days to complete the process [3].

Moreover, there have been attempts to apply the concept of lowering transformation temperature to low-carbon CFB steels ($\%C \leq 0.2\%$) because of their better weldability and wear resistance, accompanied by other high-performance features [11,17]. Indeed, the typical heat treatment used for producing such ultrafine-grained bainitic steel by isothermal tempering above the martensite start (M_s) temperature was by far unpractical, because insufficient enrichment of carbon in

austenite caused an inability of lowering transformation temperature. Subsequently, it led to a low thermal stability of austenite and allowed the formation of M/A constituent [18,19]. Hence, ausforming as a thermomechanical heat treating process can be applied in order to overcoming the limitation by means of applying external load to the untransformed austenite. The advantage of this process is to increase the thermal stability of austenite by introducing structural defects and thus to enable the bainitic transformation at a lower temperature. It also generated sub-grain boundaries, which led to a refinement of prior austenitic grain structure [20,21]. These defects could further facilitate additional nucleation sites for subsequent bainitic transformation, in which its transformation kinetics was accelerated. In contrast, occurred nuclei could then transformed to smaller amount of bainite due to mechanical stabilization of the austenite. Such mutual effects were clearly verified by experimental studies concerning ausforming heat treatment of medium/high carbon steels [22–28]. However, a few studies have been done for low-carbon steels [29,30]. The transformation kinetics of bainite and systematic correlation between ausforming parameters, microstructure evolution and mechanical properties of low-carbon steels remain unclear.

Therefore, in this work influences of processing parameters of ausforming including deformation temperature, strain and strain rate on the isothermal bainitic transformation behaviour, microstructure refinement and hardness of a low-carbon CFB steel were investigated by means of thermo-mechanical simulation. Each single control variables were systematically studied. Except for the ausforming parameters, other thermal histories of the examined samples was kept the same in the dilatometry tests of all cases. The microstructures of thermo-mechanically treated samples were characterized by light optical microscopy (LOM) and scanning electron microscopy (SEM). Afterwards, volume fraction of M/A and bainite including their morphologies were analyzed. In addition, X-ray diffraction (XRD) was employed to quantify the volume fraction of RA. It should be noted that the main focus of the current study was effects of processing parameters on emerged microstructure development. Therefore, resulting mechanical properties have been not elaborated and size of used samples in the thermal-mechanical treatment was also limited. The strength property was investigated by using a hardness measurement. Detailed discussions on the correlation of processing parameters with determined microstructure features and hardness values were provided.

2. Materials and Methods

2.1. Materials

A low-carbon CFB steel containing 0.18%C, 0.97%Si, 2.5%Mn, 0.002%B, and 0.033Ti by weight was investigated in this work. The amounts of Si and Mn in the examined steel were verified to be adequate for a development of CFB steel [31]. Hereby, the addition of Mn aimed to increase the stability of RA and hardenability of steel, whereas Si could suppress the formation of cementite in bainitic structure and facilitate an enrichment of carbon in austenite during the bainitic transformation. Moreover, adding such a little amount of Ti could also prevent the formation of boron nitride at the ferrite/austenite interfaces by forming either titanium nitride (TiN) or titanium carbonitride (Ti(C, N)) with nitrogen. The test material was initially produced in a laboratory vacuum induction furnace and cast into an 80 kg block with a cross-section of 140×140 mm². Subsequently, the ingot was homogenized at 1250°C for 2 hours and pre-forged into a final cross-section of 60×60 mm² by the semi-product simulation center (SPSC) prior to cooling down to room temperature (RT).

2.2. Dilatometry

To investigate the influences of processing parameters of ausforming on the kinetics of phase transformation, microstructure evolutions and hardness of steel, cylindrical specimens with a diameter of 5 mm and length of 10 mm were machined from the homogenized billet along the direction perpendicular to the forging direction. The thermo-mechanical experiments were carried out using a Bähr DIL805 dilatometer. Before each test, a Pt/Pt/-10 Rh thermocouple (type S) was spot-welded on the surface of central area of specimens for measuring temperature development. The specimens were then placed between two quartz rods and in the middle of an induction coil. A cooling system with helium gas and laser infrared detector for determining displacement of specimen in the radial direction were installed. Note that such measured radial displacement could be also used to gather a volumetric change of specimen. An example of radial dilatation vs. temperature diagram, which was recorded throughout the heating and cooling stages in the dilatometry test is illustrated in Figure 1a. By a heating rate of 18 °C/s from RT to the austenitizing temperature of steel at 950 °C, the observed first inflection point represented the *Ac1* temperature of 745 °C and finish temperature *Ac3* of 855 °C for the austenitic transformation. When cooling

down at a rate of 50 °C/s, the first deviation of tangent line around 390 °C was the martensite start (M_s) temperature and the temperature of about 172 °C was the martensite finish (M_f) temperature. **Fig. 1b** exhibits the continuous cooling transformation (CCT) diagram of the investigated steel, which was determined from dilatometry tests at various cooling rates after austenitizing at 950 °C for five minutes. It was found that a fully martensitic structure likely formed when a cooling rate higher than ~ 1.5 °C/s was employed.

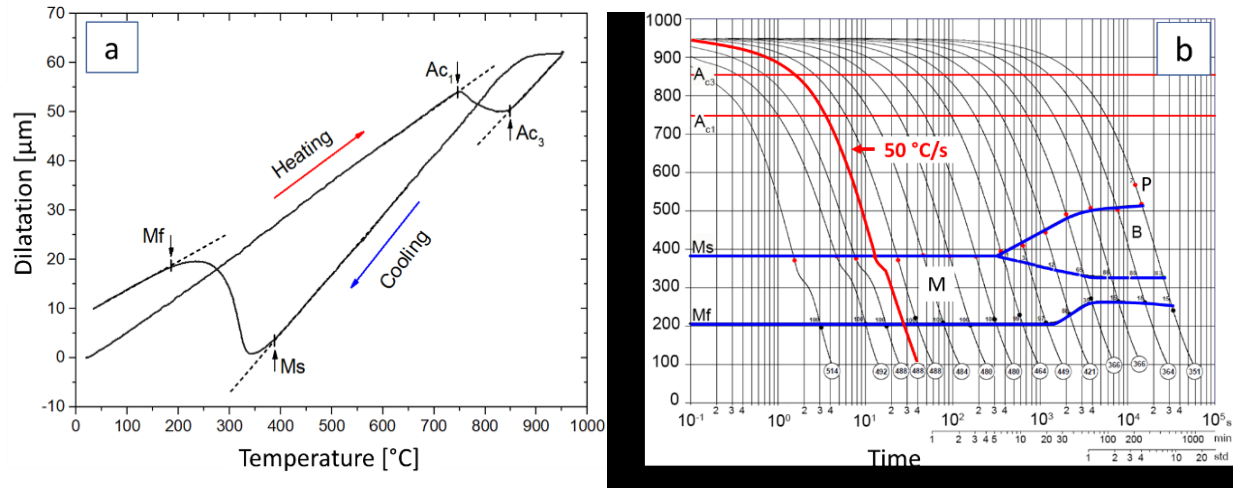


Fig. 1 (a) Radial dilatation vs. temperature during heating and cooling and (b) experimental CCT diagram of the investigated steel (M, B, and P stand for martensitic, bainitic, and pearlite transformation regimes, respectively).

In this study, four different heat-treatment routes (I to IV) were applied, as presented in **Fig. 2**. The routes I and III were designed to investigate the effect of ausforming on the M_s temperature. The decomposition behavior of austenite to bainite affected by ausforming was studied by the routes II and IV or so-called pure isothermal tempering (PIT). Note that the tempering stage defined at 400 °C was aimed to experimentally verify the martensitic transformation. The results obtained from specimens passed through routes I and II were considered as a reference for comparison with those from routes with ausforming. For specimens subjected to ausforming, M_s temperature was also identified. In the case of ausforming route III, deformation temperature was varied between 650 °C and 800 °C, while final strain and strain rate of 0.78 and 1 s⁻¹ were employed, respectively. For the ausforming route IV, all temperatures, final strains and strain rates, as given in **Table 1**, were taken into account. At the beginning of the heat treatments, all specimens were heated to the austenitizing temperature of 950 °C with the rate of 18 °C/s and held for 300 s for achieving a

homogeneous microstructure. The cooling rate to the tempering temperature of 50 °C/s was set for both specimens with and without ausforming. For the PIT treatment, specimens were soaked at the temperature of 400 °C for 1 hour and further cooled down to RT at the rate of 20 °C/s. It is noted that prior to deformation by ausforming, specimens were held for 10 s so that thermal gradient caused by the fast cooling could be first eliminated. The similar concept was also applied in [30]. During the cooling stages of each routes, radial dilatations of specimens were gathered in order to examine the phase transformation characteristics. To evaluate the kinetics of the isothermal bainitic phase transformation under different conditions, the dilatation data obtained at 400°C was additionally determined and afterwards normalized using the formula: $(d_i - d_0)/d_0$, where d_i and d_0 represent the instantaneous diameter during tempering and diameter after deformation before the isothermal holding, respectively [25].

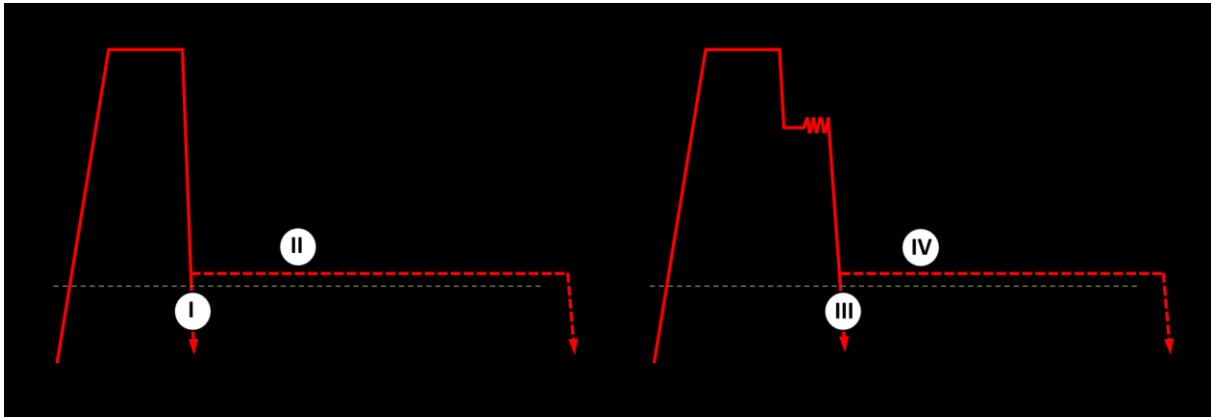


Fig. 2 Thermomechanical treatment routes through direct quenching (I, III) and tempering (II, IV) with and without ausforming.

Table 1 Variations of temperature, strain and strain rate applied in the ausforming routes III and IV.

Parameters Type of investigation	Temperature (°C)	Strain rate (s ⁻¹)	Strain (-)
Effect of deformation strain	650	1	0.15, 0.78
Effect of deformation temperature	650, 700, 750, 800	1	0.78
Effect of deformation strain rate	650	0.1, 1, 10	0.78

2.3. Microstructure analysis and hardness test

Microstructure analyses and hardness measurements were performed at the center of cross-sectional area of thermo-mechanically treated specimens parallel to the compression direction. The microstructures were examined by both light optical microscope (LOM) and scanning electron microscope (SEM). The quantitative identifications of observed phases were done by using X-ray diffraction (XRD) on BRUKER D8 diffractometer. All specimens for LOM and SEM were mechanically ground with abrasive papers (no. 600, 1200, and 2400) and then further polished with fine diamond paste. Different types of etching procedures were applied for metallographic specimens. For observing prior austenitic grains, specimens were etched with saturated picric acid and distilled water, heated at 60 °C for 30 s in a water bath, while for microstructure examination they were etched with Klemm's solution. In case of SEM investigations, etching with a 3% Nital solution was used. On the other hand, specimens prepared for XRD measurement were electro-polished by a TenuPol-5 single-jet electro-polishing device. Hereby, A2 electrolyte was employed at room temperature with the voltage and flow rate at 40 V and 12 mm/s, respectively. The XRD machine was set by using a filtered CuK α radiator, which was operated at 40 kV and 30 mA under the collection range between 30° and 120° at a step width of 0.01° with counting time of 2 s. The phase fractions of face-centered cubic (FCC) RA and body-centered cubic (BCC) bainitic ferrite or/and martensite were subsequently analyzed by the Rietveld's refinement method using MAUD software. Macro-Vickers hardness measurements were conducted, in which a constant load of 10 kg and holding time of 15 s according to the ASTM E92-17 standard were applied.

3. Results and discussions

3.1. Martensite start temperature and prior austenite grain

First, effects of ausforming and deformation temperature on the radial dilatation during martensitic transformation and prior austenitic grains of directly quenched specimens after austenitizing/ausforming heat-treatments are displayed in **Fig. 3**. It was found in **Fig. 3a** that lowering deformation temperature of ausforming resulted in shifting of the M_s temperature. It decreased from the temperature of around 382°C to 363°C when the ausforming temperature was reduced from 800°C to 650°C. This could be due to the fact that during the hot deformation crystal defects and grain boundaries were increased, while prior austenitic grain (PAG) size was reduced. As a consequence, the strength of undercooled austenite increased before the transformation of

martensite. Particularly, at lower temperatures, where effect of work hardening on the generation of substantial crystal defects was pronounced, the contribution to austenite strengthening was thus more significant. Generally, the strength of prior austenite played a major role in the subsequent phase transformation with regard to mechanical stabilization. Hereby, the austenite to martensite transformation of steel was resisted so that its M_s temperature was lowered and an isothermal bainitic transformation was enabled at low temperature [22,32]. Additionally, it is noted that during the martensitic transformation another small slope change was observed nearby the M_f temperature. Such uneven transition occurred only in the deformed specimens and its degree depended on the ausforming temperature. This phenomenon was also reported for some steels, especially highly alloyed chromium steels in [33,34]. It was evidenced that carbide precipitation and/or growth of existing carbides could lead to an inhomogeneous distribution of alloying element in austenite, which resulted in a discontinuous characteristic of austenite to martensite transformation between the M_s and M_f temperature. However, in this work, the soaking time of 300 s at the austenitization temperature of 950 °C was applied, which was sufficient for achieving a complete solid solution of austenite without remaining carbides in the steel. Note that this slope change was not observed in the specimens without ausforming and the discontinuity was more pronounced when the deformation temperature became higher. Therefore, such discontinuous transformation was likely caused by ausforming accelerated/induced carbide precipitation. It seemed that larger difference between ausforming and M_s temperature led to more noticeable slope change. Additional investigations are needed to verify this occurrence. Moreover, the PAGs of ausformed specimens were horizontally elongated, in which its magnitude directly depended on the deformation temperature. It was found that ausforming caused pancaking of prior austenite grains and it became more severe at lower ausforming temperature, for instance, at 650 °C, as depicted in **Fig. 3b-3d**. It was due to the increase of boundary areas of prior austenite per unit volume/area.

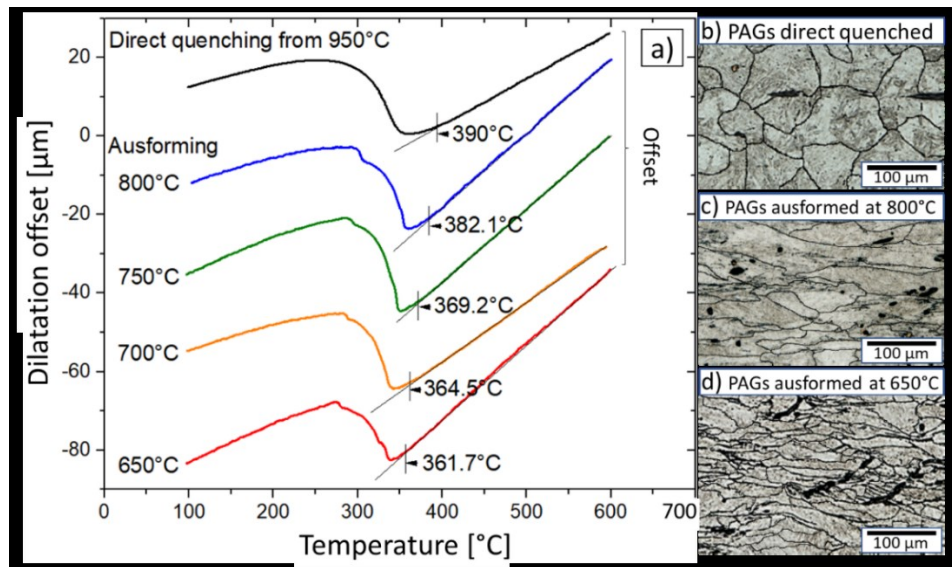


Fig. 3 a) M_s temperatures determined by the dilations and b)-d) prior austenitic grains of specimens after direct quenching from austenitization temperature (route I) and those quenched after ausforming at various temperatures (route III).

3.2. Dilatation characteristic during phase transformation

Figure 4 shows the radial dilatation vs. temperature curves of specimens during the cooling stages of applied thermomechanical treatment (routes II and IV). From the beginning of austenitization temperatures or from the ausforming temperature to the tempering temperature at 400 °C, all dilatation curves exhibited almost linear behaviour which showed no phase transformation occurred. Then, by decomposition of austenite to bainitic ferrite the curves rose up vertically until the transformation completed. Hereby, amount of transformed bainite could be approximately estimated by measuring such a vertical change [35]. In the final stage from the temperature of 400 °C to room temperature, all curves deviated from the given tangential (dashed) lines. These dashed lines were drawn individually on each experimental curve by a linear regression with respect to the deformation conditions. These obvious deviations were caused by decomposition of residual austenite into harder martensite. Larger deviation implied increased amount of transformed martensite. In **Fig. 4a**, the vertical arrows showed the estimated temperatures at the onset of the transformation. The martensitic transformation of specimen after PIT took place at the temperature of 351 °C, whereas those of specimens deformed at 650 °C/ 1 s⁻¹ until the strain of 0.15 and 0.78 were around 270 °C and 183 °C, respectively. The dilatation characteristics exhibited that lower

fraction of martensite was transformed in ausformed specimens in comparison with that in PIT specimen. In addition, variation of the ausforming temperature also significantly affected the deviation of curves, as shown in **Fig. 4b**. The decomposition of residual austenite to martensite tended to be increased when the ausforming temperature became higher. The results were in consistent with those reported in [22,32]. However, effect of varying strain rate of the ausforming on the martensitic transformation was negligible, as seen in **Fig. 4c**. The martensitic fractions in the specimens subjected to different strain rates were not much differed, especially when ausforming between the strain rate of 0.1 s^{-1} and 1 s^{-1} .

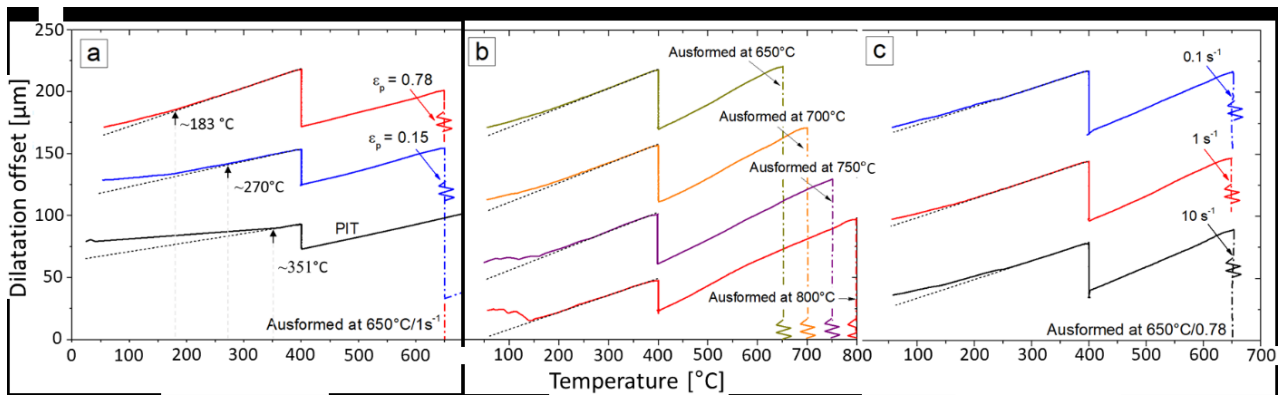


Fig. 4 Radial dilatation vs. temperature curves from the entire cooling stage after ausforming at various (a) strains (b) temperatures and (c) strain rates of specimens from route II and IV.

3.3. Kinetics of bainitic transformation

The decomposition of deformed austenite into bainite could be identified by the relative dilation at the isothermal tempering stage, since there was no other phase transformation occurred [36]. Hereby, the dilatation rate was interpreted as the rate of phase transformation. **Fig. 5a** illustrates the kinetics of bainitic transformation of specimens deformed at the temperature of 650 °C, strain rate of 1 s^{-1} until the final strains of 0.15 and 0.78 in comparison with that of PIT samples. It was found that the bainitic transformation behavior of steel could be considerably altered by applying ausforming. Both onset and completion of the transformation were accelerated when ausforming strain was increased. The magnitude of transformation in the PIT specimen was rather low. The ausforming caused crystal defects within former austenitic grains during deformation e.g. deformation bands, sub-grain boundaries and dislocation [37]. These generated defects further enhanced nucleation sites for the bainitic transformation stage. The amount of defects increased

with increasing ausforming strain. More nucleation sites implied that more austenite could be decomposed into bainite with a higher rate. The ausforming also contributed to mechanical stabilization of deformed austenite through accumulated strain and dislocations. As a result, mechanical driving force of nucleation sites became higher which was advantageous for the isothermal bainitic phase transformation, in which the total driving force required for diffusionless growth was raised [29,30]. On the other hand, retardation of the bainitic transformation because of increased ausforming temperature is presented for the examined steel in **Fig. 5b**. At high ausforming temperatures such as 800 °C, strain-induced dislocations were compensated by effect of dynamic and static recovery, in which the mechanical driving force was necessarily reduced [38]. Consequently, the total driving force for diffusionless growth was decreased, because distortion energy inherited from deformation to transformation stage was lowered. According to Zou et al. [37], reduction of driving force led to a delay of incubation time and thus decrease in the amount of bainite.

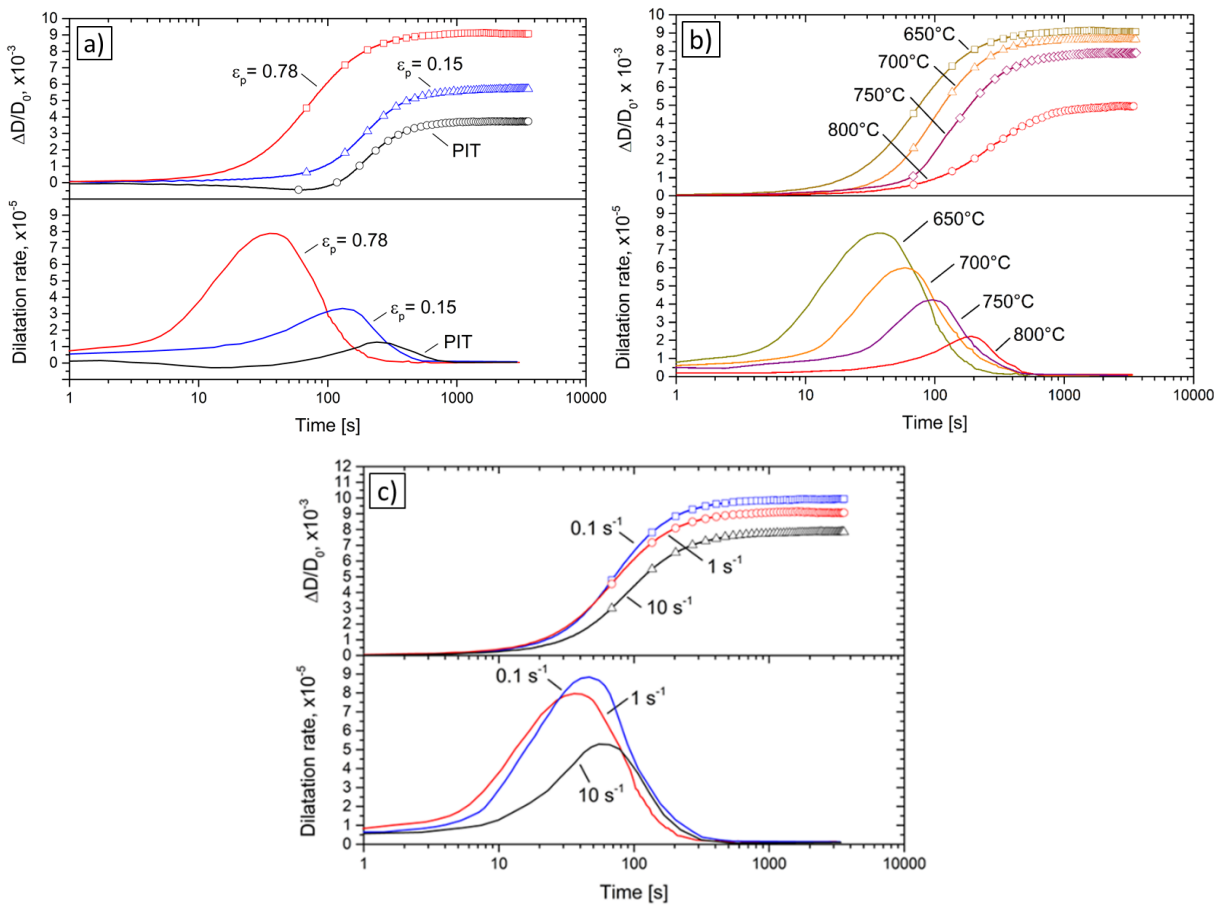


Fig. 5 Relative dilation and dilatation rate curves gathered during the isothermal tempering of specimens (a) treated with and without ausforming, (b) ausformed at various temperatures and (c) ausformed at various strain rates in comparison.

Fig. 5c depicts the influences of strain rate on the kinetics of bainitic transformation of investigated steel. In this work, it was found that the transformation rate was accelerated when lower ausforming strain rate was applied. It implied that increasing deformation rate generally led to a decrease in the amount of transformed bainite. The highest amount of transformed bainite was obtained at the strain rate of 0.1 s^{-1} . The result was inconsistent to the fact that higher strain rate increased both dislocation densities in prior austenite and nucleation sites for the bainitic transformation, which subsequently led to an acceleration of transformation kinetics. Chen et al. [29,40] performed experiments to examine effects of strain rate during ausforming on the kinetics of bainite transformation. It was though reported that such relation most likely occurred in some medium/low carbon steels, in which the ausforming caused the inconsistent mechanism of dislocation rearrangement.

3.4. Microstructure characteristics

Microstructure of the PIT specimens and specimens heat-treated and ausformed at 650°C with the strain rate of 1 s^{-1} up to the final strain of 0.78 were characterized by LOM and SEM, as demonstrated in **Fig. 6**. According to the used processing routes, three phases could form in the investigated steel, namely, BF, RA in thin film and/or block form and M/A constituent [39,40]. The presence of M/A constituent verified that the bainite transformation was incomplete. The amount of occurred martensite was consistent with the dilatation curves of the last cooling stage of the heat treatment with ausforming. By means of the color etching with Klemm's solution, in the LOM micrographs of specimens BF and martensite appeared as bright and dark brown areas, respectively, while RA was white zones [41], as illustrated in **Fig. 6a** and **6d**. The microstructures of PIT specimens showed a formation of highly elongated BF, RA, and martensitic structures, whereas those of specimens heat-treated with ausforming were obviously refined with reduced amount of martensite. This was due to that the movement of dislocations caused by ausforming increased the boundary areas of austenitic grain per unit volume and thus led to the refinement of BF and RA structures at the end of heat treatment [22,32]. Furthermore, SEM micrographs in **Fig. 6b** and **6e** exhibited well the effect of ausforming on the microstructure refinement. It is obvious

that the ausforming completely altered the microstructure of steel by replacing large blocks and elongated film-like areas with many tiny heterogeneous blocks and film-like morphologies. Observed microstructures at higher magnitude are depicted in **Fig. 6c** and **6f**. Hereby, the difference between RA and M/A constituent could be distinguished by their appearances. The RA phase was characterized in the form of either white thin-films located within sheaf-shape matrix of BF or island blocks with bright mellow appearance surrounded by matrix of granular BF. The M/A constituent was recognized as a mixture constituent, which consisted of martensite with rough appearance embedded within thin boundaries of RA, as shown with the red polygons in **Fig. 6c** and **6f**. The resulted microstructures of ausformed specimens were finer and more uniformly distributed. Though undesired M/A constituent could be considerably reduced by ausforming, the morphological distribution needed to be further controlled properly, since this may also affect the deterioration of ductility of steel [32]. Likewise, the amount of defects significantly depended on ausforming strain. Increasing the strain led to an increase in dislocation densities and splitting prior austenitic grains into several small sub-grain structures. Hereby, in the individual RA subsections, the area of growth was restricted and the ratio of carbon concentration per unit volume was increased that finally resulted in enhanced stability [7]. Furthermore, the variation of temperature and strain rate of ausforming also played an essential role in microstructure refinement due to static and dynamic recovery occurred [38,42]. When the temperature and/or strain rate of ausforming was increased, deformation induced dislocations partially vanished and the increase of sub-grains became more difficult. Hereby, the potential of grain refinement was greatly reduced and thus led to a formation of blocky RA and M/A constituent instead of film-like RA.

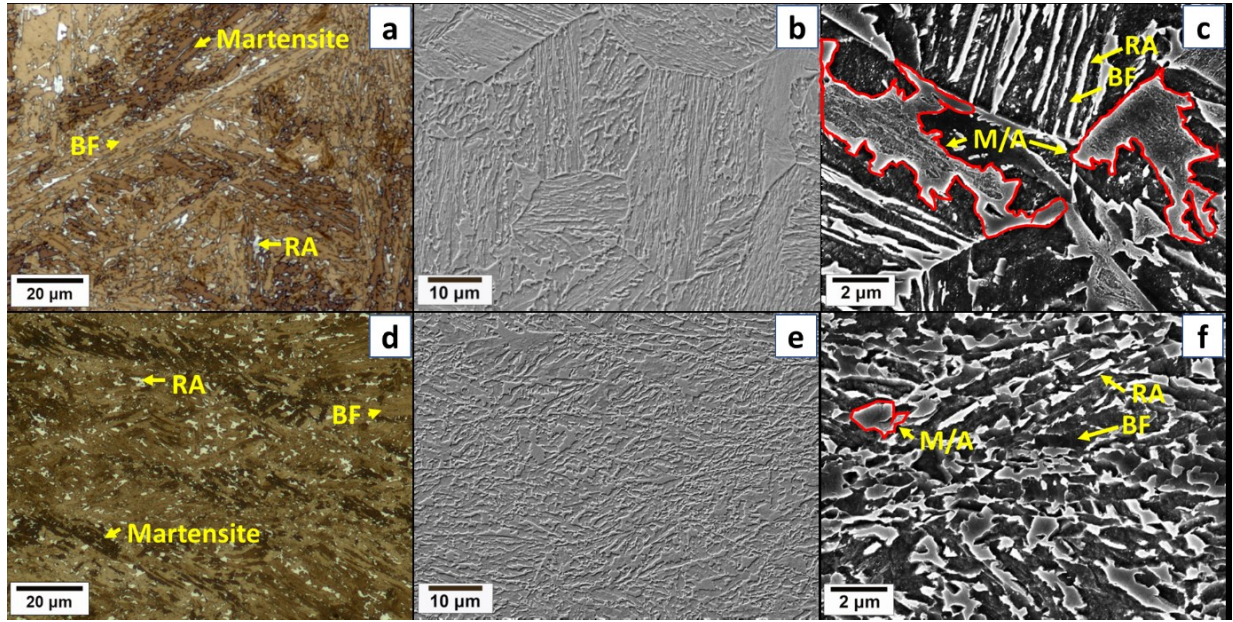


Fig. 6 Observed microstructures of specimens subjected to PIT (a-c) and ausforming (d-f) at 650 °C under the strain rate of 1 s^{-1} up to the strain of 0.78 and followed by isothermal tempering at 400 °C for 1 hr.

3.5. Phase fraction analysis

The XRD patterns of specimens undergoing various ausforming conditions were analyzed. The low relative intensity peaks of (111), (200), (220) and (311) planes, which took place at a diffraction angle of 43° , 48° , 74° , and 91° were corresponding with the diffraction planes of FCC-RA, while the other peaks concerned either BCC bainite or martensite. Note that for multiphase steels, it was relatively difficult to distinguish the pattern of the martensitic and bainitic phases, because both exhibited BCC pattern [43]. Thus, the XRD patterns obtained from the investigated steels in this work were classified into the BCC-BF and/or martensite with FCC-RA. The amount of RA was hereby calculated by means of the Rietveld refinement method incorporated with the XRD patterns. On the other hand, the area fraction of BF was estimated from LOM micrographs by an adaptive threshold method. Finally, phase fractions of martensite could be then calculated with the assumption that only three constituents, namely, RA, BF and martensite were formed in all ausformed specimens. As shown, in **Fig. 7** along with more details in **Table 2**, the phase fractions of RA and BF increased and that of martensite decreased with increasing the ausforming strain. On the other hand, increasing the ausforming temperature and strain rate noticeably caused

the reductions of RA and BF phase fractions while larger amount of martensite. This was due to grain refinement mechanism induced by ausforming, which contributed to mechanical stabilization of austenite by segmenting its grains into small sub-grains. Such enhanced austenite stability hindered the martensitic transformation. Moreover, the increase of BF phase fraction was likely because of acceleration of bainitic transformation affected by the mechanical driving force. It is noted that optimum phase fractions of examined steel would be 20% of RA, 65% of BF and 15% of martensite that were observed in the specimen deformed at the temperature, strain and strain rate of 650 °C, 0.78 and 0.1 s⁻¹, respectively. Additionally, rather high phase fraction of martensite of 63% was found in the PIT specimens due to the instability of austenite and somewhat lower formation rate of bainite.

3.6. Hardness

The macro-Vickers hardness values measured on the entire cross-sectional surface of all investigated specimens are provided in **Fig. 8**. It is seen that ausforming temperature, strain and strain rate considerably affected the hardness and thus strength of ausformed steel. The hardness decreased by increasing the ausforming strain, whereas it increased when the deformation temperature and strain rate became higher. These overall results agreed well with the ratio and individual hardness of all identified constituents in the thermo-mechanically treated specimens [44].

Table 2 Determined phase fractions of RA, BF and martensite by XRD and LOM. (Details of combination of temperature, strain, strain rate are found in **Table 1**)

Ausforming parameter	Deformation condition	RA _{XRD}	BF _{LOM}	M _{CAL}
Strain	PIT	3.2 ± 1.4	33.8 ± 3.9	63.0
	0.15	4.5 ± 0.9	38.4 ± 6.2	57.1
	0.78	18.7 ± 1.3	63.5 ± 5.6	17.8
Temperature (°C)	650	18.7 ± 1.3	63.5 ± 5.6	17.8
	700	16.5 ± 1.2	51.2 ± 6.5	32.3
	750	13.3 ± 1.5	48.8 ± 4.6	37.9
	800	8.9 ± 1.7	38.8 ± 4.9	52.3
Strain rate (s ⁻¹)	0.1	20.2 ± 1.5	64.7 ± 6.1	15.1
	1	18.7 ± 1.3	63.5 ± 5.6	17.8
	10	16.6 ± 1.2	61.7 ± 6.4	21.7

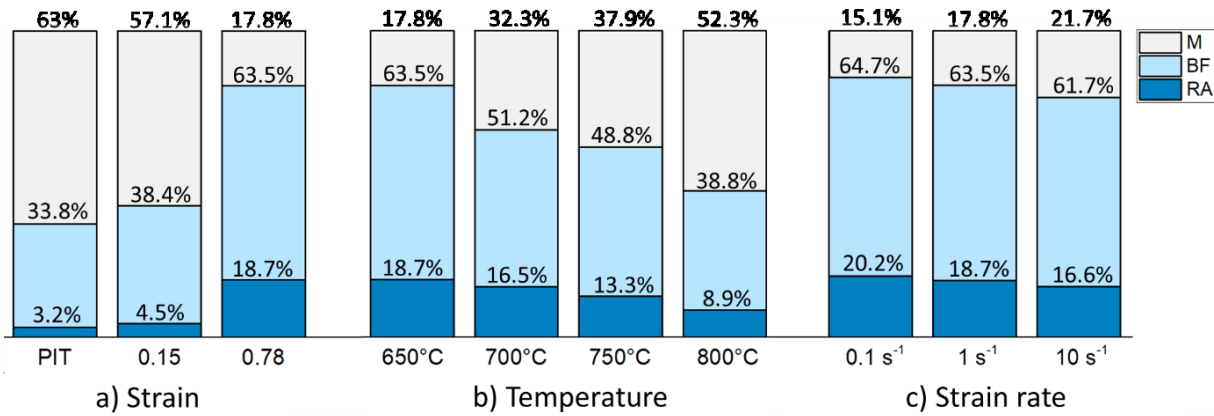


Fig. 7 Phase fractions of treated steels determined by a combination of XRD measurements (RA fraction) and image analysis using an adaptive threshold (BF). M, BF and RA stands for martensite, bainitic ferrite and retained austenite, respectively. (Details of combination of temperature, strain, strain rate are found in **Table 1**)

An increased martensitic phase fraction led to a higher hardness of specimens, while a reduction of hardness was caused by larger phase fraction of RA. The highest hardness of about 405 HV was obtained from the PIT specimens, which exhibited larger amount of martensite of 63% and a few RA of 3%. Nevertheless, the specimens deformed at 650 °C with strain and strain rate of 0.78 and 0.1 s⁻¹, respectively showed a relatively low hardness, in which 15% of martensite and 20% of RA were observed.

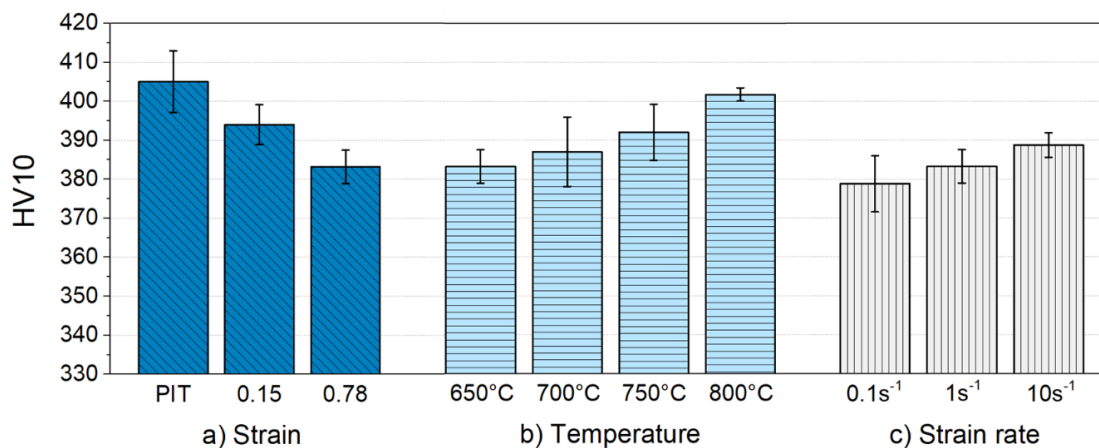


Fig. 8 Vickers hardness values as a function of different ausforming parameters: a) strain, b) temperature and c) strain rate. (Details of combination of temperature, strain, strain rate are found in **Table 1**)

4 Conclusions

The present study aimed to investigate the influences of ausforming temperature, strain and strain rate on the kinetics of isothermal transformation, microstructure characteristics and hardness of a low-carbon carbide-free bainitic steel. The conclusions can be drawn as follows:

- The applied ausforming accelerated the transformation kinetics and thus increased phase fraction of bainite in steel. This was due to the impact of mechanical driving forces on the decomposition of austenite.
- Ausforming temperature, strain and strain rate greatly affected both magnitude of defects and austenite grain size of steel. Its bainitic transformation kinetics was directly governed by the heterogeneous nucleation sites and stability of austenite.
- The ausforming refined the prior austenitic grains and increased the matrix strength. As a result, retained austenite was stabilized and thus led to lowered fractions of martensite.
- The final hardness of steel was defined by the martensitic phase fraction which depended on all ausforming parameters. The correlation between microstructure features and other mechanical properties will be further studied.

5. References

- [1] Barbacki A. The role of bainite in shaping mechanical properties of steels. *J. Mater. Process. Technol.* 1995;53(1):57–63.
- [2] Cornide J, Garcia-Mateo C, Capdevila C, Caballero FG. An assessment of the contributing factors to the nanoscale structural refinement of advanced bainitic steels. *J. Alloys Compd.* 2013;577:S43-S47.
- [3] Garcia-Mateo C, Caballero FG, Bhadeshia HKDH. Acceleration of Low-temperature Bainite. *ISIJ Int.* 2003;43(11):1821–5.
- [4] Caballero F.G., Garcia-Mateo C. The processing of nanocrystalline steels by solid reaction. In: Sung H. Whang, editor. *Nanostructured Metals and Alloys: Processing, Microstructure, Mechanical Properties and Applications*. Woodhead Publishing; 2011, p. 85–117.

-
- [5] Liu W, Zhang B, Zhao A, Guo H, Sun S. Control of morphology and dimension of blocky retained austenite in medium-carbon steel. *Mater. Res. Express* 2019;6(1):016526.
 - [6] Bhadeshia HKDH, Edmonds DV. Bainite in silicon steels: new composition–property approach Part 1. *Met. Sci. J.* 1983;17(9):411–9.
 - [7] Bhadeshia HKDH. Bainite in steels: Transformations, Microstructure and Properties. 2nd ed. London IOM Communications; 2001.
 - [8] Wang SC, Yang JR. Effects of chemical composition, rolling and cooling conditions on the amount of martensite/austenite (M/A) constituent formation in low carbon bainitic steels. *Mater. Sci. Eng., A* 1992;154(1):43–9.
 - [9] Lian J, Yang H, Vajragupta N, Münstermann S, Bleck W. A method to quantitatively upscale the damage initiation of dual-phase steels under various stress states from microscale to macroscale. *Comput. Mater. Sci.* 2014;94:245–57.
 - [10] Liu W, Liang J, Jiang Y, Zhang B, Zhao A. A study of blocky retained austenite and properties under variously heat-treated ultra-fine bainitic steel. *Mater. Res. Express* 2019;6(10):105607.
 - [11] Shimanov M, Korpala G, Terzic A, Kawalla R. Bainitic steels: their characteristics and applications. *Key Eng. Mater.* 2016;684:104–10.
 - [12] Matsuda H, Bhadeshia HKDH. Kinetics of the bainite transformation. *Proc. R. Soc. A* 2004;460(2046):1707–22.
 - [13] Yang HS, Bhadeshia HKDH. Designing low carbon, low temperature bainite. *Mater. Sci. Tech-Lond.* 2008;24(3):335–42.
 - [14] Ravi AM, Sietsma J, Santofimia MJ. Exploring bainite formation kinetics distinguishing grain-boundary and autocatalytic nucleation in high and low-Si steels. *Acta Mater.* 2016;105:155–64.
 - [15] Takahashi M. Recent progress: kinetics of the bainite transformation in steels. *Curr. Opin. Solid State Mater. Sci.* 2004;8(3-4):213–7.
 - [16] Bhadeshia HKDH. Nanostructured bainite. *Proc. R. Soc. A* 2010;466(2113):3–18.

-
- [17] Li S, Zhu R, Karaman I, Arróyave R. Development of a kinetic model for bainitic isothermal transformation in transformation-induced plasticity steels. *Acta Mater.* 2013;61(8):2884–94.
- [18] Jiang H, Wu H, Tang D, Liu Q. Influence of isothermal bainitic processing on the mechanical properties and microstructure characterization of TRIP steel. *J. Univ Sci. Technol. B.* 2008;15(5):574–9.
- [19] Saha-Podder A, Bhadeshia HKDH. Thermal stability of austenite retained in bainitic steels. *Mater. Sci. Eng., A* 2010;527(7-8):2121–8.
- [20] Shipway PH, Bhadeshia HKDH. Mechanical stabilisation of bainite. *Mater. Sci. Tech-Lond.* 1995;11(11):1116–28.
- [21] Yang JR, Huang CY, Hsieh WH, Chiou CS. Mechanical stabilisation for bainitic reaction in a Fe-Mn-Si-C bainitic steel. *J. Phys. IV France.* 1995;05(C8):497-502.
- [22] Zhao L, Qian L, Zhou Q, Li D, Wang T, Jia Z et al. The combining effects of ausforming and below-Ms or above-Ms austempering on the transformation kinetics, microstructure and mechanical properties of low-carbon bainitic steel. *Mater. Des.* 2019;183(108123):108123.
- [23] Meng JY, Zhao LJ, Huang F, Zhang FC, Qian LH. Isothermal transformation, microstructure and mechanical properties of ausformed low-carbon carbide-free bainitic steel. *Mater. Sci. Forum* 2018;941:329–33.
- [24] Yang HS, Bhadeshia HKDH. Austenite grain size and the martensite-start temperature. *Scr. Mater.* 2009;60(7):493–5.
- [25] Zhao J, Jia X, Guo K, Jia NN, Wang YF, Wang YH et al. Transformation behavior and microstructure feature of large strain ausformed low-temperature bainite in a medium C-Si rich alloy steel. *Mater. Sci. Eng., A* 2017;682:527–34.
- [26] Golchin S, Avishan B, Yazdani S. Effect of 10% ausforming on impact toughness of nano bainite austempered at 300 °C. *Mater. Sci. Eng., A* 2016;656:94–101.

-
- [27] Gong W, Tomota Y, Adachi Y, Paradowska AM, Kelleher JF, Zhang SY. Effects of ausforming temperature on bainite transformation, microstructure and variant selection in nanobainite steel. *Acta Mater.* 2013;61(11):4142–54.
- [28] Chen G, Xu G, Hu H, Yuan Q, Zhang Q. Effect of strain rate on deformation resistance during ausforming in Fe-C-Mn-Si high-strength bainite steels. *Steel Res. Int.* 2018;89(11):1800201.
- [29] Singh SB, Bhadeshia HKDH. Quantitative evidence for mechanical stabilization of bainite. *Mater. Sci. Tech-Lond.* 1996;12(7):610–2.
- [30] He BB, Xu W, Huang MX. Effect of ausforming temperature and strain on the bainitic transformation kinetics of a low carbon boron steel. *Philos. Mag.* 2015;95(11):1150–63.
- [31] Wirths V. Prozessführung und zyklisches Werkstoffverhalten von karbidfreien bainitischen Stählen [Doctoral thesis]. Aachen: Rheinisch-Westfälischen Technischen Hochschule Aachen; 2016.
- [32] Zhao L, Qian L, Liu S, Zhou Q, Meng J, Zheng C et al. Producing superfine low-carbon bainitic structure through a new combined thermo-mechanical process. *J. Alloys Compd.* 2016;685:300–13.
- [33] Ferraris SA, Danón CA. Desdoblamiento de la transformación martensítica en un acero F82H de activación neutrónica reducida. *Matéria (Rio J.)* 2018;23(2):1–10.
- [34] Tao X, Han L, Gu J. Splitting phenomenon in martensitic transformation of X12CrMoWVNbN10-1-1 steel. *Int. J. Mater. Res.* 2015;105(6):565–71.
- [35] Gui X, Gao G, Guo H, Zhao F, Tan Z, Bai B. Effect of bainitic transformation during BQ&P process on the mechanical properties in an ultrahigh strength Mn-Si-Cr-C steel. *Mater. Sci. Eng., A* 2017;684:598–605.
- [36] Tian J, Xu G, Jiang Z, Wan X, Hu H, Yuan Q. Transformation behavior and properties of carbide-free bainite steels with different Si contents. *Steel Res. Int.* 2019;90(3):1800474.
- [37] Zou H, Hu H, Xu G, Xiong Z, Dai F. Combined effects of deformation and undercooling on isothermal bainitic transformation in an Fe-C-Mn-Si alloy. *Met.* 2019;9(2):138.

-
- [38] Hu H, Xu G, Dai F, Tian J, Chen G. Critical ausforming temperature to promote isothermal bainitic transformation in prior-deformed austenite. *Mater. Sci. Tech-Lond.* 2019;35(4):420–8.
- [39] Guo H, Feng X, Zhao A, Li Q, Chai M. Effects of ausforming temperature on bainite transformation kinetics, microstructures and mechanical properties in ultra-fine bainitic steel. *J. Mater. Res. Technol.* 2019;9(2):1151.
- [40] Fan HL, Zhao AM, Li QC, Guo HH, He JG. Effects of ausforming strain on bainite transformation in nanostructured bainite steel. *Int. J. Miner. Metall. Mater.* 2017;24(3):264–70.
- [41] Kučerová L, Opatová K, Jandová A. Metallography of AHSS steels with retained austenite. In: *Microscopy and imaging science: Practical approaches to applied research and education*, p. 455–463.
- [42] Seshacharyulu T, Dutta B. Influence of prior deformation rate on the mechanism of $b \rightarrow a+b$ transformation in Ti–6Al–4V. *Scr. Mater.* 2002;46:673–8.
- [43] Talebi S, Ghasemi-Nanesa H, Jahazi M, Melkonyan H. In situ study of phase transformations during non-isothermal tempering of bainitic and martensitic microstructures. *Met.* 2017;7(9):346(1–13).
- [44] Wang X, Zurob HS, Xu G, Ye Q, Bouaziz O, Embury D. Influence of microstructural length scale on the strength and annealing behavior of pearlite, bainite, and martensite. *Metall. Mater. Trans. A* 2013;44(3):1454–61.

Chapter III

Kinetic model development of isothermal bainitic transformation of low carbon steels under ausforming conditions

Theerawat Kumnorkaew, Junhe Lian, Vitoon Uthaisangsuk, and Wolfgang Bleck

Alloys 2022; 1(1): 93-115

<https://doi.org/10.3390/alloys1010007>

Chapter III proposes a unified physics-based model to elaborate thermodynamic factors, including driving energy and activation energy interplayed with the kinetics of isothermal bainitic transformation by considering the effect of ausforming strain and alloy modification. The model is derived from the classical nucleation rate theory based on a modified T_0 concept and combined with the empirical Koistinen-Marburger (KM) equation. The nucleation rate dependence changes in activation energy, driving pressure, and carbon enrichment caused by the process contributions are also correlated with the kinetics of isothermal bainitic transformation. By means of the model, the thermodynamic stability of austenite can be appropriately adjusted with an optimal design of the processing parameters of the ausforming and alloy modification of low-carbon CFB steels. Regarding mechanical stabilization of austenite, dislocation density involving ausforming and the impact of chemical compositions are roughly estimated by XRD analysis.

Kinetic Model of Isothermal Bainitic Transformation of Low Carbon Steels under Ausforming Conditions

Theerawat Kumnorkaew^{a,*}, Junhe Lian^b, Vitoon Uthaisangsuk^c, and Wolfgang Bleck^a

^a Steel Institute, RWTH Aachen University, 52072 Aachen, Germany;

^b Department of Mechanical Engineering, Aalto University, 02150 Espoo, Finland;

^c Center for Lightweight Materials, Design and Manufacturing, Department of Mechanical Engineering, King Mongkut's University of Technology Thonburi, 10140 Bangkok, Thailand;

theerawat.kumnorkaew@iehk.rwth-aachen.de; junhe.lian@aalto.fi; vitoon.uth@kmutt.ac.th;
bleck@iehk.rwth-aachen.de

Abstract:

Carbide-free bainitic steels show attractive mechanical properties but are difficult to process because of the sluggish phase transformation kinetics. A macroscopic model based on the classical nucleation theory in conjunction with the modified Koistinen–Marburger relationship is proposed in this study to simulate the kinetics of incomplete bainitic and martensitic phase transformations with and without austenite deformation. A 0.26C-1Si-1.5Mn-1Cr-1Ni-0.003B-0.03Ti steel and a 0.18C-1Si-2.5Mn-0.2Cr-0.2Ni-0.002B-0.03Ti steel were investigated with different levels of ausforming. The concept of ausforming is expected to accelerate the onset of the bainitic transformation and to enhance the thermodynamic stability of austenite by increased dislocation density. The phase transformation kinetics of both steels is quantitatively analyzed in the study by dilatometry and X-ray diffraction so that the carbon concentration in the retained austenite and bainitic ferrite, as well as their volume fractions, is determined. A critical comparison of the numerical and experimental data demonstrates that the isothermal kinetics of bainite formation and the variation of driving energy can be satisfactorily described by the developed model. This model captures the incompleteness of the bainite phase transformation and the carbon enrichment in the austenite well. A fitting parameter can be used to elucidate the initial energy barrier caused by the ausforming. An increase in austenite stability can be described by the nucleation reaction and the thermodynamic energies associated with the change of dislocation density. The proposed model

provides an in-depth understanding of the effect of ausforming on the transformation kinetics under different low-carbon steels and is a potential tool for the future design of heat treatment processes and alloys.

Keywords: Bainitic steels; phase transformation; ausforming; carbon enrichment; activation energy; dislocation density

1. Introduction

Controlling the thermodynamic stability of austenite has been a challenging issue in the development of carbide-free bainitic (CFB) steels when considering carbon as an essential element for a bainitic transformation at low temperatures. With an addition of 1.5%wt and %Si, the decomposition of austenite occurs when supersaturated carbon from bainitic ferrite is rejected into adjacent austenitic regions and becomes robustly available for stabilization during the bainitic transformation instead of forming cementite (Fe_3C) [1–4]. The increased stability of the neighboring austenite via the enrichment of carbon thus leads to an incompleteness of the transformation that leaves two different features of the retained austenite (RA) as the secondary phase, namely film-like RA and blocky-type RA. These features of RA can be characterized by their stabilities in accordance with chemical contributions that can be statistically estimated by atom probe tomography (APT) [5,6]. The carbon-rich, thin-film RA is always more stable compared to the other type [7–10]. In light of the thermodynamic stability, Garcia Mateo et al. [11] reported that the blocky RA could also be present in various granular morphologies, depending on the carbon concentration. The morphologies with low carbon content, particularly in the central zone, are prone to decompose further into fresh martensite (FM) during ambient cooling. Even though the formation of FM is beneficial in some applications that require material with high hardness, strength, and wear resistance (e.g., railway material and agricultural parts, etc.), the existence of such a hard phase is usually an impairment when the transformation-induced plasticity (TRIP) effect is desired [3]. Therefore, the recent progress in bainitic forging steel development is aimed at refining the microstructures by means of replacing the large granular blocky RA with nano-structured film-like RA. For instance, Caballero et al. and Garcia-Mateo et al. [12,13] exploited the T_0 concept as a thermodynamic limit of CFB transformation to design advanced carbon CFB steels with an ultra-fine structure (RA thickness < 100 nm). They achieved

prominent steel properties, including strength and elongation of about 2.2–2.5 GPa and 20–30%, respectively. However, the concept is successful only in high- and medium-carbon steels (0.4–1.0 wt.%C), whereby transformation at very low temperatures above the martensite start temperature is necessary. Despite the attempt to take low-carbon steels (<0.2%C) into account, higher Gibbs free energy, associated with the insufficient C enrichment in austenite affected by the lower bulk density of C, has promoted the thermal instability of the austenite during the cooling process after isothermal holding.

Yao et al. [14] proposed an alloying modification strategy and considered a chemical Gibbs free energy change of the FCC to BCC transformation. An addition of 1.5%Ni encourages the austenite stability by means of enlarging the austenitic phase region so that an increase in the free energy difference retards the kinetics of the bainitic transformation and induces a reduction in the bainitic ferrite (BF) plate thickness. However, although the energy reduction due to another supplement of 1.5%Cr favors the bainitic transformation, a formation of iron carbide (Fe_3C) consequently deteriorates the thermal stability of the austenite. Herein, the stability of austenite likely depends on the free energy difference between the parent and the child phases. As a consequence, both Cr and Ni alloyed in nearly equivalent compositions, which causes another reduction in the driving energy by ~ 400 J/mol; thus, this is expected to enhance the thermal stability of austenite and stimulate bainitic transformation simultaneously. Hence, the enhanced stabilization of austenite is feasible by adjusting an appropriate amount of Cr and Ni addition in the concerned steel. Changle et al. [15] stated that steels alloyed with Mn content over 2.2 wt.% provide an excellent hardenability and a lower bainitic start temperature (B_s), which in turn yields an 18% volume fraction of retained austenite with a reduction in BF laths. Mn as a solid solution element is evidently effective in raising the free energy of ferrite and reducing that of austenite, causing a delay of austenite decomposition to bainite at low temperatures. Nevertheless, if the Mn content in bainitic steel exceeds its limitation and segregation occurs at the prior austenite grain boundaries, it may lead to an increase in transformation temperature and undesired brittleness.

Ausforming is one of the thermomechanical treatment processes, in which the structure of austenite is refined at its metastable temperature prior to phase transformation. The deformation plays an important part in accelerating the bainitic transformation due to increased bainitic nucleation sites, whereas raised dislocation density encourages the thermal stability of austenite.

The process parameters of ausforming, such as deformation temperature, strain, and strain rate, are also reported as being the essential controlling parameters of the kinetics of isothermal bainitic transformation [16]. A sophisticated result showed that the stability of austenite is not improved when a severe ausforming strain of 50% is applied, because of a high BF volume fraction. It is noticed that such a result is confirmed in a few works concerning low-carbon steels [17,18]. Although these qualitative conclusions can be applied to optimize the microstructure of CFB steels, a reliable physical-based model for correlating the alloying composition with processing parameters is still required because the variations of both the alloy design and the process parameters are very high. Several models have been developed for describing phase transformation of alloys, but one proposed by Bhadeshia and his co-workers has been widely employed [19,20]. Their model is based on a displacive approach, by which bainite growth without diffusion of any alloying elements is considered. In this approach, bainite formation is assumed to begin at prior nucleation sites on austenite grain boundaries and to successively form by autocatalytic nucleation at the newly formed sheaves. Consequently, the transformation of bainite is a nucleation-controlled process. The prior austenite grain size and the maximum driving energy are essential factors controlling the nucleation kinetics of bainitic transformation. Later, Magee [21] revealed that the number of nucleation sites as a function of prior austenite grain size should also be considered and can be determined by the driving energy difference. It is increased with a rise in undercooling. Van Bohemann formulated this concept to estimate the number of potential embryos for martensitic nucleation [22]. However, these displacive models use empirical constants by which the activation energy is only represented a net free energy used to activate the transformation. In the model of isothermal martensitic transformation proposed by Ghosh and Olsen [23], an energy barrier consistent with the critical driving energy needed for the nucleation should be incorporated by the sum of the strain energy, the defect-size-dependent interfacial energy, and the composition-dependent interfacial work [24]. They also introduced a model that takes autocatalytic factors into account as material constants. The effectiveness of the γ/α interface boundaries and the thickness of the bainitic plate play a significant role in the overall transformation kinetics. Meng et al. [25] reported that morphological features also affect internal stresses by the autocatalytic nucleation of martensite. A stress field, which disperses outside a transformed martensite plate, is potentially capable of triggering unstable martensite embryos to become stable nuclei and then grow up. Zou et al. [26] studied the effects of prior deformation and undercooling on the isothermal bainitic

transformation. They found that the pre-deformation provides a mechanical driving force, which further enhances the nucleation rate of bainite transformation, in addition to stresses internally generated by the dislocation density when new bainite plates are formed. Moreover, the difference in the activation energies between grain boundary nucleation and autocatalytic nucleation is proposed by Ravi et al. [27]. The autocatalytic nucleation, which is considered to have a dynamic nature, has been controlled by the degree of carbon enrichment in austenite during the transformation. Nevertheless, an empirical constant, which involves the autocatalytic term, remains undefined with any physical significance.

From the previous studies, it can be concluded that a more precise model of the bainitic transformation, especially for an ausforming process of low-carbon steels, is still to be developed. Thus, in this work, a unified physics-based model is derived to thoroughly elucidate the isothermal bainitic transformation, while taking into consideration varying ausforming strain and alloy modifications. The model is derived from the theoretical basis of the displacive transformation concerning a modified T_0 concept and the empirical Koistinen–Marburger (KM) equation. The activation energy, nucleation rate, and carbon enrichment variations caused by the process contributions are also correlated with the kinetics of isothermal bainitic transformation. By means of the model, the thermal stability of austenite can be appropriately adjusted with an optimal design of the processing parameters of the ausforming and alloy modification of low-carbon CFB steels.

2. Materials and Methods

2.1. As-Received Materials

Two as-received low-carbon steels of different compositions were chosen. The steels are identified as MC1.5Mn1NiCr and LC2.5Mn0.2NiCr steels. The chemical compositions of both steels are represented in Table 1. Manganese as the former austenite element was added to increase the stability of the retained austenite and properly elevate the hardenability of the steels. Silicon was alloyed in the amount of 1 wt.% for retarding and suppressing the formation of cementite in the bainitic structure so that retained austenite as a secondary phase was promoted. The addition of boron was to provide a shift of the diffusion-controlled ferrite/pearlite transformation to a longer time. A precipitation of boron nitride in solid solution was suppressed by alloying titanium of about 0.03 wt.%, whereas the interaction of nitrogen and titanium in the form of titanium nitride

(TiN) could be formed. The steels were individually melted in a laboratory-scale vacuum arc furnace and cast into a square ingot with a dimension of $140 \times 140 \times 525$ mm. Afterwards, the ingots were homogenized at 1250°C for 2 h, then hot-forged into square billets with a dimension of $60 \times 60 \times 1000$ mm at a finishing temperature of 950°C . The billets were slowly cooled down to room temperature. Finally, the homogenized billets were cut parallel to the forged direction to manufacture cylindrical specimens of 10 ± 0.1 mm height and 5 ± 0.1 mm diameter.

Table 1. Chemical composition of the investigated steels in wt.%.

Steel	Fe	C	Si	Mn	Cr	Ni	B	Ti
MC1.5Mn1NiCr	Bal.	0.26	1.07	1.46	0.99	0.98	0.0031	0.027
LC2.5Mn0.2NiCr	Bal.	0.18	0.97	2.50	0.20	0.21	0.0018	0.033

2.2. Experiment

The cylindrical specimens were subjected to three different heat treatment conditions. These heat treatments are distinguished between quenching and isothermal tempering, with and without austenite deformation, as follows: direct quenching (DQ), pure isothermal tempering (PIT), and ausforming followed by isothermal tempering (AIT). All heat-treating experiments were conducted on a Bähr DIL805A/D dilatometer. The machine was additionally equipped with an optical module for cross-sectional measurement, which enabled a precise investigation of the phase transformations by monitoring changes in the length of the specimen in the longitudinal and radial directions. A Pt/Pt-10 Rh thermocouple (type S) was spot-welded at the central edge of the specimens so that the temperature signal was accurately gathered from the machine. The experiments were conducted within a vacuum chamber where the specimens were located in the middle between two quartz rods inside an induction coil. A cooling gas, e.g., helium, was directly fed into the chamber through a pressure control valve. The desired temperature could be achieved by balancing the heating coil and the cooling gas. A deformation module was also installed for uniaxial compression tests. As a result, the relative volume strains were determined by considering the profile variations of the specimens in the radial and longitudinal directions, as follows [28,29].

$$\Delta V/V_0 = (1 + \varepsilon_L)(1 + \varepsilon_R)^2 - 1 \quad (1)$$

where ΔV represents the volume change of specimen, V_0 is the initial volume, ε_L is the longitudinal strain, and ε_R is the radial strain of the specimen.

For all the experiments, the specimens were first heated to the austenitizing temperature at 950 °C, at the rate of 18 °C/s, and soaked for 5 min for homogenization. The PIT specimens were subsequently cooled to 400 °C at a cooling rate of 50 °C/s and isothermally treated for 1 h before cooling to room temperatures at 20 °C/s. The AIT specimens were cooled after homogenization to a deformation temperature of 650 °C at the same rate and held for 10 s. The specimens were subsequently deformed with an ausforming strain of either of 0.15 (AIT0.15) or 0.35 (AIT0.35), at a rate of 1 s⁻¹, and cooled to the isothermal temperature within the same period, as was conducted for the PIT samples. To examine changes in the martensite start (M_s) temperature, a specimen of each material was directly quenched from the austenitizing temperature. It was defined as the DQ specimen, and the volumetric expansion result was set as a reference. The M_s locus of the DQ specimens was captured from the first deviation of the dilation curve during cooling, whereas that of the AIT specimens was traced in the same manner specifically during the secondary stage of cooling after isothermal tempering. In the case of the DQ specimens, the volumetric transformations of the martensite were calculated by using a total volumetric expansion with respect to the relative tangent of the dilatation curve as a reference, bearing in mind that in this research the M_s temperature was also empirically estimated, using the following equation [30,31].

$$M_s = 539 - 423x_C - 30.4x_{Mn} - 7.5x_{Si} + 30x_{Al} \quad (2)$$

where x_C , x_{Mn} , x_{Si} , and x_{Al} are the carbon, manganese, silicon, and aluminum contents in wt.%, respectively. The specimens for evaluating the prior austenite grain (PAG) were directly quenched from the ausforming stage to room temperature.

2.3. Characterization

In the beginning, the specimens were ground and polished with abrasive papers (grids no. 600, 1200, 2400, and 4000) and 0.1 μm diamond paste, respectively. For the PAG observation, they were chemically etched using 4 g of sodium dodecylbenzene sulfonic acid in 100 mL of aqueous saturated picric acid diluted in 100 mL of distilled water in a water bath. The optimized temperature and time for etching were 60 °C and 30 s, respectively. After etching, the average grain size of PAG (d_γ) was measured on a light optical microscope (LOM) and calculated by using

the linear intercept method based on the ASTM112-12 standard [32]. The same preparation techniques were applied to the specimens for phase quantification by X-ray diffraction (XRD) measurement, except for the solution etching. Hence, after the polishing step, all the specimens were further electro-polished by means of a TenuPol-5 single-jet electropolishing device. An A2 electrolyte was employed at room temperature with a voltage of 32 V and a flow rate of 15 mm/s. The XRD machine was operated using a filtered CrK α radiator at 40 kV and 30 mA, under the collection range between 60° and 165°, at a step width of 0.08° and a counting time of 2 s. The phase fractions of face-centered cubic (FCC) RA and body-centered cubic (BCC) bainitic ferrite or/and martensite were analyzed by the Rietveld's refinement method, using MAUD software. The carbon concentration of the retained austenite (x_C in wt.%) was estimated from its lattice parameter (a_γ), as given in Equation (3) [33]. The parameters x_{Ni} , x_{Cr} , x_N , x_{Co} , x_{Cu} , x_{Nb} , x_{Mo} , x_{Ti} , x_V , and x_W are the nickel, chromium, nitrogen, cobalt, copper, niobium, titanium, vanadium, and tungsten contents in wt.%, respectively.

$$a_\gamma(\text{\AA}) = 3.5780 + 0.0330x_C + 0.00095x_{Mn} - 0.0002x_{Ni} + 0.0006x_{Cr} \\ + 0.0056x_{Al} + 0.0220x_N + 0.0004x_{Co} + 0.0015x_{Cu} + 0.0051x_{Nb} \\ + 0.0031x_{Mo} + 0.0039x_{Ti} + 0.0018x_V + 0.0018x_W \quad (3)$$

Apart from phase quantification, the Rietveld method, which involves the Fourier analysis of the broadened peaks, was used to evaluate the microstructure parameters, such as the effective crystallite size and the average microstrain within the crystal [34]. Considering the plastically deformed materials, the Popa model was used to deconvolute the size and strain effect in the deformed crystals in accordance with the anisotropic size–strain broadening [35]. The peak shifting, broadening, and asymmetry experienced by the line profiles because of the accumulation of irradiation defects were analyzed using the Warren model [36]. The dislocation density due to the crystallite size contribution (ρ_C) was defined as the length of dislocation line per unit volume of crystal and could then be estimated using the Williamson and Smallman relation [37].

$$\rho_C = 3/D^2 \quad (4)$$

where D is the average crystal size. On the other hand, the dislocation density due to the contribution of the microstrain (ρ_S) was evaluated by the following relation.

$$\rho_S = k \frac{\langle \varepsilon_l^2 \rangle}{b^2} \quad (5)$$

where k is a material constant ($k = 0.9$ for cubic crystal), ε_l is the microstrain within the crystal domain, and b is the Burgers vector. Likewise, the average dislocation density (ρ) could be estimated from the relationship given as follows.

$$\rho = \sqrt{\rho_C \rho_S} \quad (6)$$

In order to determine the dislocation density for the bainitic transformation range, only the PIT, AIT0.15, and AIT0.35 specimens were taken into consideration. The dislocation density value of the PIT specimen was used as a reference and further compared with that of each AIT specimen so that the dislocation density influenced by the ausforming strain was calculated.

3. Transformation Models

3.1. Transformation Models

According to the thermodynamic principle of bainitic transformation [3,38,39], it has been suggested that if bainite forms under the displacive approach, the transformation can occur when the criteria of $\Delta G_m < \Delta G_N$ and $\Delta G^{\gamma \rightarrow \alpha} < -G_{SB}$ are satisfied. The first criterion is defined for the nucleation process, and the latter is for displacive growth. ΔG_m represents the maximum driving force available for the para-equilibrium nucleation. ΔG_N is the universal nucleation function, which was experimentally determined by Ali and Bhadeshia [40]. $\Delta G^{\gamma \rightarrow \alpha}$ is associated with a stored energy difference between austenite and bainite, and G_{SB} is a stored energy of bainite, which is usually considered to be 400 J/mol. A further suggestion is that ΔG_m and $\Delta G^{\gamma \rightarrow \alpha}$ are dependent on the chemical compositions of steel and undercooling [3]. The temperatures at which $\Delta G_m = \Delta G_N$ and $\Delta G^{\gamma \rightarrow \alpha} = -G_{SB}$ are called the T_h and T'_0 temperatures, respectively. Hence, it is understood that bainitic transformation can only occur when the transformation temperature is below both temperatures. In any silicon-rich steels in which the formation of cementite is most likely impossible, the concept of T'_0 can be used to indicate the incompleteness phenomena of bainitic transformation. This is with respect to carbon, which is only enriched into the adjacent austenite, instead of forming cementite, during the decomposition of austenite into bainite. The temperature is thus defined as a locus where the enrichment process of carbon ceases [10,41]. For

steels subjected to ausforming, a prior austenite grain is subdivided into several subgrains by plastic deformation such that it gives a greater defects per unit volume in an austenite grain, as shown in **Fig. 1a**. The sub-grain boundaries acting as additional defects give rise to more nucleation sites which will then facilitate the bainitic transformation. Therefore, the deformation leads to an increase in austenite free energy and enables more carbon enrichment in austenite at the beginning stage of the transformation. However, on the other hand, the dislocations generated by the growth process will arrest the transformation as it reduces the austenite free energy, as presented in **Fig. 1b**.

3.1.1. Nucleation Rate Model

By the displacive approach, the kinetics of the bainitic transformation is controlled by a nucleation rate reaction. Firstly, sub-units of bainitic ferrite (BF) are formed by activated nucleation at the interfaces of the austenite grain boundary (γ/γ interface) and the subsequent autocatalytic nucleation on the pre-existing platelets surrounding the UA (γ/α interface) [27]. The former process incorporates prior austenite grain, while the latter is essential for the growth of BF sheaves, which might arise spontaneously at the tip of previously formed sub-units due to elastic and plastic strain generations within the surrounding austenite [42].

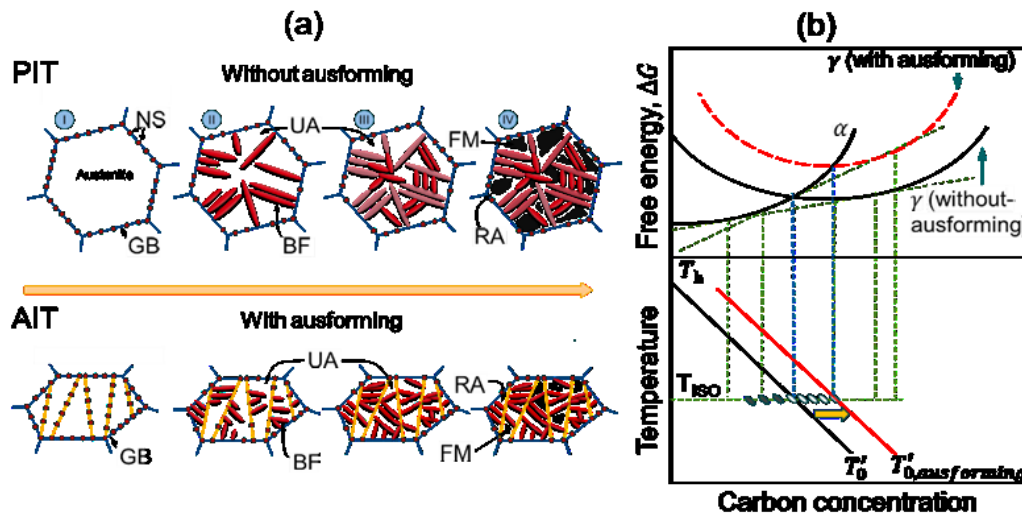


Fig. 1 (a) Graphical illustrations of the isothermal decomposition of austenite into bainite for PIT and AIT specimens, and (b) schematic diagram showing relationships of Gibbs free energy, temperature, and composition of steels under various heat treatments. NS, GB, UA, BF, and FM

stand for nucleation site, grain boundary, untransformed austenite, bainitic ferrite, and fresh martensite, respectively.

According to this hypothesis, the processes have successively continued to form bainitic sheaves until their evolutions were arrested by the mechanical stabilization of austenite. Therefore, the development of these nucleation mechanisms can be expressed as follows.

$$\left(\frac{dN}{dt}\right)_t = \left(\frac{dN}{dt}\right)_{GB} + \left(\frac{dN}{dt}\right)_{AN} \quad (7)$$

where (dN/dt) is the total nucleation rate per unit volume, $(dN/dt)_{GB}$ and $(dN/dt)_{AN}$ are the nucleation rate per unit volume arising at the austenite grain boundaries and that caused by the autocatalytic nucleation, respectively. Considering the individual nucleation rate reaction, the density of the potential nucleation sites and the activation energy play a vital role in describing the principle of the nucleation kinetics, which is expressed by Equation (8).

$$\left(\frac{dN}{dt}\right)_i = \frac{k_B T}{h} N_i \exp\left(\frac{Q_i^*}{RT}\right) \quad (8)$$

where the subscript i represents either a nucleation process at the grain boundary (GB) or the successive nucleation by autocatalytic reaction (AN). k_B is the Boltzmann constant, T is the isothermal transformation temperature, h is the Plank constant, N_i is the number of potential nucleation sites at the very beginning stage, R is the gas constant, and Q_i^* is the activation energy required for the individual nucleation process. With respect to the original Koistinen–Marburger (KM) equation [43], Van Bohemann and Seitma indicated that the nucleation density is associated with the net driving energy and undercooling [22]. The driving energy is associated with thermodynamic activation, and it thus requires two atomic processes to trigger the reaction. On the one hand, the dissociation of certain dislocation defects may partially facilitate sites for BF embryos. On the other hand, the enrichment of carbon into the surrounding austenite matrix allows a necessarily available driving force for the nucleation.

3.1.2. Activation Energy

As the activation energy accounts for the thermodynamic requirements of the nucleation processes, any energies stored within the parent phase can be presumed to be the parts of the energy barrier

necessary for the isothermal transformation. As reported by Olsen and Cohen [44], the activation energy can be determined independently with the free energy sum, as expressed by Equation (9).

$$Q_i^* = Q_0^* + K_1 \Delta G_i \quad (9)$$

where Q_0^* is considered to be the activation energy when the nucleation process is absent, given here as a fitting parameter. However, Q_0^* can be also used to estimate the existing energy required for the phase transformation when no chemical energy is involved and only the effects of undercooling and ausforming are occupied; K_1 is a fitting parameter in the model; and ΔG_i is the total molar driving force of the associated event of nucleation.

In the present study, the extra stored energy due to the deformation of austenite is formulated based on the assumption that no dynamic recrystallization occurred. Thereby, the deformation likely introduces only two energy portions to the austenite, namely the grain boundary and the change of dislocation energy. The variation of these energies depends on two factors. Firstly, the deformation elongates the austenite grains and enhances the grain boundary areas. Secondly, the deformation increases the disorder of the grain structure, which leads to an increase in the grain boundary energy per unit area ($\sigma_{\gamma/\gamma}$), roughly 10% [45,46]. Note that it is not significantly increased if the deformation stress is relatively small. However, the total driving energy required for the grain boundary nucleation is not included the effect of an increase in the number of nucleation sites because it is already involved in the initial activation energy term. The total molar driving force can thus be represented by Equation (10).

$$\Delta G_{GB} = \Delta G_{ch} + \Delta G_{\gamma/\gamma} \quad (10)$$

where ΔG_{ch} is the difference in thermodynamic Gibbs free energy between the austenite and the bainite, determined by using the MUCG83 database [47], and $\Delta G_{\gamma/\gamma}$ is the semi-coherent interfacial energy of the γ/γ interfaces required to overcome its barrier, which can be expressed as the following relationship.

$$\Delta G_{\gamma/\gamma} = 2V_{mol} \frac{\sigma_{\gamma/\gamma}}{nd} \quad (11)$$

V_{mol} is the molar volume of austenite, $\sigma_{\gamma/\gamma}$ is the semi-coherent interfacial energy at the γ/γ interfaces, n is the number of FCC cubic planes along the nucleus thickness, and d is the spacing between the cubic planes, which equals 2.5×10^{-10} m for the FCC planes [44].

Considering the spontaneous association of the nucleation events, the driving force is related to the elastic and plastic stresses generated in the adjacent austenite. In addition to the chemical driving energy change owing to the variations of carbon in BF, the stored energy associated with the stress field can also provide a particular strain accompanying the stress-energy in the surrounding austenite, due to the dislocation barrier that significantly affects the bainitic transformation. Consequently, the semi-coherent interfacial energy between austenite and bainite (γ/α interfaces), established by Dong et al. [45], is a straightforward representation of the subsequent stage of the transformation. Therefore, the total driving energy required for the iterative dynamic nature of the autocatalytic nucleation is represented by Equation (12).

$$\Delta G_{\text{AN}} = \Delta G_{\text{chA}} + \Delta G_{\gamma/\alpha} + G_{\text{dislo}} \quad (12)$$

Parameter ΔG_{chA} is the chemical free energy change depending on the degree of carbon enrichment in the austenite. $\Delta G_{\gamma/\alpha}$ is the semi-coherent interfacial energy between the austenite and bainite (γ/α interfaces). G_{dislo} is the dislocation interaction energy because of the bainitic stress field. The carbon rejected from BF during the transformation is thus specified by the chemical driving energy reduction, while the interfacial energy at the γ/α interfaces is neglected afterwards because its influence is negligible compared to the other factors [44]. Rees and Bhadeshia [20] suggested that the decrease in total energy change is caused by a mechanically induced stabilization surrounding the enrichment zone. Thus, the chemical energy change is then determined as shown in Equation (13).

$$\Delta G_{\text{chA}} = \Delta G_{\text{chAi}} \left(1 - d_s \times \left(\bar{w} + f_\alpha \frac{(\bar{w} - w_\alpha)}{(1 - f_\alpha)} \right) \right) \quad (13)$$

ΔG_{chAi} is the initial free energy change at the beginning of the transformation or grain boundary nucleation. d_s is a constant considered as a fitting parameter in the model. \bar{w} is the average carbon concentration of steel in wt.%. f_α is the fraction of bainite formed during the transformation. w_α denotes the fraction of carbon entrapped in the bainite, either in solid solution or in a form of iron

carbide, depending on the condition of the applied heat treatment and the ability of the carbon enrichment in the austenite due to the alloy addition. For the interaction energy of the bainitic stress field mentioned above, it can be given as follows.

$$G_{\text{dislo}} \approx -\frac{3E^{\gamma}}{2(1+\nu)}(\varepsilon_{22}^{\text{tr}})^2 \quad (14)$$

where $\varepsilon_{22}^{\text{tr}}$ represents the internal elastic strain state resulting from the local strain incompatibility between the bainite and austenite, E^{γ} is the elastic modulus of austenite, and ν is the Poisson ratio of austenitic steel (0.27). From Equation (9)–(14), the formation of the total energy difference required for activating the transformation at each iteration can be determined as follows.

$$\Delta Q^* = Q_{\text{GB}}^* - Q_{\text{AN}}^* \quad (15)$$

It is noted that the physical basis of such autocatalytic factors has been not adequately given in the current reported literature. Hence, the proposed model provides more details describing the particular net free energy changes caused by the elemental partitioning, particularly when the effect of ausforming is considered.

3.1.3. Potential Nucleation Site Density

In this model, the number density of the potential nucleation sites is estimated based on the original concept of Magee for athermal martensitic transformation [21]. It is reported to be linearly dependent on the undercooling temperature. In this regard, Van Bohemann and Seitsma [48] validated the increase in undercooling with a reduction in the M_s temperature due to carbon content. The higher density of nucleation sites results from the driving energy, which is increased when decreasing the transformation temperature of martensite. This concept is later reformulated to be applicable to an isothermal transformation and is given by the following expression.

$$N_0 = \emptyset(G_{\text{N}}(T_{\text{h}}) - G_{\text{N}}(T_{\text{iso}})) = \xi\Gamma(T_{\text{h}} - T_{\text{iso}}) \quad (16)$$

By analogy with the work of Magee on martensite nucleation, ξ is equal to $\alpha/(V_{\alpha}\Gamma)$. α is a material constant, and Γ is determined by the slope of $d(\Delta G_{\text{m}})/dT$, which is approximately constant in the temperature range of martensitic/bainitic transformation. V_{α} represents the average volume of the bainite sub-unit [20,22]. T_{h} is the highest temperature at which the displacive transformation

occurs. Because of the experimental investigations, the number density of the pre-existing defects can be calculated by Equation (17).

$$N_i = \frac{m}{V_\alpha} (T_h - T_{iso}) \quad (17)$$

m is the proportionality constant between the number density of the bainite nucleation sites and the degree of undercooling. In the case of martensite formation, m and α are assumed to be identical and are used as material parameters. Their values are between 0.01 and 0.07 K⁻¹ and depend slightly on the chemical composition [21,43]. A fundamental difference between the nucleation of martensite and bainite is that the density of the pre-existing defects for martensite nucleation is governed by the prior austenitic grain size, whereas the bainitic nucleation is also controlled by the structural interfaces, namely the γ/γ and γ/α interfaces. According to Van Bohemann and Seitma's report [22], m can be replaced by b_{GB} and b_{AN} with consideration of the effects of the γ/γ and γ/α interfaces, respectively. The density of the available γ/γ interfaces is dependent on the volume fraction of the remaining available austenite and the austenite grain size. The b_{GB} parameter is thus given as follows.

$$b_{GB} = \frac{Z\delta}{d_\gamma} m f_\gamma \quad (18)$$

The proportional relationship of $Z\delta/d_\gamma$ is defined as the austenite grain boundary area per unit volume, in which δ and d_γ denote the effective thickness of the prior austenitic grain boundary and the austenitic grain size, respectively. f_γ represents the fraction of the UA. In addition, when the effective thickness of the austenitic grain boundary is considered as the atomic layers of a grain in the grain boundary region, a few of the outermost atomic layers in each grain can be presumed to participate in the nucleation process. Hereby, it is suggested that an austenitic grain size is composed of two atomic layers in each grain. With regard to the autocatalytic parameter represented by b_{AN} , it is controlled by the remaining available austenitic phase fraction, at which the α/γ interfaces are formed while the bainitic transformation progresses. The parameter can therefore be given by the following equation.

$$b_{AN} = \frac{Z\delta}{d_\gamma} m f_\gamma f_\alpha \quad (19)$$

where f_α represents the volume fraction of BF. In summary, the size of the BF sub-units has an inverse relationship with the density of the nucleation sites and the remaining available austenite grains.

3.1.4. Austenitic Phase Fraction as a Function of Carbon Enrichment

As shown in Equations (17) and (18), the variations of f_γ and f_α are the critical factors when estimating the density of the nucleation sites. It is kinetically changed during the formation of BF due to the carbon enrichment in the austenite. If the stored energy of bainite caused by shear transformation is involved, the process should be completely terminated at the T'_0 locus where the free energies of austenite and bainite are identical, as presented in **Section 3.1**. By this concept, the conservation of mass balance in the bainite and austenite can be applied, and the variation of carbon concentration in the austenite associated with the locus can be given as follows.

$$w_\gamma = \bar{w} + f_\alpha \frac{(\bar{w} - w_\alpha)}{(1 - f_\alpha)} \quad (20)$$

\bar{w} represents the bulk carbon concentration of steel, and w_α is the composition of carbon in a BF sub-unit. Ravi et al. [27] used the same concept to determine the bainitic transformation temperature and found that the temperature linearly reduces with the increased carbon content in austenite, as provided in Equation (21).

$$T_h = T_{h\bar{x}} - C_1 \frac{(\bar{w} - f_\alpha w_\alpha)}{(1 - f_\alpha)} \quad (21)$$

where $T_{h\bar{x}}$ is the T_h temperature at the beginning of the transformation and is determined using thermodynamic calculation software called MUCG83 [47], and C_1 is a proportional constant relating T_h and the carbon concentration.

Moreover, the total fraction of UA, f_γ , is estimated by considering the T'_0 locus as being determined for the carbon enrichment. In this regard, a certain amount of austenite may not participate in the bainitic reaction and yields the incomplete phenomenon. It is assumed that the unavailable austenite certainly contains no potential nucleation site due to its stability. This fraction is thus subtracted while calculating the overall nucleation rate. Using the principles of the incomplete reaction phenomenon, f_γ and T'_0 can be expressed as follows.

$$f_Y = (1 - f_\alpha) \frac{(T'_0 - T_{\text{iso}})}{(T'_{0\bar{X}} - T_{\text{iso}})} \quad (22)$$

$$T'_0 = T'_{0\bar{X}} - C_2 f_\alpha \frac{(\bar{w} - w_\alpha)}{(1 - f_\alpha)} \quad (23)$$

where $T'_{0\bar{X}}$ is the T'_0 temperature at the beginning of the transformation, and C_2 is a proportional constant relating to T'_0 and the carbon concentration. Note that the influences of ausforming on the free energy change of austenite are not incorporated here due to the complexity of the implementation.

3.1.5. Bainitic Transformation Model

From Equations (7) to (23), the overall nucleation kinetics of the isothermal bainitic transformation can be summarized by the following equation.

$$\left(\frac{dN}{dt}\right)_t = \left(\frac{k_B T}{h} \frac{Z\delta}{d_Y} \frac{m}{V_\alpha} (1 - f_\alpha) \frac{(T'_0 - T_{\text{iso}})}{(T'_{0\bar{X}} - T_{\text{iso}})} (T_h - T_{\text{iso}}) \left\{ \exp\left(-\frac{Q_{\text{GB}}^*}{RT}\right) \right\} \{1 - \lambda f_\alpha\}\right) \quad (24)$$

The variable λ in this equation is represented by $\exp(\Delta Q^*/RT)$ as an autocatalytic factor. It plays an important role in the kinetics of bainitic transformation and mainly relies on the activation energy difference of the nucleation process. Thus, the autocatalytic function termed by $\{1 - \lambda f_\alpha\}$ can be given as the β parameter, which is similar to that defined in the literature [20,49]. As discussed earlier, the parameters w_α , d_s , ΔQ^* , and K_1 are given as the fitting parameters in this model, from which their physical significances can be defined.

In order to estimate the volume fraction of BF, it can be presumed that BF sheaves are formed by stacking sub-unit layers on the iterative sites of the nucleation and are therefore dependent on the number of nucleated sites. Nonetheless, the volume of a BF sub-unit examined by Matsuda and Bhadeshia [19] is not a constant value, it changes depending on the transformation temperature, which is given as follows.

$$V_\alpha = (2 \times 10^{-17}) \times \left(\frac{T_{\text{iso}} - 528}{150}\right)^3 \quad (25)$$

where V_α represents the average volume of a BF sub-unit in m^3 . Consequently, the kinetics of the isothermal bainitic transformation can be calculated by means of a numerical integration of the associated nucleation rates. The product of the integration is given by the following equation.

$$f_\alpha = \int \frac{dN}{dt} V_\alpha dt \quad (26)$$

3.2. Martensitic Transformation

As reported in a previous study [16], the UA after isothermally formed BF is not thermodynamically stable. It can be transformed to FM during ambient cooling because of the low carbon content. Therefore, only the overall kinetics equation for predicting all existing phases in the steel may not be satisfactory. To incorporate the course of martensitic transformation, the conventional KM equation [21,43,50] was modified based on Lee's equation [51] and further developed according to the fact that martensite does not directly transform from a fully austenite. The certain area of the untransformed product of austenite can be expressed as follows.

$$f_{\text{FM}} = (f_{\text{UA}}) - e^{-\alpha_{\text{FM}}(M_{\text{s,UA}} - T_{\text{RM}})^n} \quad (27)$$

f_{UA} is the phase fraction of UA and is equivalent to $1 - f_\alpha$. α_{FM} is a material parameter, which is calculated from the data reported for low-carbon steels with a high concentration of silicon and chromium [51], as given in Equation (28); $M_{\text{s,UA}}$ is a martensite start temperature after the isothermal tempering, indicated as being equal to M'_s ; and T_{RM} is room temperature. Moreover, n is also a material constant that depends on the chemical composition, as shown in Equation (29). Finally, the empirical equation of martensitic transformation can be written by Equation (30), where f_{RA} and f_{FM} are the volume fraction of the retained austenite and martensite after cooling, respectively.

$$\alpha_{\text{FM}}(K^{-1}) = 0.0231 - 0.0105x_{\text{C}} + 0.0074x_{\text{Cr}} - 0.0017x_{\text{Ni}} - 0.0193x_{\text{Mo}} \quad (28)$$

$$n = 1.4304 - 1.1836x_{\text{C}} + 0.7527x_{\text{Cr}}^2 - 0.739x_{\text{Si}} - 0.0258x_{\text{Ni}} + 0.3108x_{\text{Mo}} \quad (29)$$

$$f_{\text{UA}} = f_{\text{RA}} + f_{\text{FM}} \quad (30)$$

4. Results and Discussion

4.1. Experimentally Determined Phase Fractions

In our previous studies [16,52], no carbide precipitation was found in the examined steels with minimized alloys of around 1 wt.%Si. Therefore, the final microstructures of steel should comprise BF and RA ($\alpha + \gamma$), unless the enrichment of carbon in the UA after the bainitic transformation is thermodynamically unstable. In this circumstance, the UA can be partially decomposed to FM (α'), and the heterogeneous microstructure composed of $\alpha + \gamma + \alpha'$ consequently appears. Under thermodynamic equilibrium, the average carbon concentration in the microstructure components of steel could be expressed by $w_\alpha f_\alpha + w_{\gamma,RA} f_{\gamma,RA} + w_{\alpha'} f_{\alpha'} = \bar{w}$, where the quantity of w_α , $w_{\gamma,RA}$, and $w_{\alpha'}$ represents the carbon distribution in BF, RA, and FM, respectively, and \bar{w} is the bulk carbon content of the steels. **Fig. 2a** illustrates the results of the XRD measurements of MC1.5Mn1NiCr steel with and without ausforming. Only the phases belonging to the body-centered and face-centered structures were quantified. The bainitic, ferritic, and martensitic phases that possessed the BCC structure were displayed all together on the same crystallographic planes. The RA whose peaks appeared at the (111), (200), (220) planes was apparently observed, especially in the case of the PIT and AIT specimens, whereas the identical peaks of BF and FM exposed at the (110), (200), and (211) planes were not distinguishable. Thus, the volumetric strain response in the DQ and PIT specimens were exploited together with the volumetric fraction of the BCC obtained by the XRD measurement so that the volumetric fractions of all the constituents could be quantified rationally. **Fig. 2b** shows that the M_s temperature could be determined at the point where the cooling curve started to deviate from its tangent. A vertically measured distance between the tangent and the cooling curve at the final cooling temperature of the DQ results was given as the reference and accounted for the maximum volumetric expansion of the martensitic transformation. By comparing the reference value with the volumetric expansions for the AIT specimen using the lever rule, the martensitic phase fraction of the AIT specimen could be estimated by Equation (31).

$$f_{\alpha'}(\text{AIT}) = \frac{f_{\alpha'}(\text{DQ, XRD}) \times \alpha'(\text{AIT, DIL})}{\alpha'(\text{DQ, DIL})} \quad (31)$$

where $f_{\alpha'}(\text{DQ, XRD})$ represents the volume fraction of martensite acquired from the XRD measurement, and $\alpha'(\text{AIT, DIL})$ and $\alpha'(\text{DQ, DIL})$ are the volumetric strains obtained from the dilatation curves of the AIT and DQ specimens during cooling, respectively. As aforementioned, the total phase fraction of BF was further evaluated from the curve for the change in volume strain at the time where the BF transformation was terminated (distance AB, shown in Figure 3). With help of Equation (30), the amount of UA in the AIT specimen was calculated from the summation of the RA fraction quantified by the XRD analysis and the FM fraction from Equation (31). Subsequently, the distance BC, with regard to the UA volume fraction, was obtained by referring the distance AC to the volume fraction of all the phases. Finally, the proportionality of the dilatation locus was applied to determine the kinetics evolution of the bainitic phase transformation.

From the calculations, as shown, the percentage of the developed phases, the amount of carbon enrichment in the austenite in wt.% ($w_{\gamma, \text{RA}}$), the martensite start temperature ($M_{s, \text{exp}}$) of the steels subjected to the DQ, PIT, and the AIT heat treatments were gathered, as listed in **Table 2**. It is noteworthy that the prior deformation and its degree have played the primary role in enhancing the stability of austenite and have resulted in a decrease in the BF fraction.

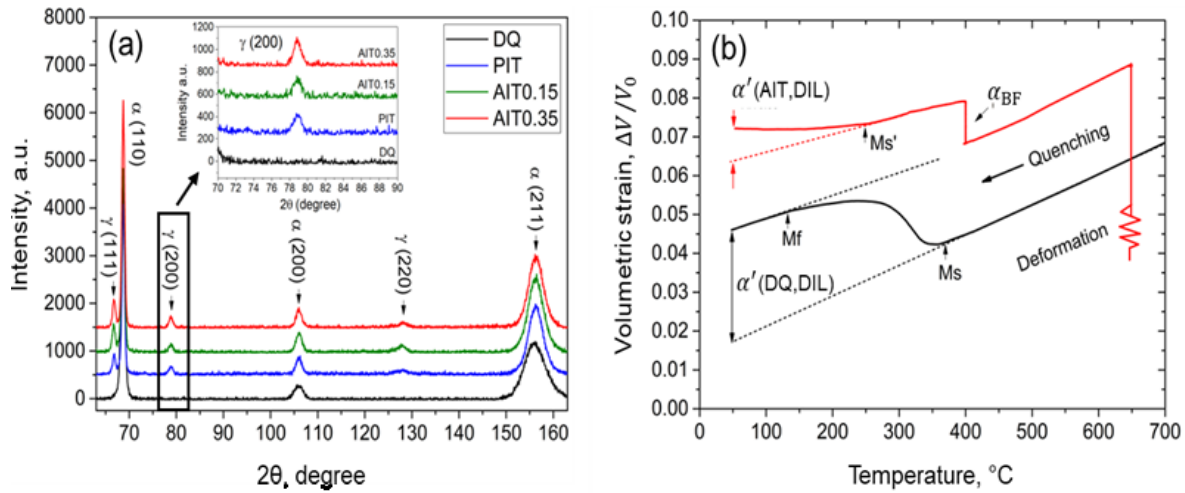


Fig. 2 (a) Phase quantifications of examined steels using XRD measurement and (b) volumetric strain of DQ and AIT specimens after cooling from austenitizing and deformation stage.

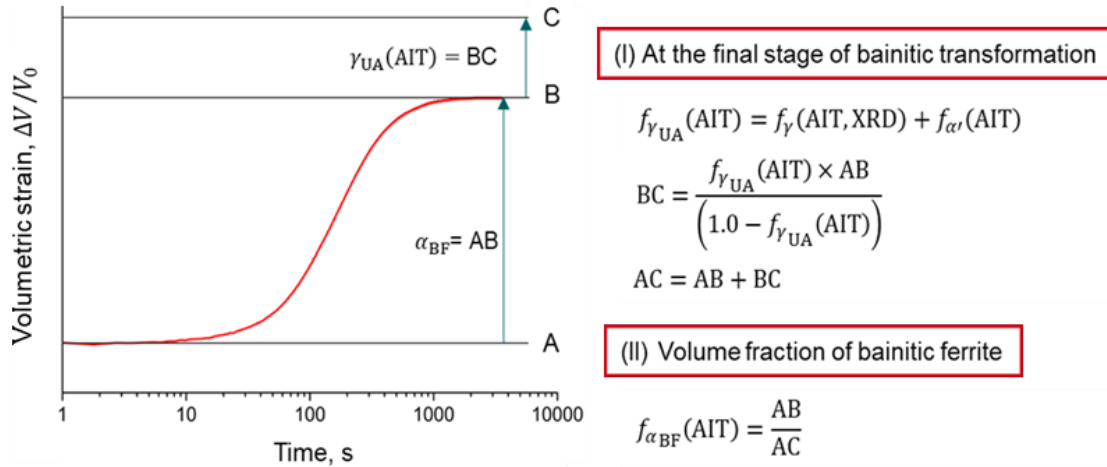


Fig. 3. Determination of the volume fraction of bainitic ferrite during tempering at 400 °C.

However, the stabilized austenite in MC1.5Mn1NiCr steel, which had a higher carbon content and low alloyed Cr and Ni contents, was not always sustained along the AIT process, especially when some UA decomposed into FM during cooling. The ausforming strains caused extreme deterioration of the thermodynamic stability of austenite, leading to a greater formation of FM with a slight reduction in the RA fraction. It seems that ausforming only influenced the FM formation, whereas the variation of RA was negligible.

Meanwhile, it is somewhat surprising that increasing the ausforming strain in the LC2.5Mn0.2NiCr specimens undergoing AIT treatment was quite effective for suppressing the phase transformation. The enrichment of the dislocation density within the plastically deformed austenite had not only accumulated while ausforming, but remained propagating during the BF formation, resulting in the suppression of the formation of FM, with the leaving of more UA as a residual product. It is also noted that the degree of carbon enrichment in austenite during bainitic transformation was directly subjected to UA stability. It was resisted once the structural stability of UA was improved. The carbon concentrations listed in the table represent the overall carbon contents in RA, which take both the products of carbon enrichment and the partitioning processes into account. Therefore, the $w_{Y,RA}$ values should be evaluated further to quantify the exact value at individual stages of the transformations.

4.2. Modelling Results

4.2.1. M_s temperature

The kinetics parameters and the theoretical start temperatures of martensite determined using the modified KM equation for both MC1.5Mn1NiCr and LC2.5Mn0.2NiCr steels under PIT and AIT conditions are presented in **Table 3**. Note that the parameters, α_{FM} and n , were dependent on the alloying composition and were not affected by the heat treatment conditions. The calculated values of α_{FM} and n for the MC1.5Mn1NiCr steel were 0.0205 and 0.96, respectively, whereas those for the LC2.5Mn0.2NiCr steel were 0.0243 and 1.06, respectively.

Table 2. Volume phase fraction determined by means of quantitative analysis of XRD measurement combined with the dilatometry results.

Material/Condition	Volume Fraction, %			$w_{Y,RA}(=x_C)$ Equation (3)
	RA	BF	FM	
MC1.5Mn1NiCr/DQ	-	-	100	-
MC1.5Mn1NiCr/PIT	15.6 ± 3.3	77.4 ± 4.2	7.0 ± 2.8	0.78
MC1.5Mn1NiCr/AIT0.15	14.6 ± 5.1	62.0 ± 6.7	23.4 ± 6.3	0.68
MC1.5Mn1NiCr/AIT0.35	13.5 ± 5.8	47.9 ± 4.5	38.6 ± 3.4	0.56
LC2.5Mn0.2NiCr/DQ	1.2 ± 0.8	-	98.5 ± 2.8	0.04
LC2.5Mn0.2NiCr/PIT	8.5 ± 2.5	83.6 ± 4.6	7.9 ± 3.9	0.45
LC2.5Mn0.2NiCr/AIT0.15	11.3 ± 3.7	77.6 ± 3.4	11.1 ± 4.5	0.51
LC2.5Mn0.2NiCr/AIT0.35	16.9 ± 3.5	74.3 ± 4.9	8.8 ± 4.1	0.89

The discrepancies between the experimental and the calculated values were highly acceptable. Clearly, the martensitic start temperature significantly depended on the heat treatment conditions and the material. For both steels, the M_s temperatures were decreased markedly with the application of ausforming. In the case of MC1.5Mn1NiCr steel, increasing the ausforming strain caused a slightly higher M_s value. The increased strain deteriorated the stability of the austenite and subsequently led to a higher fraction of FM. In contrast, the stability of the austenite in the LC2.5Mn0.2NiCr steel seemed to be effectively promoted by the enhancing of the ausforming strain in accordance with the lowered transformation temperature of the martensite. It implies that the chemical composition was of importance for adjusting the austenite stability of steel,

particularly when carbon as an austenite former element was only the most important factor in controlling the bainitic transformation at low temperature.

Table 3. Determined kinetics parameters using the modified KM equation for the examined MC1.5Mn1NiCr and LC2.5Mn0.2NiCr steels under PIT and AIT conditions.

Material/Condition	α_{FM}, K^{-1}	$n, -$	$M_{s,exp}, ^\circ C$	$M_{s,cal}, ^\circ C$
MC1.5Mn1NiCr/DQ	0.0205	0.96	354 ± 5.1	344
MC1.5Mn1NiCr/PIT	0.0205	0.96	347 ± 4.7	332
MC1.5Mn1NiCr/AIT0.15	0.0205	0.96	260 ± 7.1	255
MC1.5Mn1NiCr/AIT0.35	0.0205	0.96	265 ± 6.3	260
LC2.5Mn0.2NiCr/DQ	0.0243	1.06	388 ± 2.4	380
LC2.5Mn0.2NiCr/PIT	0.0243	1.06	351 ± 4.2	345
LC2.5Mn0.2NiCr/AIT0.15	0.0243	1.06	270 ± 3.6	263
LC2.5Mn0.2NiCr/AIT0.35	0.0243	1.06	192 ± 5.8	184

4.2.2. Model Parameters

The input parameters and the critical temperatures calculated by Bhadeshia's program (see **Section 3.1.4**) are represented in **Table 4**. It has been seen that the PAGs are decreased by the ausforming treatments and by adding either carbon or other austenite stabilizer elements due to the reduction in the driving energy for grain growth. It is suggested in [45] that the condition of the parent phase controls the driving energy for lower-temperature phase transformation. In general, the energy stored for the nucleation reaction increases with rising the number of nucleation sites and can be considerably dependent on the chemical compositions, undercooling, and prior deformation. If austenite is plastically deformed and more defects are generated as nucleation sites, the primary driving energy of the phase transformation is most probably controlled by nucleation sites increased rather than the other factors. Furthermore, the locus of $T_{h,\bar{x}}$ is hereby broadened as $T'_{0,\bar{x}}$ is suppressed. However, changes in the critical temperature were observed only as a result of the chemical contributions and the undercooling, regardless of the ausforming effect.

Table 4. Parameters used for the transformation models.

Parameter	MC1.5Mn1NiCr			LC2.5Mn0.2NiCr		
	PIT	AIT0.15	AIT0.35	PIT	AIT0.15	AIT0.35
$d_{\gamma}, \mu m$	48 ± 1.5	43 ± 3.3	35 ± 2.1	56 ± 0.9	49 ± 1.4	44 ± 2.2
T_{iso}, K		673			673	
$T_{h\bar{X}}, K$		753			983	
C_1		2304			2205	
$T'_{0\bar{X}}, K$		763			778	
C_2		8911			8537	

4.2.3. Kinetics of Bainitic Phase Transformation

Fig. 4 displays the kinetics of the bainitic transformation of MC1.5Mn1NiCr and LC2.5Mn0.2NiCr steels under PIT and AIT conditions at different ausforming strains. It shows that the calculation results fitted very well with the experimental data. The transformation kinetics presented in Figure 4a,b could be divided into three stages, namely onset, growth, and cessation. The onset was indicated at a locus, at which the first BF sub-units were formed. After that, the growth driven by the shear was kinetically captured by the progress of the BF sheaves. Finally, the transformation stopped when the decomposition of austenite was supersaturated as it reached its plateau. Ausforming had a strong influence on an acceleration of the transformation onset and a reduction in the BF volume fraction. However, for MC1.5Mn1NiCr/AIT0.35 steel, the transformation was somewhat sluggish compared to the other conditions for the same material. This circumstance could be precisely explained by the nucleation rate activity and the driving energy, as given in the next section. According to the fact that ausforming enhances the austenite stability, even though the deformation simultaneously accelerated the transformation, the drastic increase in defect density in UA during the initial progress of bainitic transformation resulted in a reduction in the BF fraction. The results were consistent with those reported in [18,53,54], particularly in the MC1.5Mn1NiCr steel. It can be seen that increasing the ausforming strain in LC2.5Mn0.2NiCr steel gave a slight difference in the lowering of the fraction of BF. In light of the chemical variations, LC2.5Mn0.2NiCr steel with a lower carbon content with adjusted Cr and Ni alloying elements possessed higher BF fractions than MC1.5Mn1NiCr steel, regardless of the

applied ausforming. It could be verified from their bulk carbon contents and the effective enrichment of carbon in austenite. Hence, it was not surprising that the lower carbon steel exhibited smaller fractions of BF, which is similar to [55].

The fitted values of w_α , d_s , Q_0^* , and K_1 obtained from the proposed model are shown in **Table 5**. Only w_α and Q_0^* were well explicable with their physical meaning. The reduction of Q_0^* values signified a decreased energy barrier of the nucleation reaction and seemed remarkably diminished by the ausforming. This parameter was associated with the kinetics acceleration of the BF transformation due to the increased number of existing nucleation sites per unit volume in UA. Considering the lower value of Q_0^* presented in the MC1.5Mn1NiCr/AIT0.15 compared with that in the MC1.5Mn1NiCr/AIT0.35, it could be described by the higher number of nucleation sites or defect densities, which essentially contributed in the later stage of the bainitic transformation. In this respect, it was not surprising that the average amount of carbon concentration in the BF supersaturation (w_α) became constricted with regard to the higher kinetics acceleration at the beginning and was most likely associated with more carbon enrichment.

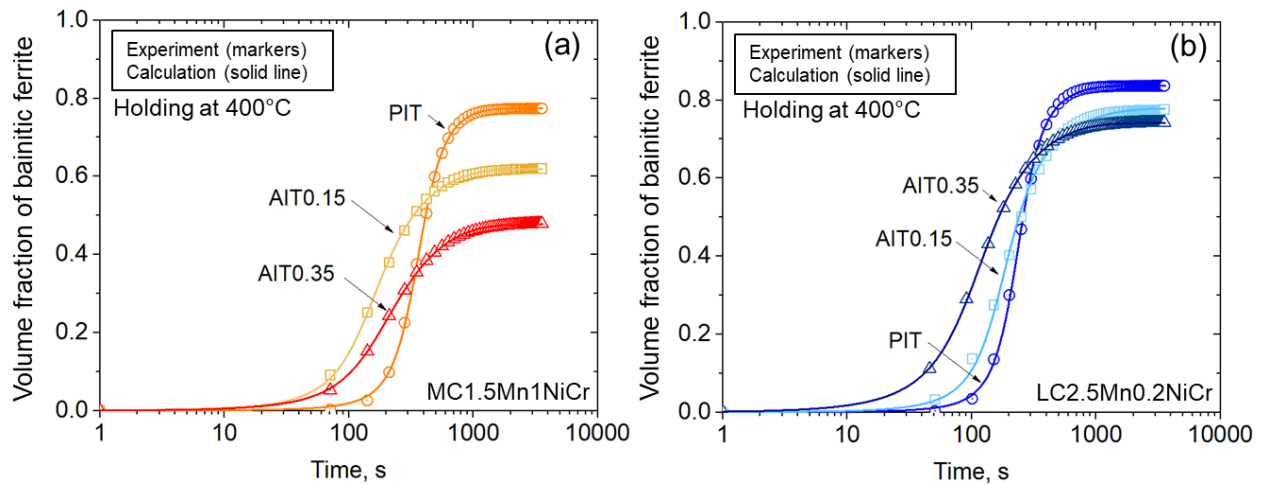


Fig. 4 The kinetics of bainitic transformation of (a) MC1.5Mn1NiCr and (b) LC2.5Mn0.2NiCr steels under PIT and AIT with the strain of 0.15 and 0.35.

However, the w_α values gathered for the present model were invariably smaller than the mean carbon concentration in the mole fraction of both of the examined MC1.5Mn1NiCr and LC2.5Mn0.2NiCr steels, namely 0.01185 and 0.00824, respectively, which is similar to Ravi's work [27]. The silicon and aluminum additions allowed the specific energy for carbon enrichment

and enabled austenite to consume with a certain amount of carbon during the enrichment process, as illustrated in **Fig. 5**. By this model, the evolution of carbon enrichment could be evaluated by the rejection of carbon from the supersaturated BF sub-unit during the austenite decomposition. The presence of RA evidenced the effectiveness of the incomplete reaction that occurred when the austenite was stabilized by the carbon enrichment. Nonetheless, the net carbon value calculated from this model could not be directly compared with the corresponding experimental values in **Table 2**, because the remaining available carbon may be further partitioned during the subsequent transformation of FM.

Table 5. Fitting parameters obtained for the used model.

Parameter	MC1.5Mn1NiCr			LC2.5Mn0.2NiCr		
	PIT	AIT0.15	AIT0.35	PIT	AIT0.15	AIT0.35
w_α , mole fraction	0.0091	0.0056	0.00081	0.0060	0.0048	0.0031
Q_0^* , kJ/mole	172.98	166.48	170.9	167.53	164.83	145.74
d_s	1.47	19.26	12.03	1.81	4.36	9.73
K_1	0.46	4.86	7.32	0.36	0.69	1.29

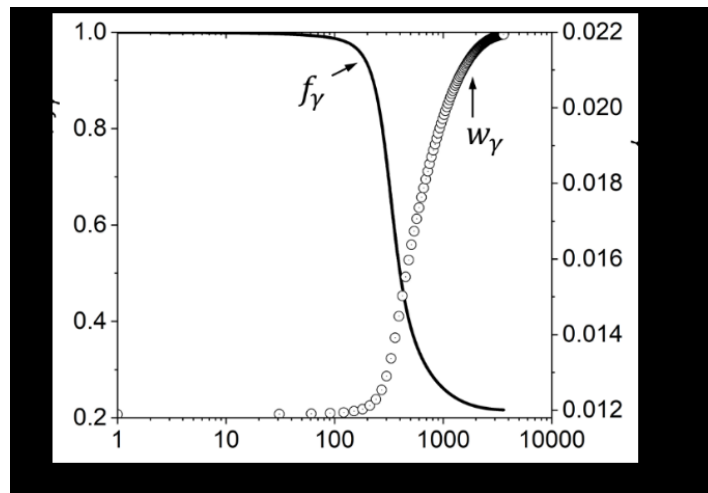


Fig. 5 Relationship between the austenite decomposition and the degree of carbon enrichment in austenite of MC1.5Mn1NiCr steel with PIT condition.

As previously mentioned in **Section 3.1.1**, the kinetics of bainitic transformation was governed by the nucleation rate mechanism, i.e., the grain boundary nucleation and the autocatalytic nucleation. The initial nucleation rate was activated by the grain boundary nucleation, which depended only

on the density of the nucleation sites. Subsequent nucleation rates were then controlled by the autocatalytic nucleation with regard to the spontaneous dissociation of the specific dislocation defects and the accumulated stored energy of the corresponding dislocations [56]. Moreover, a generation of additional defects by ausforming presumably provided more available sites while simultaneously deteriorating the activation energy of the nucleation. Enhancing the defect densities thus increased the nucleation rate by triggering the transformation onset. The nucleation kinetics of examined steels subjected to different conditions are presented in **Fig. 6**. It was hereby agreed that at the earliest stage of BF formation the driving energy for nucleation was higher than the stabilization effect, owing to the potential nucleation sites, which were generated during either the ausforming or the cooling to the transformation temperature. The formation of BF continued until the driving energy for nucleation and stored energy due to the mechanically stabilized austenite, which became identical at the maximum nucleation rate. Hereafter, the deceleration kinetics occurred, implying that the stability of the neighboring austenite was increased by the successive formations of the BF sub-units, which resulted in a reduction in stored energy for the transformation. This occurrence could be verified by the relationship between the driving energy for the autocatalytic nucleation and the corresponding number of nucleation sites, as depicted in **Fig. 7**. It is noteworthy that the nucleation rates and the driving energy values of LC2.5Mn0.2NiCr steel were all lower than those of the MC1.5Mn1NiCr steels, regardless of the heat-treated condition. This result was likely caused by the elemental distribution, which was similar to that observed in an experimental validation proposed by Wang et al. [4].

The autocatalytic driving energy could be also considered as an important factor for controlling the nucleation event. When the austenite stability became more dominant, the total driving energy stored for the phase transformation decreased. It can be observed that the driving energy was drastically increased at the initial stage of nucleus formation and then decreased gradually during the developing of the nucleation sites. The effect of ausforming almost caused degenerations of the nucleus development, accordingly, except that they occurred in MC1.5Mn1NiCr/AIT0.35 steel.

The number of nucleation sites developed in the MC1.5Mn1NiCr/AIT0.15 steel was more extensive than in the MC1.5Mn1NiCr/AIT0.35 steel, which corresponded with lower driving energy, as presented in Figure 7a. Even though the MC1.5Mn1NiCr steel consumed less driving

energy than the LC2.5Mn0.2NiCr steel, it had a small number of nucleation sites due to the existence of more dislocations. Interestingly, the driving energy of the LC2.5Mn0.2NiCr steels shown in **Fig. 7b** was significantly sensitive to ausforming, and was well described, especially at the high degree of ausforming. From the correlation between the activation energy and the driving force defined in Equation (9), it was inevitable that the initial activation energy required to overcome any obstacles played an essential role in all the nucleation events. Nevertheless, in order to extract and consider only the activation energy influenced by the other mechanisms, regardless of the energy contributed by ausforming, it was reasonable to take the activation energy difference in Equation (15) into account so that a discussion of only the effect of chemical contribution on the variation of the activation energy difference, ΔQ^* was conceivable.

In **Fig. 8**, the variations of the total activation energy difference with the evolution of the BF formation of MC1.5Mn1NiCr and LC2.5Mn0.2NiCr steels under PIT and AIT conditions are illustrated. The carbon enrichment was presumed to be the main contributor for BF formation. It was found that the ΔQ^* energies required in all the conditions of the MC1.5Mn1NiCr steel were somewhat higher than those of the LC2.5Mn0.2NiCr steel. Such a tendency corresponded well with those shown in [27,56], in which it was reported that the activation energy was dependent, on one hand, on the undercooling temperature. It was decreased with the increasing of the temperature as a higher defect density was generated. On the other hand, ΔQ^* was partially governed by the chemical element addition. In particular, those containing more carbon content acting as an austenite stabilizing element could directly lead to suppression of the bainitic transformation, accompanied by the raising of the energy required for the nucleation event.

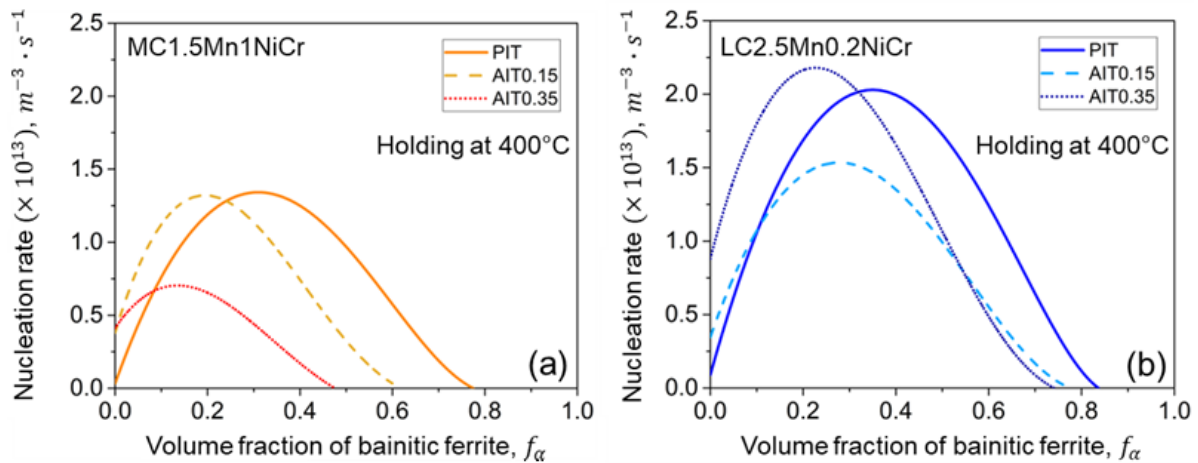


Fig. 6 Nucleation rate as a function of BF volume fraction for (a) MC1.5Mn1NiCr and (b) LC2.5Mn0.2NiCr steels under various conditions.

The maximum ΔQ^* energies obtained for both the MC1.5Mn1NiCr and the LC2.5Mn0.2NiCr steels with PIT treatment were consistently higher than those with other heat-treating conditions. It was because of the small number of potential nucleation sites in PIT steel. In this sense, the reduction of the ΔQ^* energy with respect to the evolution of the BF formation should be associated with the increased number of nucleation sites, while the termination of BF development could be associated with an overconsumption of nucleation sites in UA. Hence, the result gave rise to more stable austenite.

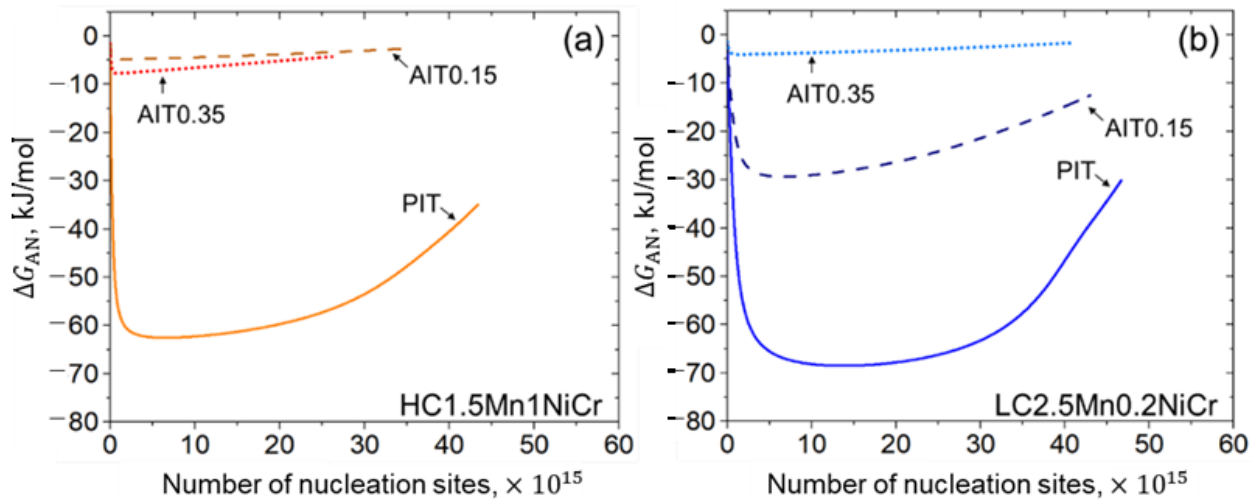


Fig. 7 Driving force for autocatalytic nucleation as a function of density of nucleation sites of (a) MC1.5Mn1NiCr and (b) LC2.5Mn0.2NiCr steels under various conditions.

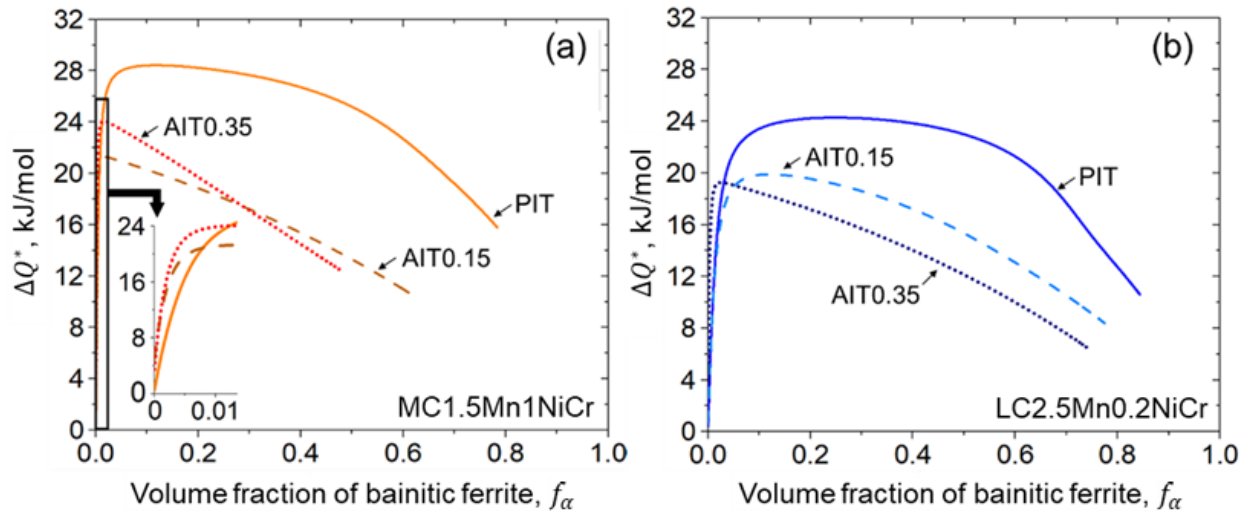


Fig. 8 Variation of total activation energy difference with bainite formation evolution of (a) MC1.5Mn1NiCr and (b) LC2.5Mn0.2NiCr steels under various conditions.

4.2.4. Dislocation Density Estimation

Figure 9a,b shows the estimated dislocation density and the PAGs of the steels under PIT, AIT0.15, and AIT0.35 conditions, respectively. As can be seen, the decreases in the PAGs were not the only factors affecting the density development of the dislocations in this study. The contribution of hard phases such as BF and FM should also be included as the formation of such structures was in fact accompanied by the accumulation of stress [57], particularly when the average dislocation density values estimated from the PIT specimens of individual steels were compared. However, the effect of carbon content on such PAG reduction could be described by the carbon-controlled nucleation mechanism during the solid solution treatment [58]. The influence of the PAGs was more pronounced in the ausformed specimens than in the PIT specimen, and thus it would be reasonable to describe it by the Hall–Petch relation [59].

Under the ausforming conditions, besides the PAGs reduction that came along with the pre-existing dislocations, the enhancement of the dislocation density was also associated with the fractions of the hard phase, as mentioned previously. The density of the pre-existing dislocation in the austenite was directly dependent on the ausforming strain, while the formations of BF and FM were governed by the thermodynamic stability of austenite and the degree of carbon enrichment, respectively. In addition, the pre-existing dislocation density affected by ausforming could be evaluated by subtracting the average density of the dislocations of any AIT specimen from the

value estimated from the PIT specimen. For the LC2.5Mn0.2NiCr steel, the additional dislocations introduced by the 0.15 and 0.35 strains were 2.4×10^{14} and $3.6 \times 10^{14} \text{ m}^{-2}$, respectively. Likewise, the estimated values of the MC1.5Mn1NiCr steel in accordance with the ausforming strains were 1.3×10^{15} and $1.5 \times 10^{15} \text{ m}^{-2}$, accordingly. Such extra dislocations can be inherited further to the tempering region and change the nucleation rate during the bainitic transformation. Therefore, it could be concluded that the presence of higher dislocations in the MC1.5Mn1NiCr steel was likely due to a strong hindrance of the nucleation reaction, in which the effect of the dislocation-induced mechanical stabilization of austenite was more pronounced. However, the conclusion with respect to ausforming the enhanced thermal stability of austenite may not be applicable for the MC1.5Mn1NiCr steel as more FM was formed. In contrast, the deformation encouraged a higher nucleation rate and was mostly available for a greater formation of nucleation sites during bainitic transformation for the LC2.5Mn0.2NiCr steel. The results hereby enabled UA to be better stabilized after the transformation, although the ausformed LC2.5Mn0.2NiCr steels had a much lower dislocation density. As a consequence, it seems that the relationship between nucleation sites and dislocation density evolutions could not be concluded as two different trends were seen in two different materials. Nevertheless, the LC2.5Mn0.2NiCr steel, with a substantial BF fraction due to the large degree of ausforming, effectively resisted the formation of FM by improving the thermal stability of austenite.

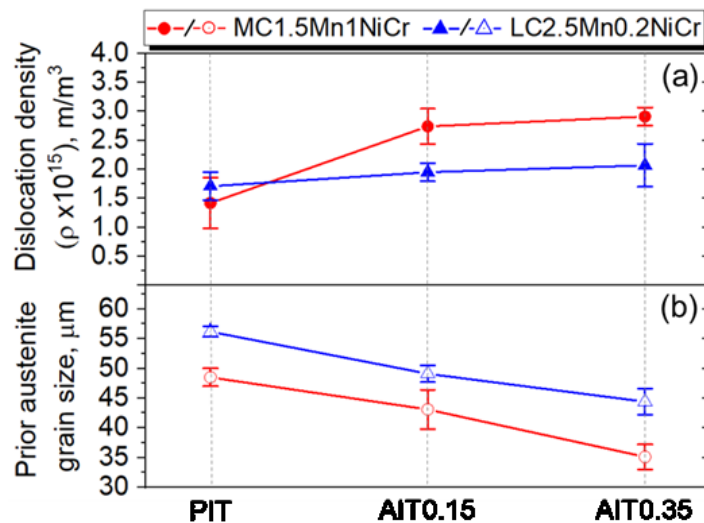


Fig. 9 (a) Dislocation density estimation and (b) prior austenite grain size of MC1.5Mn1NiCr and LC2.5Mn0.2NiCr steels under PIT, AIT0.15, and AIT0.35 treatments.

5. Conclusions/Summary

A model was formulated in this study to describe the effect of ausforming on the kinetics of isothermal bainitic transformation. The behavior of two low-carbon steels can be described based on nucleation control and the Koistinen–Marburger relationship. Different levels of ausforming were systematically characterized in experiments and further used to develop, calibrate, and validate the model. The model distinguishes grain boundary and autocatalytic nucleation. The associated driving energies are controlled by the chemical energy, interfacial energy, and stress-field energy caused by the formation of bainitic ferrite sub-units. The major conclusions are drawn in the following:

- The formation of bainitic ferrite is mainly governed by two factors: carbon enrichment in austenite and the activation energy as an energy barrier required for nucleation.
- Ausforming accelerates the onset of the bainitic phase transformation but results in sluggish transformation due to the mechanical stabilization of austenite. A higher degree of ausforming is more applicable in the steel with lower carbon content. With the substantial development of nucleation sites, even though they provide a slightly lower fraction of bainitic ferrite, the result effectively resists the formation of fresh martensite by improving the thermal stability of austenite.
- A fitting parameter representing the initial energy barrier can be used to examine the activation energy change caused by ausforming. A decrease in the energy barrier allows the acceleration of the transformation. While the transformation progresses, the driving energy for autocatalytic nucleation becomes smaller due to the enhancement of the dislocation density.
- The impact of carbon content plays a slight role in the onset period, but it is more pronounced during the progress of bainitic transformation. Minimizing carbon concentration in steel gives rise to a decrease in the net activation energy difference with the increasing of the nucleation rate. The result allocates a higher density of nucleation sites with more bainitic ferrite fractions.

6. References

- [1] Bhadeshia, H.; Edmonds, D.V. Bainite in silicon steels: New composition–property approach Part 1. *Met. Sci. J.* **1983**, *17*, 411–419. <https://doi.org/10.1179/030634583790420600>.
- [2] Caballero, F.G. Carbide-free bainite in steels. In *Phase Transformations in Steels*; Elsevier: Amsterdam, The Netherlands, 2012; pp. 436–467, ISBN 9781845699703.
- [3] Bhadeshia, H. *Bainite in Steels: Transformations, Microstructure and Properties*, 2nd ed.; IOM Communications: London, UK, 2001; ISSN 9781861251121.
- [4] Wang, S.C.; Yang, J.R. Effects of chemical composition, rolling and cooling conditions on the amount of martensite/austenite (M/A) constituent formation in low carbon bainitic steels. *Mater. Sci. Eng. A* **1992**, *154*, 43–49. [https://doi.org/10.1016/0921-5093\(92\)90361-4](https://doi.org/10.1016/0921-5093(92)90361-4).
- [5] Hofer, C.; Bliznuk, V.; Verdiere, A.; Petrov, R.; Winkelhofer, F.; Clemens, H.; Primig, S. Correlative microscopy of a carbide-free bainitic steel. *Micron* **2016**, *81*, 1–7. <https://doi.org/10.1016/j.micron.2015.10.008>.
- [6] Hofer, C.; Leitner, H.; Winkelhofer, F.; Clemens, H.; Primig, S. Structural characterization of “carbide-free” bainite in a Fe–0.2C–1.5Si–2.5Mn steel. *Mater. Charact.* **2015**, *102*, 85–91. <https://doi.org/10.1016/j.matchar.2015.02.020>.
- [7] Hu, F.; Wu, K.M. Isothermal transformation of low temperature super bainite. *Adv. Mater. Res.* **2010**, *146–147*, 1843–1848. <https://doi.org/10.4028/www.scientific.net/AMR.146-147.1843>.
- [8] Li, C.W.; Han, L.Z.; Luo, X.M.; Liu, Q.D.; Gu, J.F. Fine structure characterization of martensite/austenite constituent in low-carbon low-alloy steel by transmission electron forward scatter diffraction. *J. Microsc.* **2016**, *264*, 252–258. <https://doi.org/10.1111/jmi.12465>.
- [9] Shimanov, M.; Korpala, G.; Terzic, A.; Kawalla, R. Bainitic steels: Their characteristics and applications. *Key Eng. Mater.* **2016**, *684*, 104–110. <https://doi.org/10.4028/www.scientific.net/KEM.684.104>.

-
- [10] Takahashi, M.; Bhadeshia, H. A model for the microstructure of some advanced bainitic steels. *Mater. Trans.* **1991**, *32*, 689–696. <https://doi.org/10.2320/matertrans1989.32.689>.
- [11] Garcia-Mateo, C.; Sourmail, T.; Caballero, F.G. Bainitic Steel: Nanostructured. In *Encyclopedia of Iron, Steel, and Their Alloys*; Colás, R., Totten, G.E., Eds.; CRC Press: Boca Raton, FL, USA, 2016; pp. 271–290, ISBN 978-1-4665-1104-0.
- [12] Caballero, F.G.; Santofimia, M.J.; García-Mateo, C.; Chao, J.; Andrés, C.G. de. Theoretical design and advanced microstructure in super high strength steels. *Mater. Des.* **2009**, *30*, 2077–2083. <https://doi.org/10.1016/j.matdes.2008.08.042>.
- [13] Garcia-Mateo, C.; Caballero, F.G. Advanced high strength bainitic steels. In *Comprehensive Materials Processing*; Elsevier: Amsterdam, The Netherlands, 2014; pp. 165–190, ISBN 9780080965338.
- [14] Yao, Z.; Xu, G.; Hu, H.; Yuan, Q.; Tian, J.; Zhou, M. Effect of Ni and Cr addition on transformation and properties of low-carbon bainitic steels. *Trans. Indian Inst. Met.* **2019**, *72*, 1167–1174. <https://doi.org/10.1007/s12666-019-01590-7>.
- [15] Changle, Z.; Hanguang, F.; Shengqiang, M.; Dawei, Y.; Jian, L.; Zhenguo, X.; Yongping, L. Effect of Mn content on microstructure and properties of wear-resistant bainitic steel. *Mater. Res. Express* **2019**, *6*, 86581. <https://doi.org/10.1088/2053-1591/ab1c8d>.
- [16] Kumnorkaew, T.; Lian, J.; Uthaisangsuk, V.; Bleck, W. Effect of ausforming on microstructure and hardness characteristics of bainitic steel. *J. Mater. Res. Technol.* **2020**, *9*, 13365–13374. <https://doi.org/10.1016/j.jmrt.2020.09.016>.
- [17] Lee, C.H.; Bhadeshia, H.; Lee, H.-C. Effect of plastic deformation on the formation of acicular ferrite. *Mater. Sci. Eng. A* **2003**, *360*, 249–257. [https://doi.org/10.1016/S0921-5093\(03\)00477-5](https://doi.org/10.1016/S0921-5093(03)00477-5).
- [18] Hase, K.; Garcia-Mateo, C.; Bhadeshia, H. Bainite formation influenced by large stress. *Mater. Sci. Technol.* **2004**, *20*, 1499–1505. <https://doi.org/10.1179/026708304X6130>.
- [19] Matsuda, H.; Bhadeshia, H. Kinetics of the bainite transformation. *Proc. R. Soc. Lond. A* **2004**, *460*, 1707–1722. <https://doi.org/10.1098/rspa.2003.1225>.

-
- [20] Rees, G.I.; Bhadeshia, H. Bainitic transformation kinetics: Part 1. Modified model. *Mater. Sci. Technol.* **1992**, *8*, 994–100. <https://doi.org/10.1179/mst.1992.8.11.985>.
- [21] Magee, C.L. The kinetics of martensite formation in small particles. *Metall. Mater. Trans. B* **1971**, *2*, 2419–2430. <https://doi.org/10.1007/BF02814879>.
- [22] van Bohemen, S.M.C.; Sietsma, J. Modeling of isothermal bainite formation based on the nucleation kinetics. *Int. J. Mater. Res.* **2008**, *99*, 739–747. <https://doi.org/10.3139/146.101695>.
- [23] Ghosh, G.; Olson, G.B. Kinetics of F.C.C. \rightarrow B.C.C. heterogeneous martensitic nucleation-I. The critical driving force for athermal nucleation. *Acta Metall. Mater.* **1994**, *42*, 3361–3370. [https://doi.org/10.1016/0956-7151\(94\)90468-5](https://doi.org/10.1016/0956-7151(94)90468-5).
- [24] Ghosh, G.; Olson, G.B. Kinetics of F.C.C. \rightarrow B.C.C. heterogeneous martensitic nucleation-II. Thermal activation. *Acta Metall. Mater.* **1994**, *12*, 3371–3379. [https://doi.org/10.1016/0956-7151\(94\)90469-3](https://doi.org/10.1016/0956-7151(94)90469-3).
- [25] Meng, Q.P.; Rong, Y.H.; Hsu, T.Y. Effect of internal stress on autocatalytic nucleation of martensitic transformation. *Metall. Mater. Trans. A* **2006**, *37*, 1405–1411. <https://doi.org/10.1007/s11661-006-0085-z>.
- [26] Zou, H.; Hu, H.; Xu, G.; Xiong, Z.; Dai, F. Combined effects of deformation and undercooling on isothermal bainitic transformation in an Fe-C-Mn-Si alloy. *Metals* **2019**, *9*, 138. <https://doi.org/10.3390/met9020138>.
- [27] Ravi, A.M.; Sietsma, J.; Santofimia, M.J. Exploring bainite formation kinetics distinguishing grain-boundary and autocatalytic nucleation in high and low-Si steels. *Acta Mater.* **2016**, *105*, 155–164. <https://doi.org/10.1016/j.actamat.2015.11.044>.
- [28] Rees, G.I.; Shipway, P.H. Modelling transformation plasticity during the growth of bainite under stress. *Mater. Sci. Eng. A* **1997**, *223*, 168–178. [https://doi.org/10.1016/S0921-5093\(96\)10478-0](https://doi.org/10.1016/S0921-5093(96)10478-0).
- [29] Zhou, M.; Xu, G.; Wang, L.; Xue, Z.; Hu, H. Comprehensive analysis of the dilatation during bainitic transformation under stress. *Met. Mater. Int.* **2015**, *21*, 985–990. <https://doi.org/10.1007/s12540-015-2348-y>.

- [30] Lee, S.; Lee, S.J.; Cooman, B.C. de. Austenite stability of ultrafine-grained transformation-induced plasticity steel with Mn partitioning. *Scr. Mater.* **2011**, *65*, 225–228. <https://doi.org/10.1016/j.scriptamat.2011.04.010>.
- [31] Mahieu, J.; de Cooman, B.C.; Maki, J. Phase transformation and mechanical properties of si-free CMnAl transformation-induced plasticity-aided steel. *Metall. Mater. Trans. A* **2002**, *33*, 2573–2580. <https://doi.org/10.1007/s11661-002-0378-9>.
- [32] Abrams, H. Grain size measurement by the intercept method. *Metallography* **1971**, *4*, 59–78. [https://doi.org/10.1016/0026-0800\(71\)90005-X](https://doi.org/10.1016/0026-0800(71)90005-X).
- [33] Dyson, D.J.; Holmes, B. Effect of Alloying Additions on the Lattice Parameter of Austenite. *J. Iron Steel Inst.* **1970**, *208*, 469–474.
- [34] Lutterotti, L.; Scardi, P. Simultaneous structure and size–strain refinement by the Rietveld method. *J. Appl. Crystallogr.* **1990**, *23*, 246–252. <https://doi.org/10.1107/S0021889890002382>.
- [35] Popa, N.C. The (hkl) dependence of diffraction-line broadening caused by strain and size for all Laue groups in Rietveld refinement. *J. Appl. Crystallogr.* **1998**, *31*, 176–180. <https://doi.org/10.1107/S0021889897009795>.
- [36] Warren, B.E. *X-ray Diffraction*; Dover Publications Inc.: New York, NY, USA, 1969; ISBN 9780201085242.
- [37] Williamson, G.K.; Smallman, R.E. III. Dislocation densities in some annealed and cold-worked metals from measurements on the X-ray debye-scherrer spectrum. *Philos. Mag.* **1956**, *1*, 34–46. <https://doi.org/10.1080/14786435608238074>.
- [38] Fielding, L.C.D. The Bainite Controversy. *Mater. Sci. Technol.* **2013**, *29*, 383–399. <https://doi.org/10.1179/1743284712Y.00000000-157>.
- [39] Caballero, F.G. Bainitic Steel: Transformation Mechanisms and Properties. In *Encyclopedia of Iron, Steel, and Their Alloys*; Colás, R., Totten, G.E., Eds.; CRC Press: Boca Raton, FL, USA, 2016; pp. 291–305, ISBN 978-1-4665-1104-0.
- [40] Ali, A.; Bhadeshia, H. Nucleation of Widmanstätten ferrite. *Mater. Sci. Technol.* **1990**, *6*, 781–784. <https://doi.org/10.1179/-mst.1990.6.8.781>.

-
- [41] Bhadeshia, H.; Edmonds, D.V. The mechanism of bainite formation in steels. *Acta Mater.* **1980**, *28*, 1265–1273. [https://doi.org/10.1016/0001-6160\(80\)90082-6](https://doi.org/10.1016/0001-6160(80)90082-6).
- [42] Tszeng, T.C. Autocatalysis in bainite transformation. *Mater. Sci. Eng. A* **2000**, *293*, 185–190. [https://doi.org/10.1016/S0921-5093\(00\)01221-1](https://doi.org/10.1016/S0921-5093(00)01221-1).
- [43] Koistinen, D.; Marburger, R. A general equation prescribing the extent of the Austenite-Martensite transformation in pure iron-carbon alloys and plain carbon steels. *Acta Metall.* **1959**, *7*, 59–60. [https://doi.org/10.1016/0001-6160\(59\)-90170-1](https://doi.org/10.1016/0001-6160(59)-90170-1).
- [44] Olsen, G.B.; Cohen, M. Dislocation theory of martensitic transformations. In *Dislocations in Solids*; Nabarro, F.R.N., Ed.; Elsevier Science Publishers B.V.: Amsterdam, The Netherlands, 1986; pp. 293–408.
- [45] Dong, H.; Sun, X. Deformation Induced Ferrite Transformation. In *Ultra-Fine Grained Steels*; Weng, Y., Ed.; Springer: Berlin/Heidelberg, Germany, 2009; pp. 86–136, ISBN 978-3-540-77230-9.
- [46] Ghosh, G.; Raghavan, V. The kinetics of isothermal martensitic transformation in an Fe-23.2wt.%Ni2.8wt.%Mn alloy. *Mater. Sci. Eng. A* **1986**, *80*, 65–74. [https://doi.org/10.1016/0025-5416\(86\)90303-4](https://doi.org/10.1016/0025-5416(86)90303-4).
- [47] Bhadeshia, H. MAP Program MAP_STEEL_MUCG83. Available online: <http://www.phase-trans.msm.cam.ac.uk/map/steel/programs/mucg83.html> (accessed on 12 July 2021).
- [48] van Bohemen, S.M.C.; Sietsma, J. Kinetics of martensite formation in plain carbon steels: Critical assessment of possible influence of austenite grain boundaries and autocatalysis. *Mater. Sci. Technol.* **2014**, *30*, 1024–1033. <https://doi.org/10.1179/1743284714Y-00000000532>.
- [49] Santofimia, M.J.; van Bohemen, S.; Sietsma, J. Combining bainite and martensite in steel microstructures for light weight application. *J. S. Afr. Inst. Min. Metall.* **2013**, *113*, 143–148.

- [50] Capdevila, C.; Caballero, F.G.; Andrés, C.G. de. Determination of Ms temperature in steels: A bayesian neural network model. *ISIJ Int.* **2002**, *42*, 894–902. <https://doi.org/10.2355/isijinternational.42.894>.
- [51] Lee, J.S.; van Tyne, C.J. A kinetics model for martensite transformation in plain carbon and low-alloyed steels. *Metall. Mater. Trans. A* **2012**, *43*, 422–427. <https://doi.org/10.1007/s11661-011-0872-z>.
- [52] Wirths, V. Prozessführung und Zyklisches Werkstoffverhalten von Karbidfreien Bainitischen Stählen. Ph.D. Thesis, Rheinisch-Westfälischen Technischen Hochschule Aachen, Aachen, Germany, 2016.
- [53] Shipway, P.H.; Bhadeshia, H. Mechanical stabilisation of bainite. *Mater. Sci. Technol.* **1995**, *11*, 1116–1128. <https://doi.org/10.1179/mst.1995.11.11.1116>.
- [54] Hu, H.; Xu, G.; Wang, L.; Zhou, M.; Xue, Z. Effect of ausforming on the stability of retained austenite in a C-Mn-Si bainitic steel. *Met. Mater. Int.* **2015**, *21*, 929–935. <https://doi.org/10.1007/s12540-015-5156-5>.
- [55] Soliman, M.; Palkowski, H. Development of the low temperature bainite. *Arch. Civ. Mech. Eng.* **2016**, *16*, 403–412. <https://doi.org/10.1016/j.acme.2016.02.007>.
- [56] Shah, M.; Kumar, D.S.; Ankita, P. Phenomenological kinetic model of the nano-bainitic steels to characterize the dynamics of the autocatalytic nucleation process. *SN Appl. Sci.* **2020**, *2*, 635. <https://doi.org/10.1007/s42452-020-2395-y>.
- [57] PEET, M.J.; Bhadeshia, H. Surface relief due to bainite transformation at 473 K (200 °C). *Metall. Mater. Trans. A* **2011**, *42*, 3344–3348. <https://doi.org/10.1007/s11661-011-0755-3>.
- [58] Castro Cerda, F.M.; Sabirov, I.; Goulas, C.; Sietsma, J.; Monsalve, A.; Petrov, R.H. Austenite formation in 0.2% C and 0.45% C steels under conventional and ultrafast heating. *Mater. Des.* **2017**, *116*, 448–460. <https://doi.org/10.1016/j.matdes.2016.12.009>.
- [59] Narutani, T.; Takamura, J. Grain-size strengthening in terms of dislocation density measured by resistivity. *Acta Metall. Mater.* **1991**, *39*, 2037–2049. [https://doi.org/10.1016/0956-7151\(91\)90173-X](https://doi.org/10.1016/0956-7151(91)90173-X).

Chapter IV

Low carbon bainitic steel processed by ausforming: Heterogeneous microstructure and mechanical properties

Theerawat Kumnorkaew, Junhe Lian, Vitoon Uthaisangsuk,

Jiali Zhang, and Wolfgang Bleck

Materials Characterization 2022; 194: 112466

<https://doi.org/10.1016/j.matchar.2022.112466>

Chapter IV characterizes the enhancements of thermodynamic stability of austenite on microstructure heterogeneity and tensile properties of a low carbon bainitic steel processed by ausforming and a single stage of isothermal bainitic transformation. Microstructure characterizations done by EBSD, XRD, and dilatometric experiments bring about a better understanding of how the thermodynamic stability of austenite enhances the tensile properties of the steel. Tensile properties of the steel are improved due to the adjusted heterogeneous microstructure and well balance of its phase constituents, especially the minimized fraction of fresh martensite. The significantly increased strengths are mainly attributed to microstructure refinement as well as the enrichment of geometrically necessary dislocations (GNDs) within the bainitic ferrite and retained austenite. Moreover, a large fraction of retained austenite has a significant impact on the enhancement of both uniform elongation and strength, benefitting from the transformation-induced plasticity (TRIP) effect. Apart from that, grain boundary strengthening and a large fraction of highly stable retained austenite lead to effective retardation of void nucleation, consequently preventing the formation of macro/micro-cracks during post-necking.

Low carbon bainitic steel processed by ausforming: Heterogeneous microstructure and mechanical properties

Theerawat Kumnorkaew^{a,*}, Junhe Lian^b, Vitoon Uthaisangsuk^c,
Jiali Zhang^d, and Wolfgang Bleck^a

^a Steel Institute of RWTH Aachen University, 52072 Aachen, Germany.

^b Department of Mechanical Engineering, Aalto University, 02150 Espoo, Finland.

^c Center for Lightweight Materials, Design and Manufacturing, Department of Mechanical Engineering, King Mongkut's University of Technology Thonburi, 10140 Bangkok, Thailand.

^d Institute for Materials Applications in Mechanical Engineering, RWTH Aachen University, 52062 Aachen, Germany

theerawat.kumnorkaew@iehk.rwth-aachen.de; junhe.lian@aalto.fi; vitoon.uth@kmutt.ac.th;

j.zhang@iwm.rwth-aachen.de; bleck@iehk.rwth-aachen.de

Highlights:

- Ausforming improves the thermodynamic stability of the retained austenite.
- Ausformed microstructure with high GND densities hinder martensite transformation.
- Strength and ductility are enhanced by the developed heterogeneous microstructure.
- Microstructural refinement retards macro/microcracks formation up to fracture.

Abstract:

Thermodynamic stability of austenite is a primary factor affecting mechanical properties of low-carbon bainitic steels. In this work, ausforming was applied to a low-carbon steel, in which additional dislocations and defects were induced in austenite prior to isothermal transformation of bainite at a relatively low temperature. Hence, the stability of the retained austenite was improved, and the formation of fresh martensite during the secondary stage of cooling was suppressed. Results of microstructure characterizations by electron backscatter diffraction (EBSD), X-ray diffraction (XRD), and dilatometry were examined. The correlations between the process parameters and developed heterogeneous microstructures were established. It was found that the volume fraction of retained austenite was greatly promoted along with the reductions of fresh martensite and bainitic ferrite. Tensile properties of the bainitic steel were enhanced due to the occurred heterogeneous microstructure and fair balance of its phase constituents. The significantly increased strengths were mainly attributed to microstructure refinement as well as the enrichment of geometrically necessary dislocations (GNDs) within the bainitic ferrite and retained austenite. Furthermore, a large fraction of retained austenite showed a significant impact on the enhancement of both uniform elongation and strength, benefitting from the transformation-induced plasticity (TRIP) effect. The presence of microcracks and tiny dimples with thick tearing edges in the vicinity of the inclusions in the fractographs were directly related to the refined microstructure, which certainly provided a remarkable ability to reduce the formation of macro/micro-cracks and prolong the post-necking.

Keywords: Thermodynamic stability of austenite; ausforming; heterogeneous microstructure; mechanical properties; GND density; TRIP effect

1. Introduction

Over the past decades, bainitic steels have attracted much attention in the automotive industry and become a new forefront of modern steels for forged components due to their lightweight and remarkable mechanical properties, which can be achieved at a low cost. It is well-known that lightweight components play a crucial role in improving vehicle performance by reducing average fuel consumption, accompanying depreciation of the average CO₂ emission [1]. As reported by

Sugimoto [2,3], bainitic forged steels, composed of lath-like bainitic ferrite and film-like retained austenite, possess an outstanding balance in tensile strength, ductility, and toughness. It was also found that the bainitic ferrite with thicknesses of less than 100 nm has a great resistance in micro-crack initiation and effectively improves toughness by inhibiting cleavage fracture. Nevertheless, heat treatment is time-consuming because of the high stability of austenite. Generally, these components are manufactured via hot forging followed by a simple process of heat treatment; isothermal tempering, or controlled cooling. These two heat treatments must be within a temperature range far below pearlitic formation but above the temperature where martensite can form [2,3]. Additions of elements, such as Mn, Cr, Si, Cu, Ni, Mo, and S, can bring about a wide range of mechanical properties through microstructural adjustment; however, a thorough understanding of microstructural evolution during heat treatment is necessarily required [4–6]. An optimum alloy design with a reduction of expensive alloy elements such as Ni and Cr to a range of 0.1–0.2 wt.% allows steel production through a single-step isothermal heat treatment process [7,8]. In addition, approximately 1.0 wt.% of Si is found to be adequate to arrest carbide precipitation during bainitic transformation.

According to the displacive theory proposed by Bhadeshia [9], bainitic transformation starts by paraequilibrium nucleation of bainitic ferrite and progresses by their shear growth without diffusion. During the diffusionless growth, any exceeded carbon from supersaturated bainitic ferrite plates is ejected into the adjacent austenite along with dislocation debris arising in the vicinity of bainitic laths, leading to the so-called “incomplete reaction phenomenon”. The transformation is ceased when the carbon content of austenite reaches the value predicted at T_0 curve. The T_0 curve is the locus of values where austenite and ferrite of the same chemical composition have identical driving energy. Bhadeshia and Edmond [10] explained that diffusionless transformation only occurs at temperatures below the T_0 temperature when the chemical driving energy of retained austenite becomes less than that of bainitic ferrite of the same carbon concentration. For carbide-free steels, the concept of T_0 can be used to estimate the volume fraction of retained austenite apart from that of bainitic ferrite, depending on the carbon content of austenite and the transformation temperature. According to the lever rule [9,11], the volume fraction of bainitic ferrite can be increased by decreasing the transformation temperature. The temperature should be above the martensite start (M_s) temperature so that austenite is only decomposed into bainitic ferrite during the transformation. Lowering the M_s temperature has been

an essential technique to maximize the volume fraction of bainitic ferrite while maintaining the retained austenite fraction by reducing the feasibility of martensitic transformation during cooling operation [11]. Apart from the design of alloy composition [12–16], various heat treatment techniques [17–21] have also been employed to alter an appropriate mixture of heterogeneous microstructures. However, the primary fresh martensite is highly promoted by the thermodynamic instability of austenite, especially in low-carbon steel (< 0.2 wt.%C) [22–24], in the form of granular features of austenite and/or martensite-austenite constituent (M/A). These austenite islands remain to exist and consequently lead to a drastic formation of secondary fresh and brittle martensite in an early stage of deformation [25]. It is reported that the excessive formation of fresh martensite leads to the deterioration of toughness, ductility, and fatigue properties, indicating a dissatisfactory TRIP effect on the steel.

Ausforming is a thermomechanical treatment technique that combines a plastic deformation of metastable austenite with bainitic transformation. Crystal defects such as grain boundaries and dislocations substantially developed by the deformation are expected to facilitate bainitic ferrite formation due to increased nucleation sites [9]. The defects incorporated surrounding the bainitic ferrite lattices are prone to impart the driving force for bainitic growth, particularly at the initial stage of the bainitic transformation. Eventually, substantial debris of dislocations from the displacive transformation accompanying carbon enrichment successively introduced into austenite hinders the progress of the bainitic reaction due to the mechanical stabilization phenomenon. However, the hinderance of the bainitic progress at the early stage of the transformation is undesirable as more nucleation sites available for martensitic transformation could be provided [26]. As observed in various studies, ausforming has been mostly applied to medium (0.3 wt.% $< C < 0.5$ wt.%) and high ($C > 0.5$ wt.%) carbon steels [18,27–29] rather than to low carbon steels. Many studies paid more attention to shortening the kinetics incubation than considering the transformation-induced dislocations since plenty of defects from grain refinement and supercooling may likely lead to overstabilization of austenite. In this case, small deformation has been widely applied so that planar dislocations remain on the active slip planes to assist bainitic transformation accompanied by a strong variant selection [30]. On the contrary, for low carbon steels, where grain refinement includes the defects obtained by undercooling at a very low M_s temperature is virtually impossible, ausforming with a large deformation strain was proposed to compensate for what can be achieved in high and medium carbon steels. For instance, He et al.

[31] varied a wide range of the compressive strain to steels containing 0.2 wt.%C, then observed that the maximum fraction of bainite with a drastic reduction of fresh martensite is reached at a strain of 25% over a temperature range between 600 to 700°C. The decrease in the average volume of fresh martensite is occupied by the formation of bainitic ferrite sheaf. The dislocations intensively dispersed within individual sheaves consequently reduce the interfacial energy available for martensite transformation [32]. Also, Zhao et al. [33] held a consistent opinion that the dislocations dispersed across the fine thickness of bainitic ferrite laths (<100 nm) lead to an enhancement of material strengthening. Nevertheless, their analysis only aimed at reducing bainitic thickness, while the dislocations that interact with the parent structure were not mentioned. In terms of the mechanical response, defects induced by ausforming could lead to changes in grain size, morphology, and carbon enrichment in austenite upon phase transformation, thus resulting in variations of uniform elongation due to the transformation-induced plasticity (TRIP) effect. However, the effect of microstructure refinement on post-necking behavior and the link between the ausforming process, isothermal phase transformation, microstructural evolution, and tensile properties of low-carbon steels (< 0.2 wt.%C) have never been thoroughly presented.

Therefore, this research aims to systematically investigate the isothermal transformation kinetics, phase constituents, and mechanical properties related to the microstructural evolution of low-carbon bainitic steel that is processed either by the conventional process of isothermal heat treatment or by applying ausforming prior to the isothermal heat treatment. This investigation also aims to explore the possibility of establishing advanced high-strength steels to improve strength and ductility via the ausforming process. Factors such as dislocation density and grain refinement are thoroughly described to emphasize their contributions to the enhancement of mechanical properties. The outcome is expected to provide an approach for designing and preparing bainitic steels with low carbon content and facilitating the application of such steels.

2. Experimental procedures

2.1. Material

An experimental low-carbon steel with a chemical composition presented in **Table 1** was employed in the present study. The alloy was prepared by melting in a laboratory-scale vacuum arc furnace and subsequently cast to an 80 kg ingot with dimensions of 140 mm×140 mm×525

mm. The ingot was delivered further for homogenization at 1250°C for 2h and sequentially hot-forged into 60 mm² cross-sectional billets at a finishing temperature of 950°C. The billets were manufactured into small-scale rectangular specimens (20 mm×20 mm×65 mm) and cylindrical specimens (Ø5 mm×10 mm) for thermal-/thermomechanical processes.

Table 1 Chemical composition of the investigated steel in wt.%.

C	Si	Mn	Cr	Ni	B	Ti	Fe
0.18	0.97	2.50	0.20	0.21	0.0018	0.033	Balance

2.2. Ausforming process

All thermal-/thermomechanical treatments were performed at the Steel Institute, RWTH Aachen University, using a Thermomechanical Treatment Simulator TTS820 (TA Instruments GmbH, Hüllhorst, Germany). These apparatuses enabled the experimental simulations of compressive operation from which the secondary tensile specimens can be produced after the treatment process. The primary rectangular specimens were treated with different processes: PIT (pure isothermal tempering) and AIT (ausforming prior to isothermal tempering). But only the heating and tempering stages were identical, as illustrated in **Fig. 1a**. At the very beginning stage, all specimens were heated to an austenitizing temperature of 950°C at 18°C/s and held for 5 min for homogenization. Then, the specimens were isothermally treated at 400°C for 60 min to ensure that the decomposition from austenite to bainite was completed. For the PIT process, a specimen was defined as a reference. It was cooled from the austenitizing temperature directly to the isothermal tempering stage at 50°C/s for bainitic transformation before cooling further to room temperature at 20°C/s. For the AIT process, two austenitized specimens were cooled to a temperature of 650°C (T_{def}) at 50°C/s. Individual specimens were soaked for 10 s before being compressed to different strains (φ) at a strain rate ($\dot{\varphi}$) of 1 s⁻¹ in the direction transversal to the length of the specimen. The specimen deformed to a small strain of 0.15 called “AIT0.15”, whereas the other to a higher strain of 0.35 called “AIT0.35”. After the deformation, these specimens were tempered and cooled with the same conditions as the PIT specimen.

To examine the kinetics behavior of bainitic transformation and measure the locus variation of martensitic start (M_s) temperature, the cylindrical specimens were employed in a Bähr DIL805A/D

high-resolution dilatometer (TA Instruments GmbH, Hüllhorst, Germany). The machine was equipped with a deformation module and an optical contactless module so that contraction/expansion in both radial and longitudinal directions of the specimens could be fully captured. The dilatometry specimens were deformed in the lateral direction, unlike the specimens carried out in the TTS machine due to its operational direction. Relative volume strain ($\Delta V/V$) was calculated to represent the overall kinetic behavior of bainite during the operation using the following formula:

$$(1 + \varepsilon_L)(1 + \varepsilon_R)^2 - 1 \quad (15)$$

where ε_L and ε_R represent the instantaneous strains in longitudinal and radial directions, respectively. A reference dilatometry specimen for this investigation was made by the direct quenching (DQ) process. It was directly quenched from the austenitizing temperature to room temperature at 50 °C/s, according to the processing diagram described elsewhere [24]. Meanwhile, as mentioned earlier, the other three specimens were conducted under the PIT and AIT processes.

2.3. Mechanical tensile testing

After the thermal-/thermomechanical treatments, the primary specimens were manufactured into cylindrical tensile specimens according to EN10002 (see **Fig. 1b**). The mechanical properties of the secondary specimens were evaluated using quasi-static tensile testing. The tensile tests were carried out at room temperature and at a constant crosshead speed of 0.5 mm/min using a screw-driven ZWICK Z100 machine (Zwick GmbH & Co. KG, Ulm, Germany). A mechanical strain gauge with a length of 15 mm was used to trace the elongation of the specimen during tensile deformation.

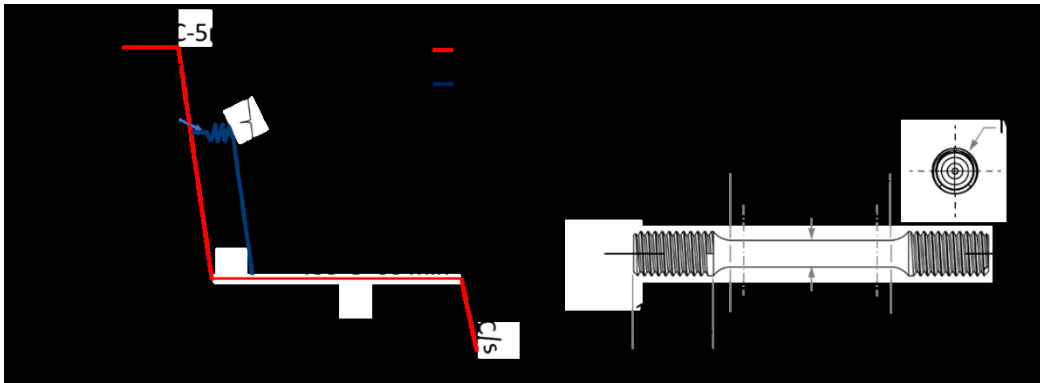


Fig. 1 (a) Temperature-time schedule indicating the pure isothermal tempering (PIT) and the ausforming prior to isothermal tempering (AIT) processes, which were conducted in the thermomechanical treatment simulator and high-resolution dilatometer (b) dimension of the tensile specimen

2.4. Characterization methods

The primary PIT and AIT specimens were identically prepared for metallographic characterization. They were embedded in bakerite material using a Qpress 50 (OPAL X-PRESS, X-P50). Later, the metallographic specimens were mechanically ground with water-abrasive papers (No. 600, 1200, 2400, and 4000), followed by polishing with a fine diamond paste of 0.1 μm through a SAPHIR 560 machine (ATM GmbH, Mammelzen, Germany). After polishing, the specimens were additionally electro-polished by a LectroPol-5 electropolishing device (Struers A/S, Ballerup, Denmark) at room temperature for 15 s at 32 V and in A2 struers solution. A SEIFERT Analytical X-Ray Diffraction (XRD) machine (XRD Eigenmann GmbH, Schnaittach, Germany) was set up using a Vanadium filtered $\text{CrK}\alpha$ radiator, which was operated at 40 kV and 40 mA under the collective range between 60° and 165° with a step size of 0.05° and a counting time of 2 s. The fractions of face-centered cubic (fcc-RA) and body-centered cubic (bcc) were subsequently analyzed by Rietveld's refinement method using MAUD software [34]. The carbon concentration within the austenite, x_C (wt.%), was estimated from its lattice parameter a_γ [35] as:

$$a_\gamma(\text{\AA}) = 3.556 + 0.0453x_C + 0.00095x_{Mn} + 0.0056x_{Al} \quad (16)$$

where x_{Mn} and x_{Al} are in wt.%.

However, XRD analysis could not successfully distinguish between bainitic ferrite and fresh martensite due to structure and lattice similarity. A simple method was thus carried out by combining the results from the dilatometry and XRD analysis, as described in [24], to quantify the volume fraction of the individual structures. Qualitative measurements of bainitic ferrite packets, retained austenite, and fresh martensite microstructures in different features were carried out by a field-emission scanning electron microscope (Zeiss Sigma FE-SEM, Carl Zeiss Microscopy GmbH, Jena, Germany) using In-Lens detector. Afterward, the electron backscatter diffraction (EBSD) technique was applied to approach the crystallographic information of the specimens based on the Kikuchi pattern [36]. The analysis was conducted at 20 kV under a measuring step

size of 60 nm in the Zeiss Sigma FE-SEM equipped with a NordlysNano-EBSD detector (Oxford instrument, Abingdon, UK). The data obtained by EBSD measurement was post-processed and analyzed using the MATLAB-based MTEX toolbox [37]. The half-quadratic filter developed by Bergmann et al. [38] was applied to resolve any measurement error that may occur from a poor calibration of the EBSD system and noise in the Kikuchi pattern so that the non-indexed points can be assigned. It was also suggested that this filter could preserve better inner grain boundaries than other commonly used spline filters, thus suitable for analyzing sub-granular features [39]. Fracture analyses were carried out on the top surface of failed specimens after tensile tests in the SEM using a secondary electron (SE) detector.

3. Results and discussion

3.1. Transformation evaluation

The relative volume strain of PIT and AIT specimens observed along the cooling and the isothermal tempering stages are shown in **Fig. 2**. A direct quenching (DQ) curve shown in **Fig. 2a** was set as a reference to specify M_s temperature and used to compare with the PIT and AIT curves. The bainitic volume strain at 400 °C and the martensitic volume strain at the final cooling stage is indicated by α_B and α' , respectively. The effect of ausforming played a significant role in the thermal stability improvement of austenite since the α_B and α' are decreased with increasing the ausforming strains. This result was more pronounced in the secondary stage of austenite decomposition upon cooling to room temperature in which M_s temperature and the formation of α' were resisted by austenite strengthening. It can be referred to as the mechanical stabilization of austenite caused by carbon enrichment and dislocation density developments [26]. Additionally, the kinetic aspects of isothermal bainitic transformation (α_B region) shown in **Fig. 2b** indicate that the incubation time for the bainitic nucleation obtained in AIT0.35 specimen was shortened over ~50 s compared with PIT specimen. The transformation kinetics was initially accelerated, then became sluggish in the later stage. Notably, this kinetic acceleration strongly depended on the magnitude of ausforming and was inversely proportional to the subsequent progress of the transformation. The results thus led to a reduction of bainitic ferrite fraction with a substantially longer time required for the completion. In comparison, the PIT specimen required ~1121 s to reach the transformation plateau, while the AIT0.15 and AIT0.35 specimens possessed dramatically longer duration up to ~2130 s and ~3279 s, respectively. Also, the volume fraction of

BF was reduced from ~ 0.84 to ~ 0.76 . These incidents are congruent with experimental validation and thermodynamic calculation conducted by van Bohemann [40], who clarified that the shortened incubation time is attributed to an increase in available nucleation sites of plastically deformed austenite. In this sense, more available nucleation sites then reduced the energy barrier required for the transformation, enhancing the nucleation driving force. Although such a circumstance that improves the formation of bainitic ferrite occurred only in the preliminary stage of the transformation, the dislocations consecutively developed together with the carbon enrichment led to the deceleration of the progress of the transformation. Similar results were described in a recent study [41] that the sluggish reaction is directly associated with a reduction of the net driving energy. The continuous decrease in the net driving energy is due to the mechanical stabilization of the untransformed austenite, which increased while the transformation progressed. Nevertheless, this mechanism leads to hinder the further progress of bainitic ferrite as the austenite becomes essentially strengthened, resulting in a reduction of bainitic ferrite fraction. Likewise, the subsequent transformation of fresh martensite can become thermodynamically difficult during cooling to room temperature.

Hence, the results of the previous descriptions can be summarized by the volumetric reduction of the bainitic ferrite (BF) and fresh martensite (FM) along with a considerable increment of retained austenite (RA) in AIT0.15 and AIT0.35 specimens, respectively. As can be seen from **Fig. 3a**, almost 16% of retained austenite has remained in AIT 0.35 specimen. In this way, it can be concluded that ausforming also effectively allowed the enrichment of carbon into austenite, as displayed in **Fig. 3b**, regardless of the carbon partitioning into austenite during the secondary decomposition of the untransformed austenite to FM.

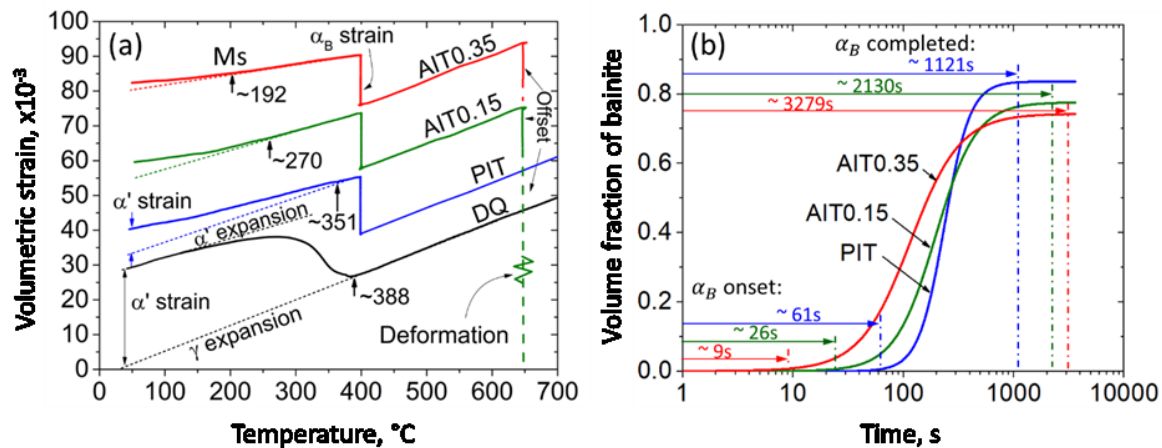


Fig. 2 (a) Volumetric dilation change of the dilatometry specimens during cooling after an austenitizing temperature of 950°C (DQ/PIT specimens) or the ausforming temperature of 650°C (AIT specimens), (b) kinetic of bainitic transformation of PIT and AIT specimens during the isothermal transformation at 400°C

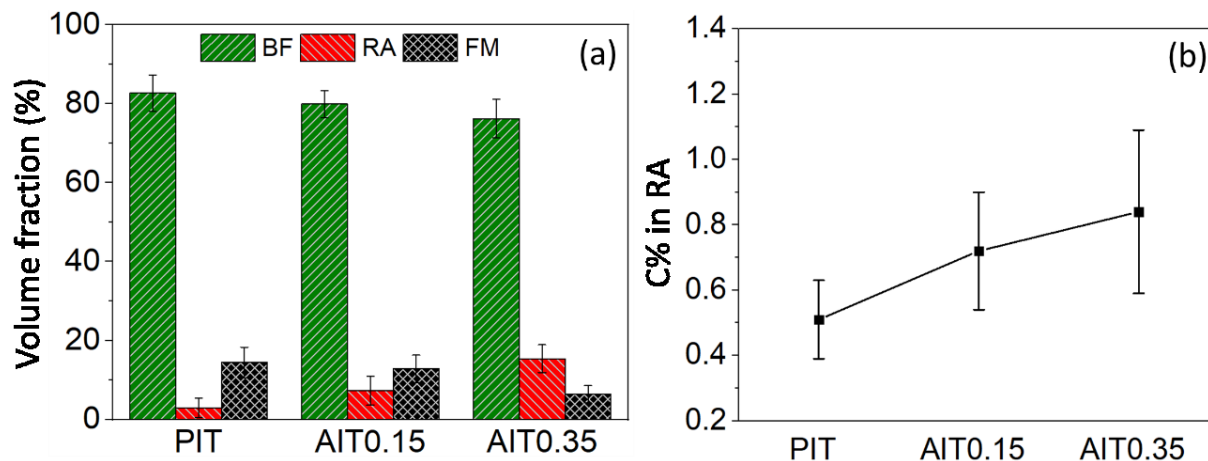


Fig. 3 (a) Volume percentage of bainitic ferrite (BF), retained austenite (RA) and fresh martensite (FM) in the heat-treated specimens carried out by XRD analysis combined with the dilatometric method and (b) carbon content in weight percent of RA

3.2. Analysis of heterogeneous microstructure

The SEM (In-Lens) micrographs of PIT specimen are displayed in **Fig. 4**. It revealed that a prior austenite grain was divided into several packets of BF with different orientations, as defined by the red highlighted boundaries shown in **Fig. 4a**. The largest packet within individual prior austenite grain boundary (PAGB) consists of BF laths entrapped between RA films, which

arranged in almost the same orientation [9,42,43]. On the other hand, the small packets consist of RA grains or FM blocks located between lath-like and granular features of BF grains. From the morphological aspect, the granular structures of BF as a component of a single BF packet could be better indicated with the assistance of EBSD by defining a grain tolerance angle of 5 degrees and a minimum grain size of 2 pixels. Regarding the RA feature, the presence of blocky or film-like RA shown in **Fig. 4b** was dependent upon the BF feature. Film-like RA is unique and always located between the BF laths, whereas blocky RA is surrounded by several grains of granular BF. The morphological difference of RA can be characterized by their brightness levels, which are related to their carbon concentration [41]. The brightness of blocky RA depends on its size and is always lower than that of the film-like feature. In addition, it can be noticed that FM is mainly formed within the large grains of blocky RA and has lower brightness but does not lower than the BF matrix.

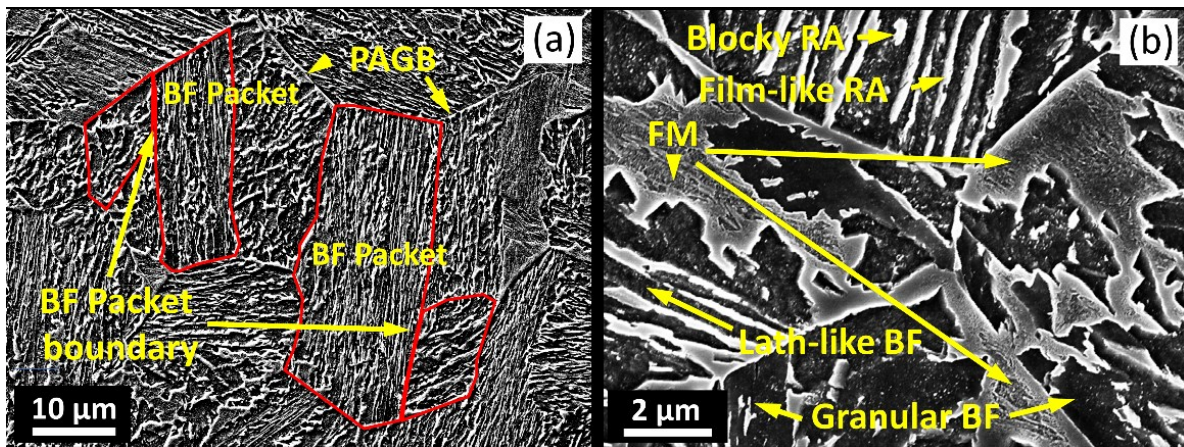


Fig. 4 SEM micrographs of PIT specimen obtained from an In-Lens detector, showing examples of (a) components of bainitic ferrite packets within prior austenite grains (PAGs) and (b) microstructures of bainitic ferrite (BF), retained austenite (RA), and fresh martensite (FM) in different features.

Fig. 5 shows EBSD inverse pole figure maps in the z-direction (IPF-z), misorientation angle distribution maps, corresponding misorientation angle data, statistics of average grain size based on Euler angle, and the average grain size for bcc (BF/FM) and fcc (RA) of the PIT, AIT0.15, and AIT0.35 specimens. The IPF-z maps of bcc structures demonstrated in **Fig. 5a-5c** were colored relative to different orientations and perpendicular to the deformed direction. All structures formed within a PAG consist of elongated and granular grains of FM and BF. As revealed in **Fig. 5b** and

Fig. 5c, it is more evident that BF/FM regions were divided into several small BF packets and FM blocks arranged almost perpendicular to the ausforming direction, especially in the AIT0.35 specimen with the highest magnitude of the deformation. Although the BF and FM regions in AIT0.35 seem more refined than those in PIT and AIT0.15 specimens (see in black marks), the grain size distributions shown in **Fig. 5g** indicate that only the percentage of grains with sizes less than 2 μm was decreased with a slight increase in the percentage of larger grains. However, the statistical evidence could not be fully concluded towards microstructural development. Therefore, in **Fig. 5h**, statistical results of the average grain sizes obtained by the IPF-z maps of fcc-RA were considered and compared to those of bcc structures. On the one hand, it can be noted that the average grain size of bcc represented by the black line was slightly reduced from 1.75 to 1.3 μm with increasing the magnitude of ausforming, and the minimum average grain size of bcc was found in the AIT0.35 specimen. On the other hand, reducing the average grain size of bcc significantly raised the average RA grain size despite having negligible differences, as shown in the red line.

It is straightforward to notice that the average grain size of bcc depends on the magnitude of the deformation, contrary to that of fcc, which most likely resulted from the interaction between the defects and carbon content in the austenite. The morphology of RA can only be presented in two features: film-like and blocky types, depending on the amount of carbon enrichment and the dislocations generated in the matrix around RA [21]. The concentration of carbon enriched in each feature was quantitatively measured by atom probe tomography (APT), in which the different carbon concentrations and the positions of the individual features were revealed [25,41,42]. The RA films entrapped between the adjacent subunits of BF have higher carbon content than the RA blocks, which are usually surrounded by BF grains or intervened between sheaves/packets of BF. Besides the carbon enrichment in austenite during bainitic transformation, the decomposition of austenite into BF and FM was accompanied by the generation of dislocations [32]. Although the dislocation clusters around the individual features of RA have never been separately quantified, it could still be assumed that the number of dislocations should be related to that of the carbon enriched in austenite by the principal [9]. However, this could be difficult to justify straightforwardly since the ausforming divided the prior austenite grain (PAG) into several subgrains and introduced plenty of dislocations into the untransformed austenite. The dislocations could assist the transformation, thereby leading to more carbon segregating into the large RA

blocks. The misorientation angle distributions of the studied steels displayed in **Fig. 5d-5f** reveal the alteration of the grain-to-grain angle. The low misorientation ($2^\circ \leq \theta < 15^\circ$) of sub-grain boundaries is denoted by red lines, whereas the high misorientation region of $15^\circ \leq \theta < 55^\circ$ and $55^\circ \leq \theta < 65^\circ$ of high-angle boundaries are represented by blue and black lines, respectively. The PAG boundaries were classified by the region of misorientation angle between 15° and 55° in which the bainitic-ferritic boundaries were also found within this range. For the quantitative analysis, the relative frequency of different misorientations is shown in **Fig. 5i**. The fragmentation of a higher quantity of PAG and subgrain boundaries was associated with the development of dislocation density. It corresponded to a decrease in the high-angle boundaries due to BF and FM reduction. The stress fields generated by dislocations at low-angle grain boundaries were responsible for the atomic arrangement and contributed to the stability improvement of RA [44].

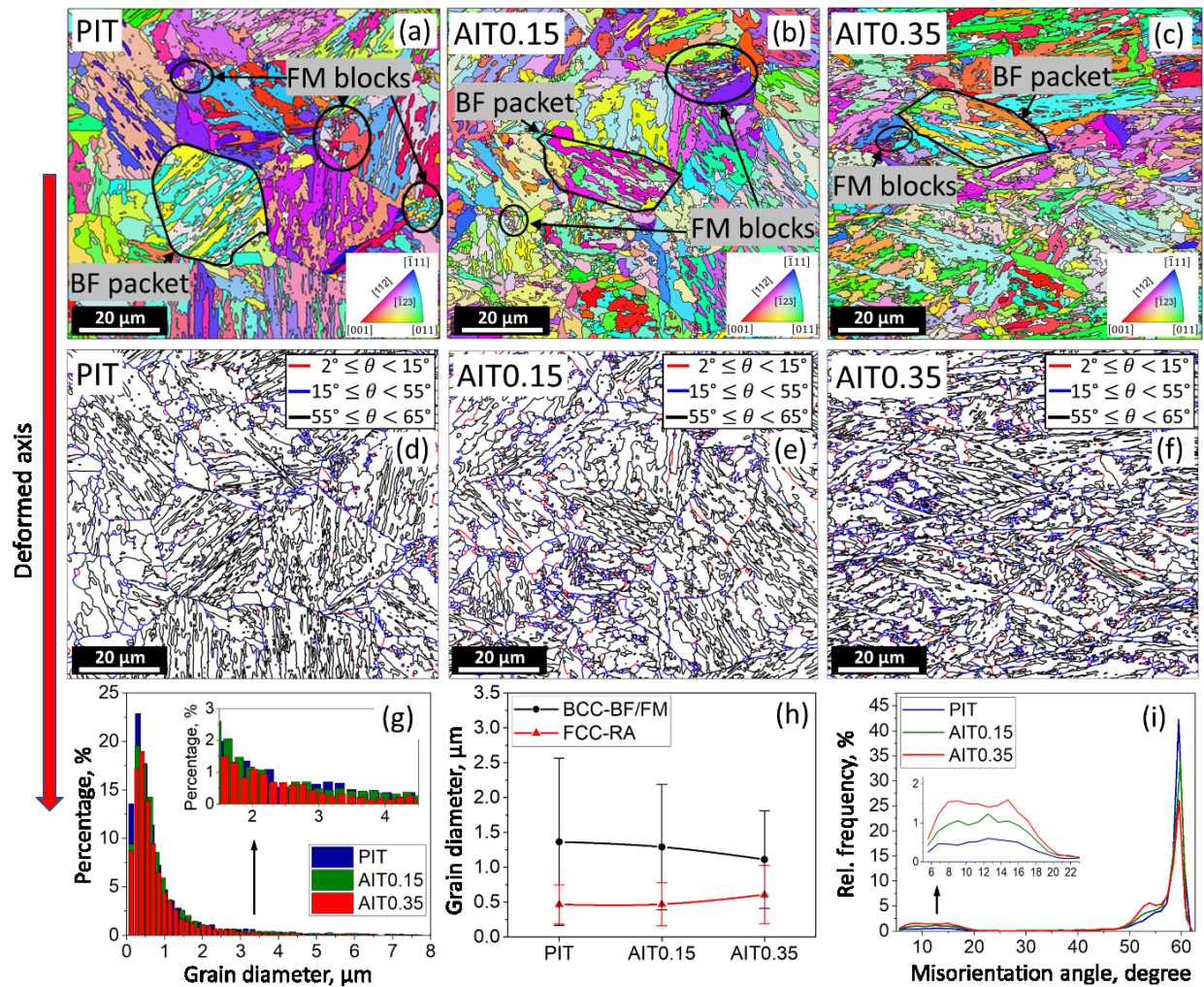


Fig. 5 (a)-(c) Inverse pole figure (IPF) maps \perp the deformed direction of the PIT, AIT0.15, and AIT0.35 specimens; (d)-(f) Misorientation angle distribution maps according to low and high angle separation of PIT, AIT0.15 and AIT0.35 specimens; (g) Statistics of grain size distribution; (h) Average grain size of bcc (BF/FM) and fcc (RA); (i) Relative frequency of misorientation angle depending on the treatment conditions. BF, FM, and RA refer to bainitic ferrite, fresh martensite, and retained austenite, respectively.

Owing to the microstructural complexity, image quality (IQ) maps obtained by EBSD, based on the intensity of the Kikuchi bands, were used to conduct a quantitative analysis of the bcc phase. As stated by Suzuki [45], if there is no damage caused by specimen preparation, contamination, or formation of oxide on the surface of the specimen, the IQ map can be reflective of the degree of structural distortion in the diffracted volume. The low crystal distortion degree is strongly displayed on the greyscale IQ map in brightened regions, which reflects its high IQ values. On the contrary, grain boundaries and highly distorted structures, such as FM with low IQ values, would display dark regions. The IQ map, statistical data of the IQ value, and phase maps superimposed with the corresponding IQ maps obtained on EBSD data of the PIT, AIT0.15, and AIT0.35 specimens are presented in **Fig. 6**. Moreover, **Fig. 6a** shows a selected IQ map of the PIT specimen. As aforementioned, grain boundaries and FM are visualized in the dark to black colors, whereas the bright regions represent lower distortion in the composite structures of BF. In this work, the relative frequency of the IQ on the scanned regions was plotted with respect to the IQ values to differentiate the microstructural constituents of FM and BF. For instance, two subareas with clearly different image qualities were extracted to demonstrate the analyses. Subarea1 should comprise grain boundaries, FM (showing in low IQ values), and BF in high IQ values, whereas a brightened Subarea2 could be as BF microstructure. Slightly different shades in the BF regions were assumed to be associated with the microstructural distinction, by which shear components and the formation of dislocations within the individual structure according to the phase transformation were involved.

The histograms of IQ values were analyzed by the deconvolution of the sum of multiple Gaussian peaks [46]. For instance, the data of Subarea1, as shown in **Fig. 6b**, was deconvoluted into three Gaussian peaks. The Gaussian peak that laid in the range of low IQ values was referred to FM, while those of higher IQ values were associated with BF. In addition, the intersection between the adjacent peaks was assumed to be a threshold between two components. However, the double

outliers that appeared within the BF region were composed of a superposition of two Gaussian peaks, which were assumed to be parts of bainite and ferrite, respectively. Subsequently, the heterogeneous components of BF were characterized further with the IQ plot of Subarea2 (**Fig. 6c**). It can be seen that bainite and ferrite microstructures were separated at a threshold of about 100 with bainite and ferrite corresponding to lower and higher ranges, respectively. Additionally, the thresholds of the IQ histogram of the entire region were found to be consistent with that of the Subarea1 for PIT specimen (**Fig. 6d**). Interestingly, the threshold value between FM and BF and that between bainite and ferrite were shifted towards higher ranges when the magnitude of ausforming was increased, as shown in **Fig. 6e-6f**. Particularly, in the range of bainite and ferrite, the thresholds are proven to be higher than 100. The highest threshold of FM over the value of 80 was found in the AIT0.35 specimen with a significant reduction of the total area under the deconvoluted peak of FM. The reduction of FM fraction with an increased threshold in the IQ histogram was somewhat related to the increases in low-angle grain boundaries and their neighboring substructures with highly accumulated dislocation density in the untransformed austenite. Although it was reported that increasing the defect density in PAGs would induce more nucleation sites for bainitic transformation, the dislocations excessively generated by ausforming and during the progress of BF formation could be turned to enhance the thermal stability of austenite. Based on the displacive theory of bainitic transformation [9], the latter reduced the nucleation sites available for martensitic transformation and left more austenite untransformed during the subsequent cooling, as presented in **Fig. 6g-6i**. To quantify the total fraction of bainite and ferrite, the area under each deconvolution peak of the IQ histograms was calculated. The fraction of bainite for PIT, AIT0.15, and AIT0.35 specimens were about 32.6%, 30.8%, and 24.3%, while that of ferrite were about 47.7%, 48.1%, and 49.7%, respectively. These could be evaluated that ausforming devaluated the bainite fraction but promoted the fraction of ferrite.

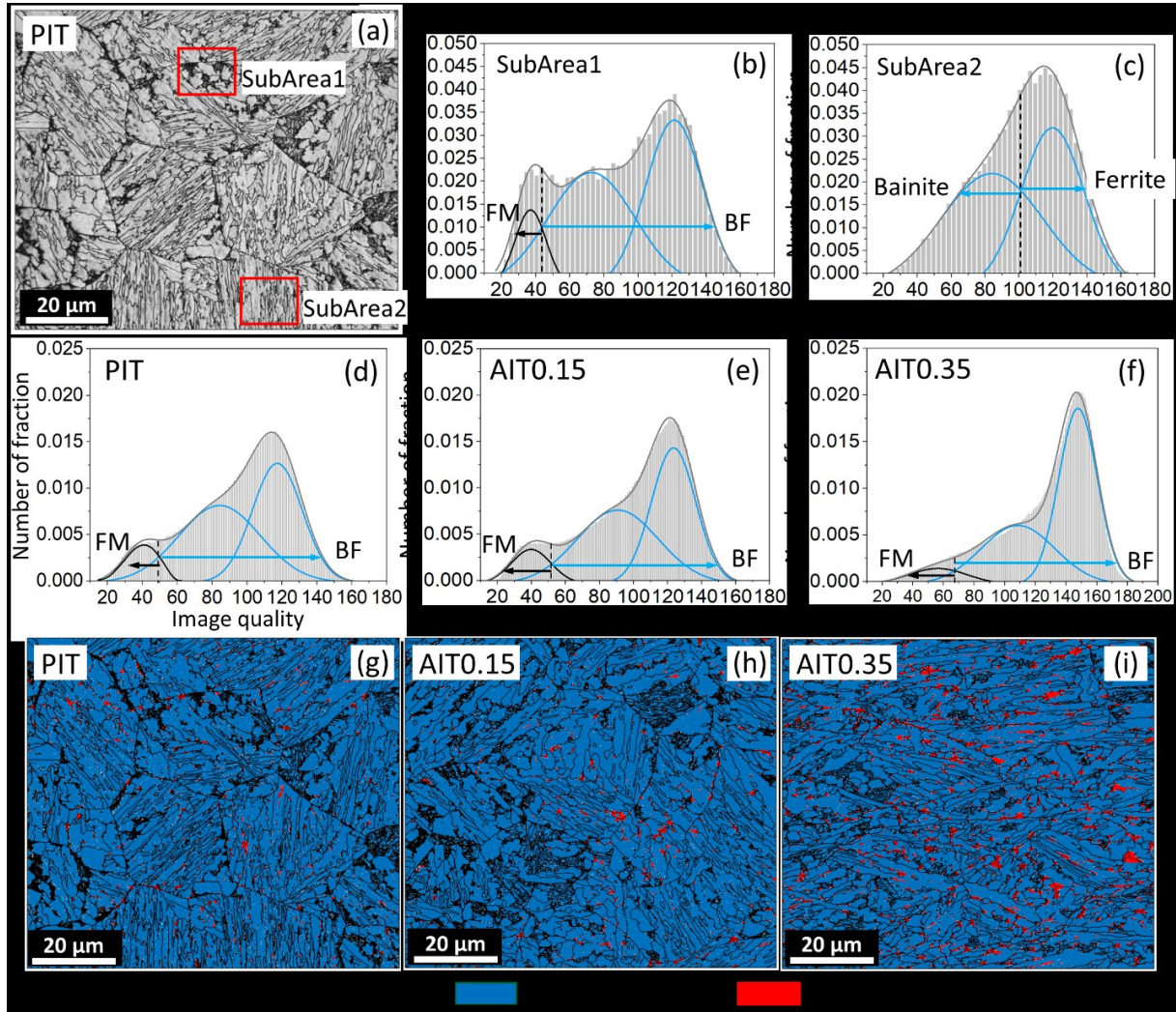


Fig. 6 (a) EBSD-IQ map of PIT specimen indicating two representative areas for a determination of bainite/ferrite threshold; (b) and (c) statistical intensity of Kikuchi pattern of structural distribution fitted with Gaussian multiple peaks method applied in Subarea1 and 2, respectively; (d)-(f) variation of the statistical intensity of fresh martensite and bainitic ferrite in PIT, AIT0.15, and AIT0.35 specimens; (g)-(i) IQ map superimposed by phase maps indicating the increase in retained austenite fraction caused by ausforming.

3.3. Local plastic strain and stress concentration

The local strain distribution was also evaluated by EBSD kernel average misorientation (KAM) maps. In general, the calculation of KAM provides the average misorientation around a measured point corresponding to all surrounding points of EBSD data. Therefore, the variation of KAM

value can be interpreted in terms of the degree of local lattice distortion or local plastic strain [47]. For the KAM analyses, the first-order neighbors were employed as the local dislocation structures of the deformed material could already be nicely revolved without costing too much computational time. The variation of color in the KAM map visualizes local strain distribution, i.e., the blue color represents no strain, while green and red represent fairly and highly strained regions, respectively. Therefore, the local strain distributions stored in PIT and AIT specimens can be seen in **Fig. 7a-7c**. A highly concentrated strain in KAM is observed in the AIT0.35 specimen, whereas lower strain concentrations are observed in the AIT0.15 and PIT specimens. Although the graphical illustrations cannot clearly distinguish those KAM specimens, the statistical data and the calculation of the local average KAM values (**Fig. 7d**) can help to confirm what was discussed previously in **Section 3.2**. The local maximum and minimum average KAM were found in AIT0.35 and PIT with values of 0.82 and 0.70, respectively. KAM calculation was carried out separately in phases with the different crystal structures (fcc and bcc) to examine the local strain distribution in individual structures, especially in RA. The average KAM values of specimens that underwent the PIT and AIT treatments are shown in **Fig. 7e**. The average KAM values of bcc and fcc are raised as the magnitude of ausforming increases, while the KAM value obtained in RA is always lower than that in BF and FM in all cases.

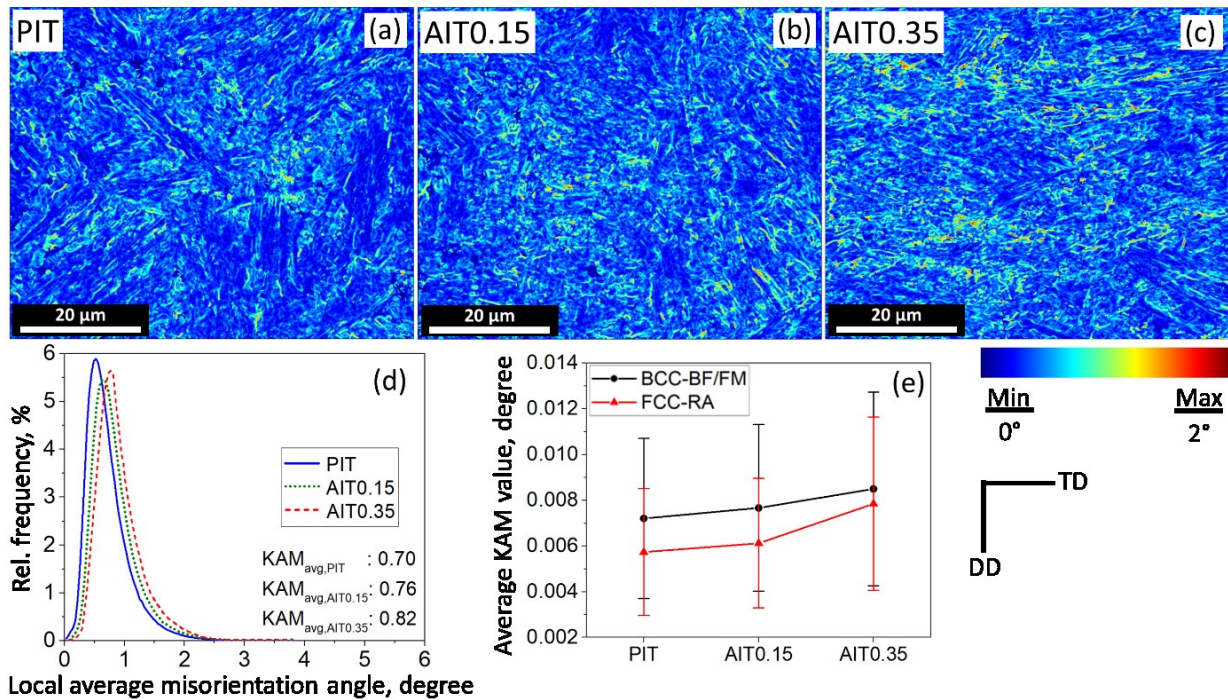


Fig. 7 (a)-(c) Kernel average misorientation (KAM) maps of PIT, AIT0.15, and AIT0.35 specimens, respectively. (d) Relative frequency of KAM angle, (e) average KAM value of bcc (BF/FM) and fcc (RA) structures based on specimen conditions. BF, FM, and RA refer to bainitic ferrite, fresh martensite, and retained austenite, respectively.

Furthermore, the local dislocation density was estimated based on lattice curvature, so-called geometrically necessary dislocation (GND). Like the analyses of KAM values, the distributions of GND density in RA and BF grains were analyzed separately, and the color gradient in the GND density maps represents the intensity of dislocations at specific locations. Following this, the GND density maps of PIT (**Fig. 8a** and **8c**) and AIT0.35 (**Fig. 8b** and **8d**) specimens were calculated. The red spots and green spread areas correspond to the high intensity of dislocations, while the blue-based matrix corresponds to the lowest intensity of dislocations. The GND density map of BF was visualized by superimposing it with the highly distorted structure of FM. The distribution of GND density in RA and BF grains was directly proportional to the magnitude of ausforming since the fraction of high GND density areas increased with increasing the ausforming strain. In the PIT specimen, the dislocations piled up along the grain boundaries and at BF/blocky FM interface tips. However, these dislocations barely spread out to the BF grain boundaries or into RA grains, as the overall intensity of dislocations was somewhat lower. In contrast, the high GND density induced by ausforming for the AIT0.35 specimen was dispersed throughout both structures (**Fig. 8b** for BF and **Fig. 8d** for RA), particularly near the slender interfaces between BF substructures, RA and FM. Herein, the high intensity of dislocations accumulated in RA and BF grains might lead to a higher tensile strength.

In general, the overall increasing trend of GND densities in both BF and RA may be directly related to the highly distributed stress and generated dislocations during applying ausforming. Compared to the PIT specimens, an increasing number of elongated BF substructures with a high intensity of dislocations in AIT specimens can likely result in pronounced yield and tensile strengths. Similarly, the inheritance of GND density into RA grains stabilized the untransformed austenite and thus made RA grains became more stable. This would lead to the fact that less RA undergoes martensitic transformation during tensile test and degrades the total elongation of the ausformed materials [48]. However, considering the large volume fractions and small grain sizes of the RA in these AIT materials, they would still contribute to the total elongation and partially help to rise

the material strengths. These aspects will be discussed in detail in the following section together with the mechanical properties of the materials.

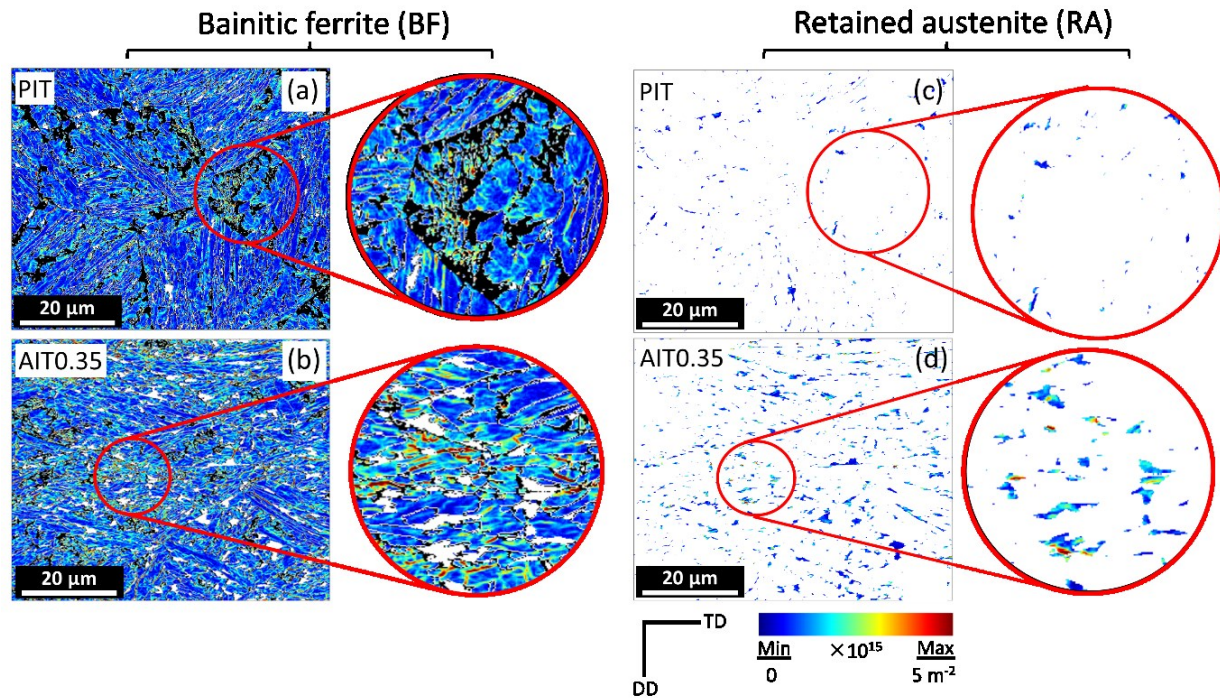


Fig. 8 Distribution of geometrically necessary dislocation (GND) density in PIT and AIT0.35 specimens for (a) and (b) bainitic ferrite superimposed with black-colored region fresh martensite and white-colored retained austenite, and for (c) and (d) retained austenite superimposed with bainitic ferrite and fresh martensite indicated by white regions.

The average GND density graph shows that the average GND densities in BF were consistently higher than that in RA for all cases. The values in BF obtained for PIT, AIT0.15, and AIT0.35 specimens are 1.103×10^{15} , 1.213×10^{15} and $1.571 \times 10^{15} \text{ m}^{-2}$, respectively, while the averaged values of RA are 8×10^{14} , 9.7×10^{14} and $1.2 \times 10^{15} \text{ m}^{-2}$, respectively. (as shown in **Fig. 9**)

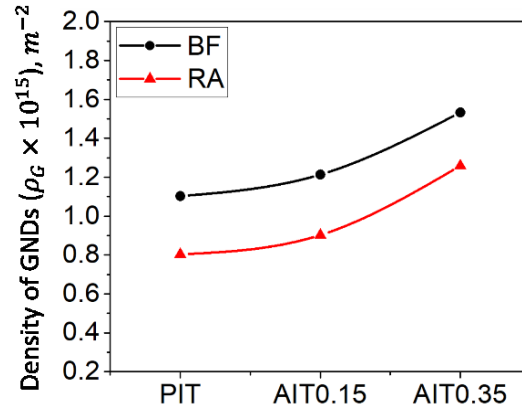


Fig. 9 Increase in average GND density in bainitic ferrite (BF) and retained austenite (RA) in PIT, AIT0.15, and AIT0.35 specimens

3.4. Mechanical properties

The engineering stress-strain curves of the PIT, AIT0.15, and AIT0.35 specimens depicted in **Fig. 10a** were utilized to evaluate tensile properties of the heat-treated materials. The results show that the yield strengths (YS) and ultimate tensile strengths (UTS) of both AIT specimens were improved by increasing the magnitude of the ausforming. In addition, the total elongations (A_5) were not diminished despite considerable increases in the strengths. These results contradicted the typical mechanical properties of bainitic TRIP steels [49,50], where a substantial enhancement of strength often leads to deterioration of the ductility. The tensile properties of all specimens are also summarized in **Table 2**. An excellent yield-to-tensile strength (YS/UTS) ratio is observed in AIT0.35 specimen. This implies that such a high magnitude of ausforming provided a substantial work hardening capability. The increase in values of YS, UTS, and YS/UTS could be associated with the contribution of the following mechanisms: 1) grain refinement according to the well-known Hall-Petch effect [51,52]; 2) increased GND densities in RA and the surrounding BF layers, as already pointed out in the previous section; and 3) TRIP effect [53]. Note that the influence of pre-existing FM on the material strengthening might be insignificant because the FM fraction was too small. The enhanced total elongation, which included both uniform elongation and post-necking regime, of AIT specimens can be attributed to a larger volume of RA which underwent strain-induced TRIP effect and the prolonged elongation to fracture caused by geometric softening [54]. This regime refers to as post-necking. As the post-necking regime is mainly determined by the capability of the materials in arresting cracks and preventing catastrophic failure, the

mechanisms in the post-necking regime will be further discussed in regard to the fractography in the last section.

The deformation behaviors of PIT, AIT0.15, and AIT0.35 specimens were further analyzed by the work hardening rate curves (represented by dotted curves), as depicted in **Fig. 10b**. A sudden drop in work hardening rate at low strains is ascribed to dislocation movements and dislocation generation within lattice structures of the material [55,56]. When plastic strain increases, the interaction of dislocations becomes prominent, as a consequence of competition between the formation of new dislocations, inhibition of their mobility, and processes that allow them to be organized and to annihilate each other. As a result, work hardening of material occurs while cross-section of specimen is continuously reduced so that work hardening rate is lowered. The reduction of the work-hardening rate continues up to a necking point where the true stress-strain curve intersects with the work hardening rate curve. However, there are significant differences between these three materials. AIT specimens exhibit a greater initial work hardening rate at true strains below ~ 0.01 when compared with PIT specimen. It seems that the refined microstructure and the pre-existing higher GND density in RA and surrounding BF only affected the increase in YS. They did not play any role in the initial work hardening rate since no effect of these two factors was found conspicuously. Hence, the initial work hardening rate behavior was influenced by higher fractions of the softened phases (i.e., BF and RA), at which substantial dislocations were allowed to develop. In contrast, AIT specimens exponentially decreased at lower hardening rates compared to PIT specimen when the strains progressed (> 0.01). The presence of such lower work hardening rates is involved in highly accumulated dislocations during the initial plastic deformation [55,56]. Nevertheless, it is observed that the work hardening rate curve of PIT specimen decreases significantly after achieving the strain of ~ 0.053 , while that of AIT specimens gradually declines at the higher rates before coming to their necking points. This behavior could be elucidated in terms of the formation of FM through the strain-induced TRIP effect of RA. The contribution of the TRIP effect of RA in the AIT0.15 and AIT0.35 specimens should be directly related to their volume fractions. It is plausible that the substantial amount of RA in AIT0.35 specimen led to a significantly higher uniform elongation than in AIT0.15 specimen. This will be discussed further in the next section in connection with the volume fractions of the RA measured corresponding to the equivalent plastic strains measured at different positions on the cross-section of the tensile

specimens. Overall, ausforming enhanced the YS, UTS, and YS/UTS ratio accompanying with the delayed necking and prolonged post-necking regime.

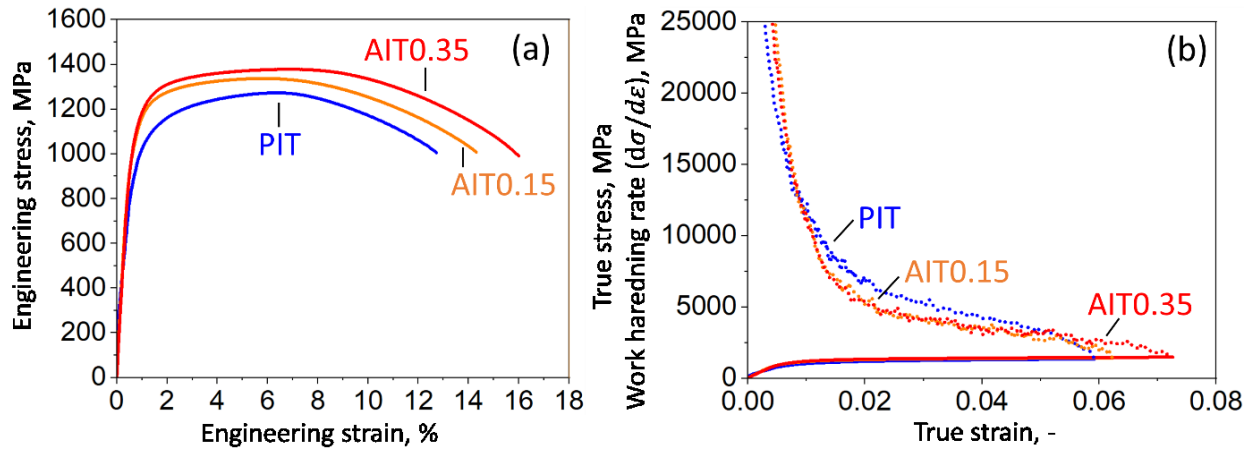


Fig. 10 (a) Engineering stress-strain curves (b) true stress and instantaneous work hardening rate ($d\sigma/d\varepsilon$) as a function of true strain of PIT, AIT0.15, and AIT0.35 specimens

Table 2 Tensile properties of PIT, AIT0.15, and AIT0.35 specimens. YS, UTS, A_5 , and YS/UTS stand for yield strength, tensile strength, total elongation, and yield-to-tensile ratio, respectively.

Specimen	YS, MPa	UTS, MPa	A_5 , %	YS/UTS
PIT(ref)	930	1269	12.7	0.73
AIT0.15	1057	1337	14.3	0.79
AIT0.35	1112	1390	16.1	0.80

3.5. TRIP effect

Since RA played a dominant role in the transformation into FM when plastic deformation occurred, the amount of RA was evaluated at the specific locations on the cross-sectional areas of the PIT and AIT specimens after fracture. Assuming that the location of 2 mm and 4 mm from the fracture surface possessed different plastic strains and those areas of each specimen could respond to the TRIP effect differently. In this study, the finite element analysis was conducted to predict the plastic strains at the evaluated locations. The 1/8 smooth-rounded tensile specimens were modeled, using ABAQUS software with the dynamic-explicit solver, by defining boundary conditions similar to the experiments. The element type C3D8R was selected with a minimum mesh size of

0.05 mm. As a result, the reaction force and displacement data obtained from the finite element simulation were compared with the experimental data, as illustrated in **Fig. 11a**. The displacement at the fracture point was taken into consideration so that the equivalent plastic strain (PEEQ) distribution was evaluated (see **Fig. 11b**). The PEEQ values were determined at 2 mm and at 4 mm from the fracture surface, which were the locations where RA fractions were observed by XRD measurement. It was found that the RA fractions at the specimen shoulder were nearly the same as that of the initial specimen. Supposing the percentages of RA fraction were plotted as a function of the PEEQ, the relationship between those values could be made using the linear regression method [57], as depicted in **Fig. 11c**. The coefficient (m) of the linearly fitted line was used to analyze the reduction rate of RA when it was subjected to the plastic strain. Comparing the results obtained from PIT to AIT0.15 and 0.35 specimens, it was found that AIT0.35 specimen has a much higher reduction rate of RA than the other specimens. This is because of its original high-volume fraction of RA, which allowed more transformability of RA during plastic deformation. However, the RA in this specimen possessed high mechanical stability, the transformation of RA was likely not activated in the early stage of plastic deformation, but it was effectively transformed into FM in the later stage before necking. As a consequence, work hardening rate of this specimen was still high at the high true strain region, as in **Fig. 10b**.

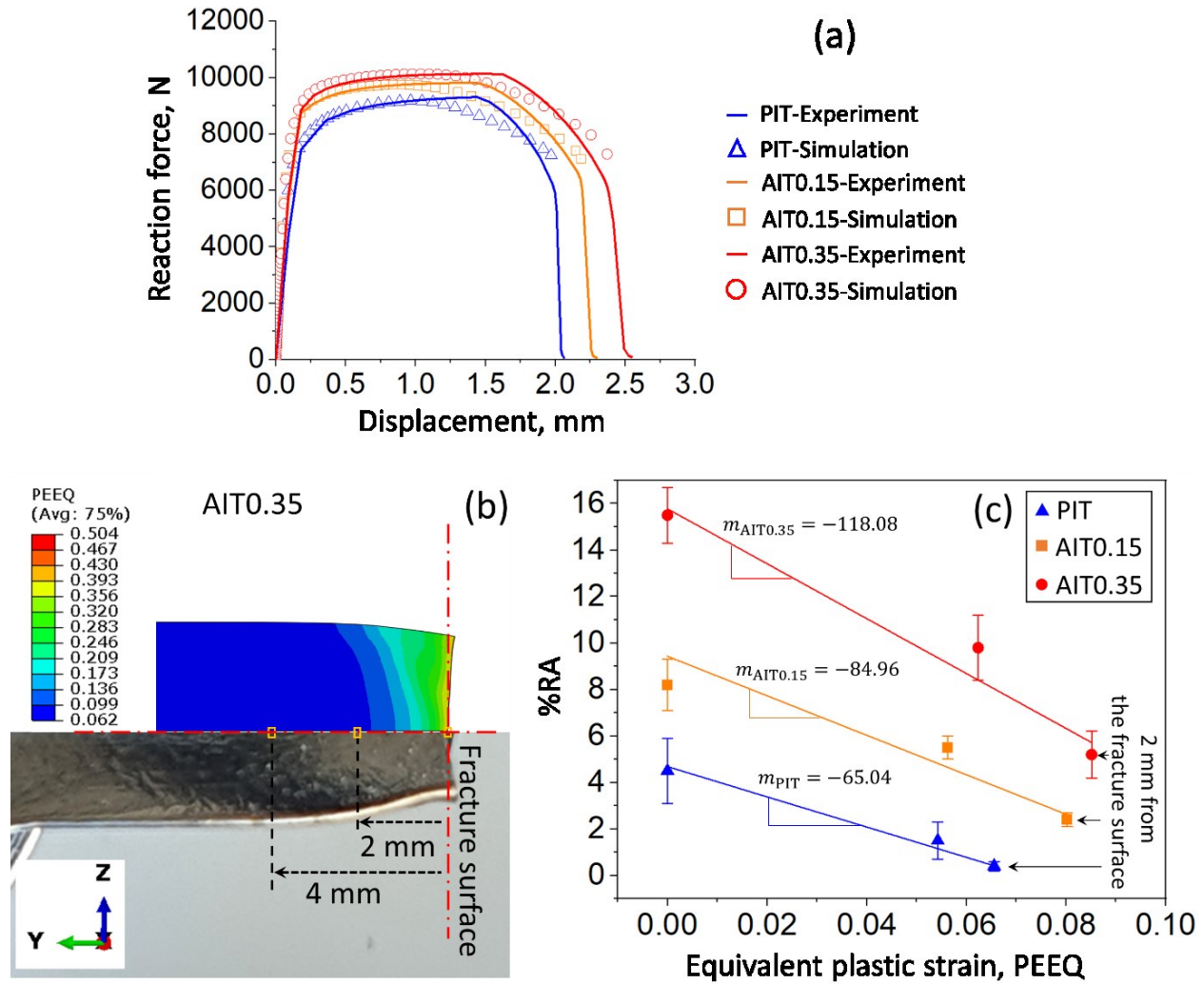


Fig. 11 (a) Force-displacement response of PIT, AIT0.15, and AIT0.35 specimens obtained from the experiment and simulation, (b) positions for XRD measurement on AIT0.35 specimen after tensile test superimposed with strain field measured from the finite element simulation at the fracture point and (c) percentage of retained austenite (RA) as a function of equivalent plastic strain values obtained from the different locations apart from the fracture surface.

3.6. Fracture morphology

The SEM fractography characteristics were viewed directly on the fracture surfaces of PIT and AIT0.35 specimens at different magnifications, as shown in **Fig. 12**. Hereby, the role and contribution of microstructure effects on the strength and ductility of the steels were studied. First, macroscopic features of the fracture surface of PIT and AIT0.35 specimens are depicted in **Fig.**

12a, and **Fig. 12d**, respectively. They generally exhibited ductile fracture morphology with the presence of macro-/microcracks near the center of the reduced cross-section, at which fracture was presumably initiated under tensile loading. The fracture surface of the PIT specimen had an excessive number of large macrocracks which developed towards the center of the specimen, whereas a few microcracks ($< 90 \mu\text{m}$) were observed in the AIT0.35 specimen away from the center. The microstructural feature strongly governed the formation of microcracks and their growth paths. This also led to a subsequent occurrence of voids and resulted in overall strength and plastic deformation capacities. A refined microstructure with a higher density of pre-existing dislocations was essential to impeding dislocations piled up at the grain/subgrain boundaries [58,59]. Apart from promoting increased yield strength, such grain boundary strengthening induced effective retardation of void nucleation during the post-necking stage. According to the microscopic feature of dimples near microcracks, illustrated in **Fig. 12b**, and **Fig. 12e**, the AIT0.35 specimen showed a high density of very-fine elongated dimples and small deep holes associated with extensive plastic deformation within the post-necking regime. Next to the dimples, the typical appearance of tear ridges was found in the PIT specimen (**Fig. 12c**). The tear ridges were relatively broad and filled with secondary voids around holes and dimples, unlike those observed in the AIT0.35 specimen (**Fig. 12f**). The formation of thickened and elongated valleys of the tear ridges in the AIT0.35 specimen suggested higher resistance to fracture and was consistent with its larger post-necking elongation, compared with those in the PIT specimen. Nevertheless, such greater resistance against fracture was supposed to be also relevant to the contribution of more fraction of retained austenite with high stability, besides the effect of grain boundary strengthening. As a consequence, the great ability of AIT0.35 specimen against macro-/microcrack formation during the cross-sectional reduction in the post-necking regime was provided.

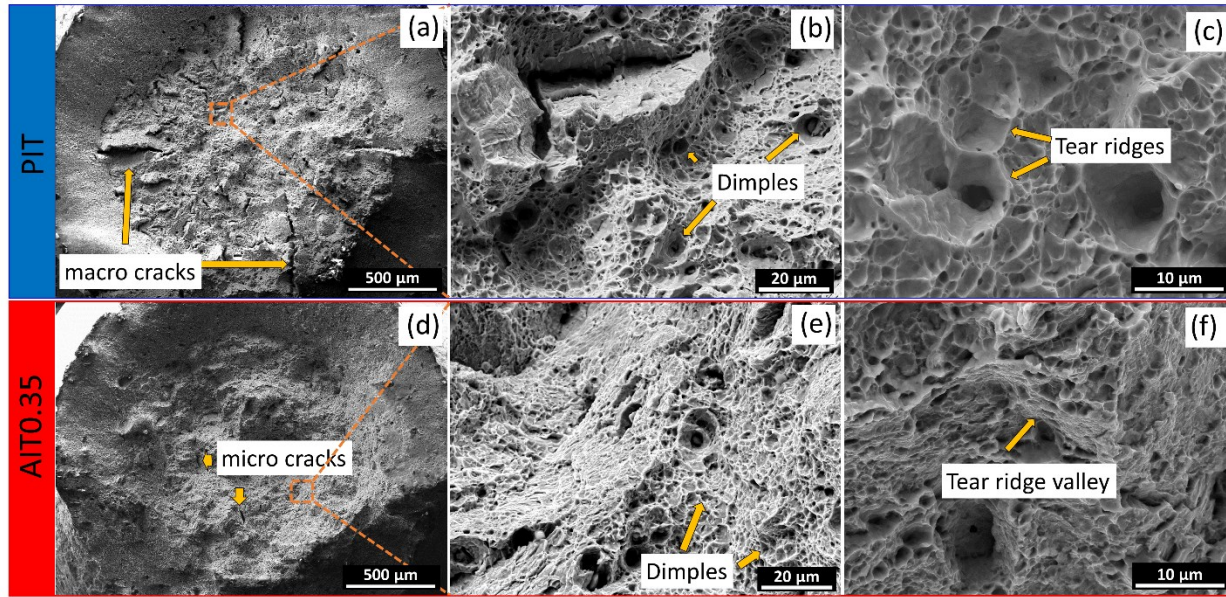


Fig. 12 SEM fractography of cup fracture surfaces of PIT and AIT0.35 specimens, showing; (a), (d) Overall fractography of failure normal to the stress axis; (b), (e) Magnified observation in the area of near macro-and-microscopic cracks; (c), (f) Highly magnified observation showing characteristics of tear ridges and their valley

4. Conclusions

The relationship between the ausforming process and the development of heterogeneous microstructure along with the improved mechanical properties of a low carbon Fe-0.18C-2.5Mn-1Si-0.2Cr-0.2Ni (wt.%) steel was investigated in this work. The major findings are as follows:

- Compared to the conventional pure isothermal tempering process, applying ausforming accelerates the onset of bainitic transformation. However, increasing in thermodynamic stability of austenite retards the completion of the bainitic transformation, which in turn leads to a reduction of the fresh martensite.
- The ausforming provides an increase in low-angle substructures with high dislocation density, which results in a reduction of the nucleation sites available for the martensitic transformation and therefore leaves more untransformed austenite after the subsequent cooling.

- The increases in yield strength, tensile strength, and total elongation of the studied low-carbon bainitic steel are due to the development of the heterogeneous microstructure, which contains about 16% retained austenite, 76% bainitic ferrite, and 8% fresh martensite. The elongation is mainly controlled by the dislocation slip and strain-induced plasticity effect of the retained austenite. At the same time, the high yield strength and ultimate tensile strength are governed by the refined microstructure and the stored high dislocation density.
- Apart from the enhanced strengths, grain boundary strengthening and a large amount of highly stable retained austenite induce effective retardation of void nucleation and help to prevent the formation of macro/micro-cracks during post-necking.

5 References

- [1] H.-W. Raedt, F. Wilke, C.-S. Ernst, Lightweight forging initiative phase II: Lightweight design potential for a light commercial vehicle, *ATZ. Worldw.* 118 (2016) 48–53. <https://doi.org/10.1007/s38311-015-0110-1>.
- [2] K. Sugimoto, S. Sato, G. Arai, Hot forging of ultra high-strength TRIP-aided steel, *MSF* 638-642 (2010) 3074–3079. <https://doi.org/10.4028/www.scientific.net/MSF.638-642.3074>.
- [3] K. Sugimoto, T. Hojo, A.K. Srivastava, Low and medium carbon advanced high-strength forging steels for automotive applications, *Metals* 9 (2019) 1263. <https://doi.org/10.3390/met9121263>.
- [4] W. Bleck, M. Bambach, V. Wirths, Microalloyed engineering steels with improved performance, in: *HSLA Steels 2015, Microalloying 2015 & Offshore Engineering Steels 2015*, Springer International Publishing, Cham, 2016, pp. 97–107.
- [5] F.G. Caballero, M.J. Santofimia, C. García-Mateo, J. Chao, C.G. de Andrés, Theoretical design and advanced microstructure in super high strength steels, *Mater. Des.* 30 (2009) 2077–2083. <https://doi.org/10.1016/j.matdes.2008.08.042>.
- [6] C. Garcia-Mateo, T. Sourmail, F.G. Caballero, Bainitic Steel: Nanostructured, in: R. Colás, G.E. Totten (Eds.), *Encyclopedia of Iron, Steel, and Their Alloys*, CRC Press, 2016, pp. 271–290.
- [7] V. Wirths, R. Wagener, W. Bleck, T. Melz, Bainitic forging steels for cyclic loading, *AMR* 922 (2014) 813–818. <https://doi.org/10.4028/www.scientific.net/AMR.922.813>.
- [8] V. Wirths, *Prozessführung und zyklisches Werkstoffverhalten von karbidfreien bainitischen Stählen*. Doctoral thesis, Aachen, 2016.

- [9] H. Bhadeshia, *Bainite in steels: Transformations, Microstructure and Properties*, secondnd., London IOM Communications, 2001.
- [10] H. Bhadeshia, D.V. Edmonds, Bainite in silicon steels: new composition–property approach Part 1, *Met. Sci. J.* 17 (1983) 411–419. <https://doi.org/10.1179/030634583790420600>.
- [11] H.S. Yang, H. Bhadeshia, Designing low carbon, low temperature bainite, *Mater. Sci. Tech-Lond.* 24 (2008) 335–342. <https://doi.org/10.1179/174328408X275982>.
- [12] F. G. Caballero and H. K. D. H. Bhadeshia, High-strength bainitic steels, *Int. J. Sci.* 1 (2004) 15–23. <https://doi.org/10.2355/isijinternational.45.1736>.
- [13] H. Guo, P. Zhou, A.M. Zhao, C. Zhi, R. Ding, J.X. Wang, Effects of Mn and Cr contents on microstructures and mechanical properties of low temperature bainitic steel, *J. Iron. Steel Res. Int.* 24 (2017) 290–295. [https://doi.org/10.1016/S1006-706X\(17\)30042-0](https://doi.org/10.1016/S1006-706X(17)30042-0).
- [14] J. Tian, G. Xu, M. Zhou, H. Hu, X. Wan, The effects of Cr and Al addition on transformation and properties in low-carbon bainitic steels, *Metals* 7 (2017) 40. <https://doi.org/10.3390/met7020040>.
- [15] Z. Yao, G. Xu, H. Hu, Q. Yuan, J. Tian, M. Zhou, Effect of Ni and Cr addition on transformation and properties of low-carbon bainitic steels, *Trans. Indian Inst. Met.* 72 (2019) 1167–1174. <https://doi.org/10.1007/s12666-019-01590-7>.
- [16] K. Zhu, C. Mager, M. Huang, Effect of substitution of Si by Al on the microstructure and mechanical properties of bainitic transformation-induced plasticity steels, *J. Mater. Sci. Technol.* 33 (2017) 1475–1486. <https://doi.org/10.1016/j.jmst.2017.09.002>.
- [17] L. Qian, Q. Zhou, F. Zhang, J. Meng, M. Zhang, Y. Tian, Microstructure and mechanical properties of a low carbon carbide-free bainitic steel co-alloyed with Al and Si, *Mater. Des.* 39 (2012) 264–268. <https://doi.org/10.1016/j.matdes.2012.02.053>.
- [18] X. Gui, G. Gao, H. Guo, F. Zhao, Z. Tan, B. Bai, Effect of bainitic transformation during BQ&P process on the mechanical properties in an ultrahigh strength Mn-Si-Cr-C steel, *Mater. Sci. Eng. A.* 684 (2017) 598–605. <https://doi.org/10.1016/j.msea.2016.12.097>.
- [19] M. Soliman, H. Mostafa, A.S. El-Sabbagh, H. Palkowski, Low temperature bainite in steel with 0.26wt% C, *Mater. Sci. Eng. A.* 527 (2010) 7706–7713. <https://doi.org/10.1016/j.msea.2010.08.037>.
- [20] L. Zhao, L. Qian, J. Meng, Q. Zhou, F. Zhang, Below-Ms austempering to obtain refined bainitic structure and enhanced mechanical properties in low-C high-Si/Al steels, *Scr. Mater.* 112 (2016) 96–100. <https://doi.org/10.1016/j.scriptamat.2015.09.022>.
- [21] W. Liu, B. Zhang, A. Zhao, H. Guo, S. Sun, Control of morphology and dimension of blocky retained austenite in medium-carbon steel, *Mater. Res. Express* 6 (2019) 016526. <https://doi.org/10.1088/2053-1591/aae561>.

-
- [22] M. Soliman, H. Palkowski, Development of the low temperature bainite, *Arch. Civ. Mech. Eng.* 16 (2016) 403–412. <https://doi.org/10.1016/j.acme.2016.02.007>.
- [23] J. Cornide, C. Garcia-Mateo, C. Capdevila, F.G. Caballero, An assessment of the contributing factors to the nanoscale structural refinement of advanced bainitic steels, *J. Alloys Compd.* 577 (2013) S43–S47. <https://doi.org/10.1016/j.jallcom.2011.11.066>.
- [24] T. Kumnorkaew, J. Lian, V. Uthaisangskuk, W. Bleck, Effect of ausforming on microstructure and hardness characteristics of bainitic steel, *J. Mater. Res. Technol.* 9 (2020) 13365–13374. <https://doi.org/10.1016/j.jmrt.2020.09.016>.
- [25] C. Hofer, S. Primig, H. Clemens, F. Winkelhofer, R. Schnitzer, Influence of heat treatment on microstructure stability and mechanical properties of a carbide-free bainitic steel, *Adv. Eng. Mater.* 19 (2017) 1600658. <https://doi.org/10.1002/adem.201600658>.
- [26] S. Chatterjee, H.-S. Wang, J.R. Yang, H.K.D.H. Bhadeshia, Mechanical stabilisation of austenite, *Mater. Sci. Tech-Lond.* 22 (2006) 641–644. <https://doi.org/10.1179/174328406X86128>.
- [27] H. Guo, X. Feng, A. Zhao, Q. Li, M. Chai, Effects of ausforming temperature on bainite transformation kinetics, microstructures and mechanical properties in ultra-fine bainitic steel, *J. Mater. Res. Technol.* 9 (2019) 1151. <https://doi.org/10.1016/j.jmrt.2019.11.085>.
- [28] M. Zhang, Y.H. Wang, C.L. Zheng, F.C. Zhang, T.S. Wang, Effects of ausforming on isothermal bainite transformation behaviour and microstructural refinement in medium-carbon Si–Al-rich alloy steel, *Mater. Des.* 62 (2014) 168–174. <https://doi.org/10.1016/j.matdes.2014.05.024>.
- [29] J. Zhao, X. Jia, K. Guo, N.N. Jia, Y.F. Wang, Y.H. Wang, T.S. Wang, Transformation behavior and microstructure feature of large strain ausformed low-temperature bainite in a medium C-Si rich alloy steel, *Mater. Sci. Eng., A* 682 (2017) 527–534. <https://doi.org/10.1016/j.msea.2016.11.073>.
- [30] W. Gong, Y. Tomota, Y. Adachi, A.M. Paradowska, J.F. Kelleher, S.Y. Zhang, Effects of ausforming temperature on bainite transformation, microstructure and variant selection in nanobainite steel, *Acta Mater.* 61 (2013) 4142–4154. <https://doi.org/10.1016/j.actamat.2013.03.041>.
- [31] B.B. He, W. Xu, M.X. Huang, Effect of ausforming temperature and strain on the bainitic transformation kinetics of a low carbon boron steel, *Philos. Mag.* 95 (2015) 1150–1163. <https://doi.org/10.1080/14786435.2015.1025886>.
- [32] S.H. He, B.B. He, K.Y. Zhu, M.X. Huang, Evolution of dislocation density in bainitic steel: Modeling and experiments, *Acta Mater.* 149 (2018) 46–56. <https://doi.org/10.1016/j.actamat.2018.02.023>.

- [33] L. Zhao, L. Qian, Q. Zhou, D. Li, T. Wang, Z. Jia, F. Zhang, J. Meng, The combining effects of ausforming and below-Ms or above-Ms austempering on the transformation kinetics, microstructure and mechanical properties of low-carbon bainitic steel, *Mater. Des.* 183 (2019) 108123. <https://doi.org/10.1016/j.matdes.2019.108123>.
- [34] L. Lutterotti, Maud: a Rietveld analysis program designed for the internet and experiment integration, *Acta Crystallogr. A* 56 (2000) s54-s54. <https://doi.org/10.1107/S0108767300021954>.
- [35] N. Vandijks, A. Butt, L. Zhao, J. Sietsma, S. Offerman, J. Wright, S. van der Zwaag, Thermal stability of retained austenite in TRIP steels studied by synchrotron X-ray diffraction during cooling, *Acta Mater.* 53 (2005) 5439–5447. <https://doi.org/10.1016/j.actamat.2005.08.017>.
- [36] D. Stojakovic, Electron backscatter diffraction in materials characterization, *Process. Appl. Ceram.* 6 (2012) 1–13. <https://doi.org/10.2298/PAC1201001S>.
- [37] F. Bachmann, R. Hielscher, H. Schaeben, Texture analysis with MTEX – Free and open source software toolbox, *SSP* 160 (2010) 63–68. <https://doi.org/10.4028/www.scientific.net/SSP.160.63>.
- [38] R. Bergmann, R.H. Chan, R. Hielscher, J. Persch, G. Steidl, Restoration of manifold-valued images by half-quadratic minimization, *IPI* 10 (2016) 281–304. <https://doi.org/10.3934/ipi.2016001>.
- [39] P. Lehto, H. Remes, EBSD characterisation of grain size distribution and grain substructures for ferritic steel weld metals, *Weld World* 66 (2022) 363–377. <https://doi.org/10.1007/s40194-021-01225-w>.
- [40] S. van Bohemen, Bainite growth retardation due to mechanical stabilisation of austenite, *Acta. Mater.* 7 (2019) 100384. <https://doi.org/10.1016/j.mtla.2019.100384>.
- [41] T. Kumnorkaew, J. Lian, V. Uthaisangskuk, W. Bleck, Kinetic model of isothermal bainitic transformation of low carbon steels under ausforming conditions, *Alloys* 1 (2022) 93–115. <https://doi.org/10.3390/alloys1010007>.
- [42] M.-C. Kim, Y. Jun Oh, J. Hwa Hong, Characterization of boundaries and determination of effective grain size in Mn-Mo-Ni low alloy steel from the view of misorientation, *Scr. Mater.* 43 (2000) 205–211. [https://doi.org/10.1016/S1359-6462\(00\)00392-4](https://doi.org/10.1016/S1359-6462(00)00392-4).
- [43] B. Guo, L. Fan, Q. Wang, Z. Fu, Q. Wang, F. Zhang, The role of the bainitic packet in control of impact toughness in a simulated CGHAZ of X90 pipeline steel, *Metals* 6 (2016) 1–13. <https://doi.org/10.3390/met6110256>.
- [44] X. Zhang, J. Li, L. Yan, X. He, Effect of film-like retained austenite on low temperature toughness of high strength offshore steel, *Mater. Res. Express. (Materials Research Express)* 6 (2019) 116530. <https://doi.org/10.1088/2053-1591/ab445c>.

-
- [45] S. Suzuki, Features of Transmission EBSD and its Application, *JOM*. 65 (2013) 1254–1263. <https://doi.org/10.1007/s11837-013-0700-6>.
- [46] K. Chen, H. Li, Z. Jiang, F. Liu, C. Kang, X. Ma, B. Zhao, Multiphase microstructure formation and its effect on fracture behavior of medium carbon high silicon high strength steel, *J. Mater. Sci. Technol.* 72 (2021) 81–92. <https://doi.org/10.1016/j.jmst.2020.09.034>.
- [47] A. Winkelmann, B.M. Jablon, V.S. Tong, C. Trager-Cowan, K.P. Mingard, Improving EBSD precision by orientation refinement with full pattern matching, *J. Microsc.* 277 (2020) 79–92. <https://doi.org/10.1111/jmi.12870>.
- [48] M.C. Taboada, A. Iza-Mendia, I. Gutiérrez, D. Jorge-Badiola, Substructure development and damage initiation in a carbide-free bainitic steel upon tensile test, *Metals* 9 (2019) 1261. <https://doi.org/10.3390/met9121261>.
- [49] C. Garcia-Mateo, F.G. Caballero, Advanced high strength bainitic steels, in: *Comprehensive Materials Processing*, Elsevier, 2014, pp. 165–190.
- [50] M. Shimanov, G. Korpala, A. Terzic, R. Kawalla, Bainitic steels: their characteristics and applications, *Key Eng. Mater.* 684 (2016) 104–110. <https://doi.org/10.4028/www.scientific.net/KEM.684.104>.
- [51] E.O. Hall, The Deformation and Ageing of Mild Steel: III Discussion of Results, *Proc. Phys. Soc. B* 64 (1951) 747–753. <https://doi.org/10.1088/0370-1301/64/9/303>.
- [52] N. Hansen, Hall–Petch relation and boundary strengthening, *Scr. Mater.* 51 (2004) 801–806. <https://doi.org/10.1016/j.scriptamat.2004.06.002>.
- [53] K. Sugimoto, N. Usui, M. Kobayashi, S. Hashimoto, Effects of volume fraction and stability of retained austenite on ductility of TRIP-aided dual-phase steels, *ISIJ Int.* 32 (1992) 1311–1318. <https://doi.org/10.2355/isijinternational.32.1311>.
- [54] Günter Gottstein, *Physical Foundations of Materials Science*, first ed., Springer Berlin, Heidelberg, Springer-Verlag Berlin Heidelberg 2004, 2004.
- [55] T. Li, J. Zheng, Z. Chen, Description of full-range strain hardening behavior of steels, *Springerplus* 5 (2016) 1316. <https://doi.org/10.1186/s40064-016-2998-3>.
- [56] H.M. U.F. Kocks, Physics and phenomenology of strain hardening: the FCC case, *Prog. Mater. Sci.* 48 (2003) 171–273. [https://doi.org/10.1016/S0079-6425\(02\)00003-8](https://doi.org/10.1016/S0079-6425(02)00003-8).
- [57] A. Schneider, G. Hommel, M. Blettner, Linear Regression Analysis, *Dtsch Arztebl Int.* 107 (2010) 776–782. <https://doi.org/10.3238/arztebl.2010.0776>.
- [58] H.-S. Park, R.E. Rudd, R.M. Cavallo, N.R. Barton, A. Arsenlis, J.L. Belof, K.J.M. Blobaum, B.S. El-dasher, J.N. Florando, C.M. Huntington, B.R. Maddox, M.J. May, C. Plechaty, S.T. Prisbrey, B.A. Remington, R.J. Wallace, C.E. Wehrenberg, M.J. Wilson, A.J. Comley, E. Giraldez, A. Nikroo, M. Farrell, G. Randall, G.T. Gray, Grain-size-

- independent plastic flow at ultrahigh pressures and strain rates, *Phys. Rev. Lett.* 114 (2015) 65502. <https://doi.org/10.1103/PhysRevLett.114.065502>.
- [59] S.R. Aghdaee, V. Soleimanian, Dislocations, crystallite size, and planar faults in nanocrystalline ceria, *Powder Diffr.* 24 (2009) 228–233. <https://doi.org/10.1154/1.3187210>.

Chapter V Conclusions and future studies

The effect of ausforming on the thermodynamic stability of austenite in low carbon steels, composed of carbon $<0.2\%$ wt., has been investigated and characterized through the kinetics of isothermal bainitic transformation, resistance to fresh martensite formation, microstructure analysis, and mechanical properties. Furthermore, the nucleation rate influenced by changes in the activation energy and enriched carbon in the austenite caused by ausforming has been analyzed by a unified physics-based model developed in this dissertation. The main conclusions are summarized below.

- Ausforming as a thermomechanical heat treatment process combining a plastic deformation of austenite at a high temperature with a single process of isothermal heat treatment at 400°C is employed to deal with the thermodynamic stability of austenite in low carbon steels. This process refines the austenite grain structure, then minimizes available nucleation sites for a subsequent decomposition of austenite to fresh martensite during cooling operation. The result achieves a desirable microstructure by increasing the volume fraction of retained austenite with a slightly decreased bainitic ferrite fraction.
- As compared with the conventional process of isothermal bainitic heat treatment, applying a prior plastic deformation of austenite remains applicable in this study. However, process parameters of ausforming, such as deformation temperature, strain, and strain rate, need to be controlled to define an appropriate condition so that the desired microstructure can be achieved.
- The effect of ausforming on the kinetics behavior of isothermal bainitic transformation and resistance to fresh martensite formation can be analyzed via a unified physics-based model derived from the classical nucleation rate theory and combined with the Koistinen-Marburger equation. Through detailed analysis of the kinetics behavior, it is revealed that the activation energy, driving pressure, and carbon enrichment in the austenite play a significant role in changing the nucleation rate. The nucleation rate is accelerated due to increased nucleation sites, then sluggish by the mechanical stabilization of austenite. The latter is affected by the increased carbon enrichment and dislocation density in the austenite.

- Mechanical properties evaluated in this study are strongly related to microstructure heterogeneity and phase constituents of the steel. Grain refinement and existing high dislocation structures enhanced strengthening behavior, while the amount of retained austenite fraction is essential to improve the strain-induced plasticity effect of the retained austenite. The effective prevention of macro/micro-crack formation during post-necking is due to grain boundary strengthening and a large amount of highly stable retained austenite.

Although the mechanical property improvement in this study provides a possibility to design low carbon carbide-free bainitic steels by ausforming process, other experimental validations should be carried out to fulfill the specific requirements for forged steel components. Furthermore, an improvement of the thermodynamic stability of austenite proposed in this dissertation is mainly focused on the variation of the kinetics behavior of isothermal bainitic transformation to the carbon enrichment in austenite. Meanwhile, the influence of other alloy elements on the same aspect has not been considered. Thus, the following investigations need to be considered in future studies.

- Effect of ausforming on toughness and fatigue properties. Apart from tensile and hardness properties employed in this dissertation, toughness and dynamic fatigue properties are also required for forged steel components under general service operations. Therefore, further experiments need to be validated for the completeness of mechanical property evaluation.
- Application of ausforming combined with other processing routes of heat treatment. Since the processing route applied after ausforming is vital to enhance the thermodynamic stability of austenite, other processes such as quenching-partitioning or tempering below M_s temperature should also be carried out.
- Effect of ausforming on the kinetics behavior of bainitic transformations, heterogeneous microstructure, and mechanical properties should be considered in the entire range of low-carbon steels.
- Effect of austenite former elements on their thermodynamic stability. The research summarized in this dissertation mainly focuses on improving the thermodynamic stability of austenite affected by the capability of carbon enriched in austenite. However, other substitutional elements, such as Mn and Ni interact with the stability improvement of austenite, were not considered. Therefore, the influence of these elemental contributions on

the kinetics behaviors and microstructure development should also be examined and characterized further in subsequent studies.

- Even though the experimental kinetics transformation is fitted well with the model, changes in the kinetics parameters during bainitic transformation are not experimentally validated. Consequently, experimental validations of the activation energy, carbon enrichment in austenite, and dislocation density evolutions during isothermal bainitic transformation are also required.

Curriculum vitae

Personal information

Surname, given name	Kumnorkaew, Theerawat
Address	Adalbertsteinweg 52, 52070 Aachen, Germany
Nationality	Thai
Date of birth	October 31 st , 1987
Place of birth	Chiangmai, Thailand
Phone	017665318397
E-mail	theerawat.kumnorkaew@iehk.rwth-aachen.de

Educational background

2010 – 2013	Master of Engineering, Mechanical Engineering, King Mongkut's University of Technology Thonburi, Thailand
2006 – 2010	Bachelor of Engineering, Mechanical Engineering, King Mongkut's University of Technology Thonburi, Thailand
2001 – 2006	High School Diploma, Mathematics–Science Programme, Yupparaj Wittayalai School, Thailand

Professional experience

Since 08/2018	Research associate in materials integrity group, Steel Institute, RWTH Aachen University, Germany
07/2016 – 08/2018	Research associate in materials simulation group, Steel Institute, RWTH Aachen University, Germany
02/2014 – 07/2016	University Lecturer in Mechanical Engineering division, Faculty of Engineering, Rajamangala University of Technology Krungthep, Thailand

Professional experience

04/2009 – 05/2009	Student Intern, Boiler Maintenance department, Electricity Generating Authority of Thailand, Lampang, Thailand
04/2008 – 05/2008	Student Intern, Maintenance department, Thai Composites Co., Ltd., Chonburi, Thailand

